VALIDATION OF NON-INVASIVE STANDING ARTERIAL STIFFNESS MEASUREMENTS USING BALLISTOCARDRIOGRAPHY AND PHOTOPLETHYSMOGRAPHY

A DISSERTATION

SUBMITTED TO THE DEPARTMENT OF BIOENGINEERING

AND THE COMMITTEE ON GRADUATE STUDIES

OF STANFORD UNIVERSITY

IN PARTIAL FULFILLMENT OF THE REQUIREMENTS

FOR THE DEGREE OF

DOCTOR OF PHILOSOPHY

Richard Matthew Wiard

June 2012

This dissertation is online at: http://purl.stanford.edu/cc955ph0602

I certify that I have read this dissertation and that, in my opinion, it is fully adequate in scope and quality as a dissertation for the degree of Doctor of Philosophy.

Gregory Kovacs, Primary Adviser

I certify that I have read this dissertation and that, in my opinion, it is fully adequate in scope and quality as a dissertation for the degree of Doctor of Philosophy.

Charles Taylor

I certify that I have read this dissertation and that, in my opinion, it is fully adequate in scope and quality as a dissertation for the degree of Doctor of Philosophy.

Laurent Giovangrandi

Approved for the Stanford University Committee on Graduate Studies.

Patricia J. Gumport, Vice Provost Graduate Education

This signature page was generated electronically upon submission of this dissertation in electronic format. An original signed hard copy of the signature page is on file in University Archives.

Abstract

More than 76 million Americans have hypertension, or high blood pressure, which can shorten life by 10-15 years if left untreated. Hypertension increases the risk of developing cardiovascular diseases (CVD) such as stroke, heart attack, congestive heart failure, or kidney failure that are often debilitating and impact quality of life. Prevention is the key to minimize CVD risk and increase longevity, but accurate prognosis of a future disease is difficult. Elevated blood pressure (BP) is generally the first sign of risk, but measuring pressure alone does not provide insight to where in the body problems may exist. Therefore, other screening tests are needed to more specifically isolate the underlying cause, which would improve the selection process of prescribing medications, or diet and exercise changes. And similar to BP measurements, such hypertensive screening tests may need to be performed at home to improve accuracy, since doctor's visits often trigger physiological responses that falsely elevate and lower BP.

To address these concerns this work describes the design and validation of a home based noninvasive system (a bathroom scale) to measure aortic pulse wave velocity (PWV), to assess arterial stiffness, which is a clinical risk factor for certain CV diseases. The purpose of this work was four-fold: to develop a home monitoring device with simple user operation; to develop biomechanical theories as to why forces in the aortic arch can be sensed synchronously at the feet; clinically validate the biomechanical theory; and to demonstrate potential clinical utility of standing PWV measurements for trending and prognosis.

The PWV scale is comprised of two different sensing technologies, ballistocardiography and photoplethysmography, which are embedded in the scale to measure pulse arrival times in the aortic arch and the foot—simply by standing on the scale. Using this system, PWV can be routinely determined in less than 30-seconds—significantly faster than commercial systems using trained operators.

To validate this PWV system, a novel biomechanical theory was developed called Central Aortic Forces (CAF) to explain how the cardiovascular forces inside the body can be synchronously sensed outside the body. The computational models accurately predicted the amplitude of forces in the aortic arch (2-3 Newtons at rest), which were empirically confirmed in a clinical study; the empirical results agreed within 10% of the theory. To demonstrate trending abilities, a longitudinal PWV study was also performed over a four month duration, with results highly correlated to the applanation methods. Finally, an age study was conducted to characterize arterial aging, which matched well ($p<0.01$) in slope and intercept major clinical trials published in the literature using applanation PWV (clinical gold standard). Examples are given on how such a system may improve prognosis to detect early vascular aging in young adults, otherwise masked in standard blood pressure measurements.

Acknowledgements

I credit the completion of this thesis to several people and wish to acknowledge those who contributed technically, financially, and provided emotional support. A doctoral program in bioengineering was not part of my original plan when I started the masters program in mechanical engineering. But after meeting a special group of people residing on the 2nd floor of the Paul G. Allen Center that shared a similar passion for medical devices, it was only natural to stay. Taking part in the Stanford Transducers Lab has truly been some of the greatest times of my life.

First, I would like to thank my principal advisor, and dear friend, Professor Gregory Kovacs. Greg was very patient (and kind) while I searched for a thesis topic and broadened my knowledge beyond mechanical engineering—venturing further into electrical engineering, the life sciences, and clinical research. I must emphasize he was patient! Greg is a rare individual who follows his passions and it is a joy to watch him live them out. From his extended family vacations exploring the savannahs, to climbing mountains and exploring volcanos—to the times he spends teaching enjoyable courses in electronics while chairing outdoor coffee sessions after lectures with his students. In government, he's served his country at DARPA finding worthwhile technologies to invest in. Greg also introduced me to NASA, by running biomedical experiments in a weightless environment. It's hard for me to say that Greg shows up for work…he shows up for life. I have been blessed by Greg's kindness that he's included me in several of these experiences. There is more life to be lived after Stanford, and I am certain that Greg will continue to be a part of many of those adventures.

Next, I would like to thank Laurent Giovangrandi, who co-advised this research. Laurent is wonderful man and gifted in every regard; a single paragraph will not do justice explaining this. I am indebted to him for the countless hours he spent working with me as a mentor, team member, and editing of several manuscripts. He stepped up and kept the lab running smoothly while Greg was away at DARPA and did a fantastic job. Laurent continuously challenged me to develop sound theories to support the experimental work, and he never lacked ideas on how to advance the research when we thought we reached the edges. We consumed lots of caffeine in the process (enough to support a small island economy). Outside of work, we covered a lot of distance together on our road bikes including some fifty mile treks from Stanford, over the mountains, down to wonderful Pacific Ocean beaches—and back. You may even find our names recorded in the ledger at The Bike Hut barn on Tanitas Creek Road, if you happen to be there.

To my friend and colleague Omer Inan, I owe some of my deepest thanks and respect to. Early on, he accepted a challenge from Greg to investigate the ballistocardiogram for his thesis—in hopes to revitalize the field after the medical community dismissed it. With a brave effort, Omer ventured down an abandoned road and reignited the field; where five years later he is chairing an invited session at the annual IEEE Engineers in Medicine and Biology Society conference. Somehow, Omer did all these amazing

things while raising two wonderful children, with his lovely wife Erin. He may say coffee should be part of this list. As his clinical work progressed, it became a source of inspiration for me to continue developing the physical theories which became a central theme in this thesis. Omer has been a good friend and source of encouragement during the Ph.D. process.

Everyone in the Stanford Transducers Lab, both past and present, deserves acknowledgements. Mozziyar Etemadi, for his key contributions to early BCG work; he is now at UCSF in the Ph.D./MD program and on a path to do more amazing things. To Michael Chen, I thank you for your willingness to volunteer as the first test subject for many of my (pre-) protocols—whether it takes place in artic or desert like conditions at the Gilbert Lifesciences temperature chambers. To Mikael Evander, who was always curious and willing to participate. I thank Shruthi Baskaran who helped to recruit subjects for the clinical studies. And to the other members of the lab past and present: Corey Mccall, Bill Esposito, Burak Dura, Shilpi Roy, Bernie Rihn, Amy Droitcour, Hollis Whittington, Gaylin Yee, Walt Wyman, Joy Ku, Keya Pandia, Sandy Plewa, and Claire Nicholas—thank you.

Next, I would like to thank Professors' Dwight Nishimura, Kenneth Waldron, and Craig Heller for serving on my quals, defense, and reading committees. I would like to thank Dr. Glenn Chertow in Nephrology—he supported this work by loaning test equipment and offered sound advice on how to structure the clinical studies. A special thank you is due to Olgalydia Urbano-Winegar in the Bioengineering Department. She encouraged early on me to apply to bioengineering for doctoral studies, when I was first became interested. When defense time approached, she was there just like day one, helping me navigate the university procedures to finish. Her constant smile will be in my memories always.

I am especially grateful to Professor Charles Taylor as a lecturer, examiner, and reading committee member. Charley understands hemodynamics like no other; he devoted his career to teaching courses and to develop blood flow simulation software that is far advanced of anything currently available. These simulation tools were utilized in Chapter 3 to show the relationship between hemodynamics and ballistocardiogram forces. Within his lab, I thank C. Alberto Figueroa and Hyun Jin Kim for the time they invested in the simulation work. At the present time, these simulations require an amount of computing power not commonly available. In the future, readers may wonder why these problems were so hard to solve in the first place.

I would like to thank Johnson & Johnson Company, Intuity Medical, and the Stanford Electrical Engineering department for their financial sponsorship during my tenure. I am grateful to Dennis Hager, currently at Edwards Lifesciences, who championed the initial support within Johnson & Johnson. And to Chris Countryman, I thank you for our friendship and the way you helped with the final push to complete this thesis.

To the late Jim Williams, I appreciate the inspiration he fostered in our lab. Without his contributions, our lab may not have not pursued ballistocardiography in the first place. He had an open door policy at Linear Technology and let me visit him to discuss circuits and possible ways to improve them. Also at Linear, I thank Balazs Lugosi who supplied our lab with sample components for many of the circuits that were built.

And to my family, I would like to thank my brother and sisters for their understanding and patience, when I decided to go back to school. And my deepest appreciation is owed to my parents, Cecil and Jessie Wiard. They raised me in a loving home and were superb role models of the Christian faith I share and hope to pass down to the next generation. They created a stable environment to grow and discover my passions. I had many interests—bordering between the fine line of typical and eclectic, which I usually pursued with equal tenacity. Sometimes this learning process came through the school of hard knocks, where personal disappointments became the some of the most important life lessons. But, my parents were always there for me, with loving support to go discover what lies next…

To my brother, David Wiard.

For convincing me to give college a try at a time when I thought playing baseball was more important.

Table of Contents

List of Tables

List of Figures

1 Introduction—Hypertension…a Call for Prevention

"…I will prevent disease whenever I can, for prevention is preferable to cure."

Selection from the Hippocratic Oath, modern version, by Dr. Louis Lasagna, 1964

1.1 Background

Through our curiosities in science, medicine, and engineering we are realizing increasing life spans. This advancement has resulted from immunizations, innovation in medical devices and pharmaceuticals, and equally through public health initiatives to promote awareness. However, with such life expectancy increase, major causes of death are now different than before. Attention needs to be given to the current leading cause—and preventive measures along with medications and devices may be the remedy. Hypertension, or high blood pressure, is the number one cause of premature deaths worldwide. However, our ability to diagnose the underlying causes of hypertension is mainly empirical—even with today's technologies. An overview of hypertension is presented in this chapter along with one potential technology (which is the work of this thesis) aimed to improve the prognosis of the risks related to hypertension.

1.1.1 Public Health in the 21st Century

Over the past century alone, life expectancy has nearly doubled worldwide as shown in Figure 1.1. To calibrate the reader to the level of this significance, the average life expectancy was 30-45 years in the early twentieth century. During the Middles Ages (5^{th} to the 15^{th} century) the average person lived to be 30 years old, and 28 years old in the classical eras of Greece and Rome over two millennia ago [1]. As of 2011, the current world average life expectancy is 67.2 years old (and 78.2 years old for the United States). Reviewing life expectancy data in Figure 1.1, a metric related to socio-economic status (SES) correlates well to prolonging life. Developed nations are the largest benefactors, followed by nations with developing economies, and lastly by impoverished nations. Healthcare-related factors associated with economic strength include improved access to physicians, vaccinations, surgical procedures, and medical device and/or pharmaceutical therapies to manage disease [2]. Technology has become essential to living longer, and future advances offer the promise to extend life even further.

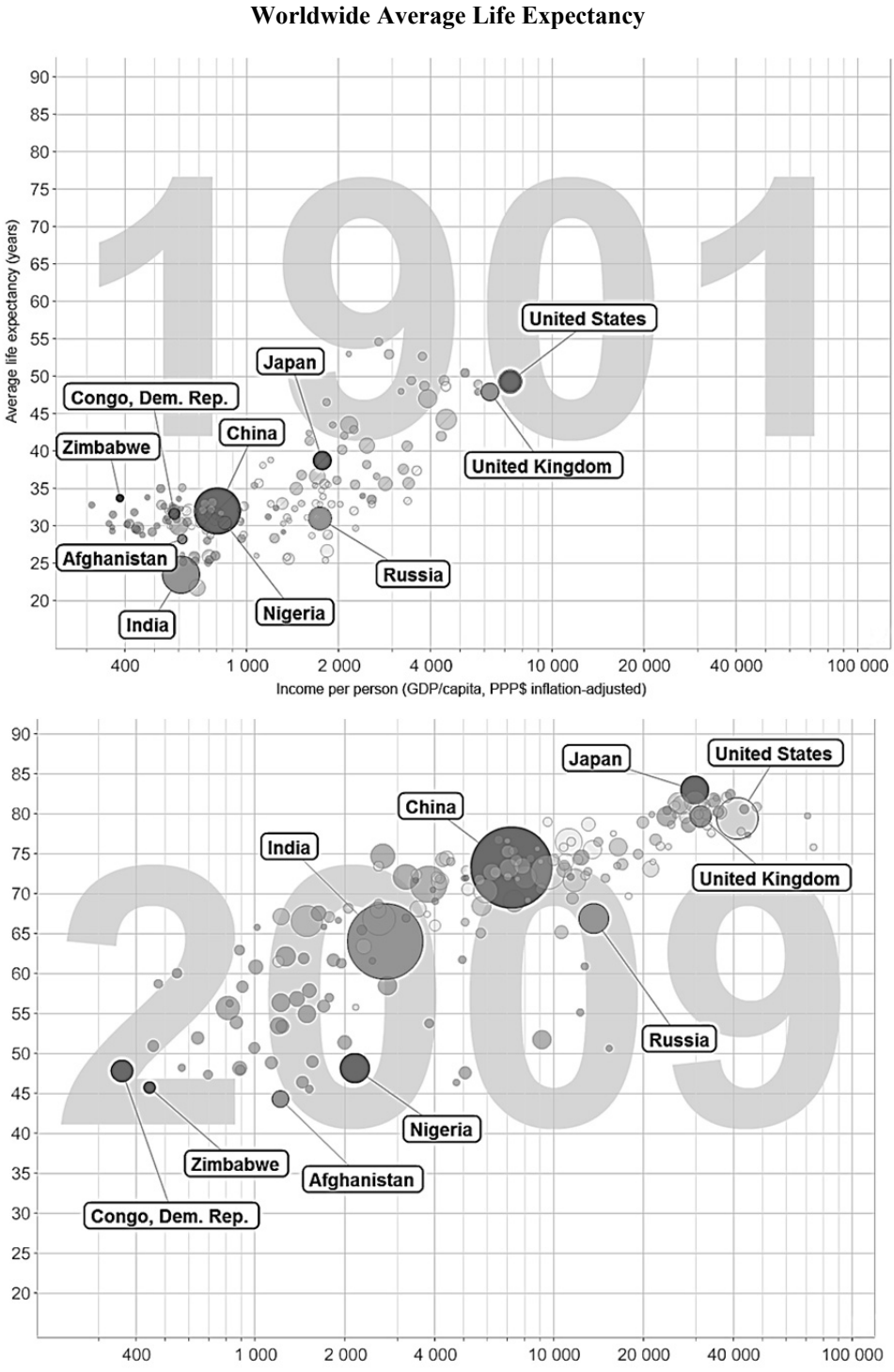

Figure 1.1: Average life expectancy (in years) sub-grouped by country versus inflation-adjusted personal income (normalized to national GDP by country) for the years 1901 and 2009. During this one-hundred-plus-year period the average life expectancy has nearly doubled worldwide. Source: Data aggregated by [3].

1.1.2 Cost and Benefit in Healthcare

A second examination of Figure 1.1 reveals two things. First, there is increased life expectancy from 1901-2009 presumably due to vaccinations, devices, drugs, and awareness. Second, there is increased life expectancy with SES, where the linear gains in life expectancy come at exponential cost. This cost-benefit proportion certainly has a point of diminishing return, but where? The United States is one such country wrestling with this economic and moral question, as growing healthcare costs are stifling the economy and the annualized increases in healthcare spending are predicted to bankrupt portions of the Medicare system by 2019. As new procedures are developed, what price should be paid for an added year of life? In one recent analysis, the renal dialysis cost-effectiveness standard model was revised, and $129,000 was proposed as the value of human life, in order to make a treatment worth its cost, if the treatment guaranteed one year of "quality life" [4]. Countries such as Canada, Australia, and England have formulated cost-effectiveness thresholds to determine whether new medical technology should be adopted, but the practice is meeting resistance by the Medicare system in the United States [5]. This intent here is not to reconcile the value of technology on human life, but rather to motivate the reader to consider the technologies discussed herein, which may have significant impact on quality of life with minimal cost, and can achieve broad adoption in various healthcare systems worldwide.

1.1.3 Future Outlook of Public Health

Mortality data from countries with high life expectancy may offer clues to guide research efforts to extend life further. In the United States, cardiovascular disease (CVD) is the leading cause of death in the older population (see Figure 1.2), followed by cancer. CVD accounts for one-third of deaths by the fifth decade of life and over one-half of deaths by the seventh decade. Of all leading causes of death, CVD is the only cause that increases monotonically throughout adult life. This age-dependent mortality rate is not limited to the United States. The World Health Organization reports that CVD is the overall leading cause of death worldwide, accounting for one-third of all deaths [6]. As new ways to prolong life are realized, the prevalence of CVD may continue to grow as the leading cause of death. It is therefore important to understand how CVD originates to discover better approaches to delay it, if possible.

1.1.4 Cardiovascular Disease

Cardiovascular disease (CVD) is the class of disorders involving the heart or blood vessels that leads to diminished function, organ failure, or a related cause of death. Major CVDs include stroke, ischemic heart disease, and renal failure where vascular damage or occlusions lead to death. Various interventions and devices are available to restore organ function and/or circulation once the particular form of CVD is diagnosed—often at high cost. However, treating the common risk factor associated with major CVD—hypertension—may be more practical to realize improved cost-benefits.

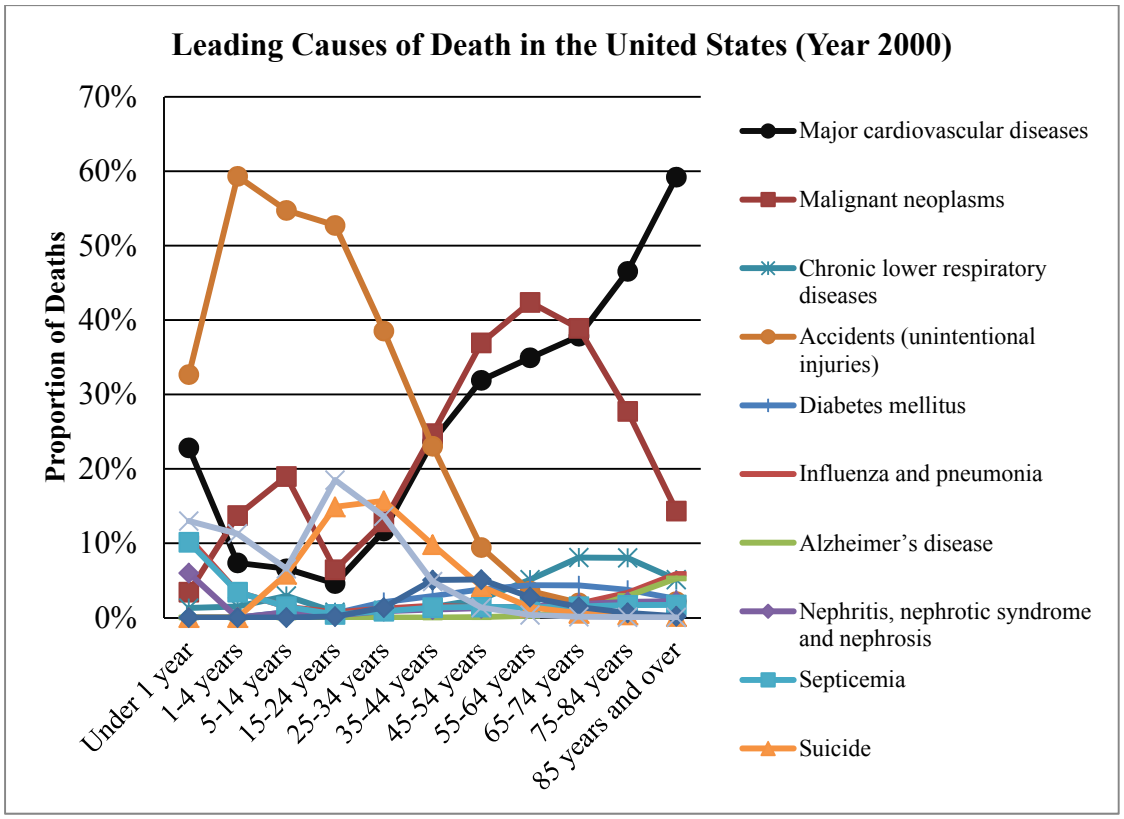

Figure 1.2: Leading cause of death in the United States stratified by age. Beginning at age 55, all major causes of death decrease or level off except cardiovascular disease (CVD). CVD continues to increase in prevalence monotonically at age fifteen. Source: National Vital Statistics Report, Death: Final Data for 2000 [7].

1.2 Hypertension: A Preventable Cause of Death

Hypertension is the chronic elevation of blood pressure and the leading cause of CVD both in the United States and the world. Michael O'Rourke best describes it as: "…hypertension is not a disease but a problem of magnitude, that high blood pressure, however measured or expressed, increases the load on the heart and the stresses on arteries, and accelerates cardiovascular degeneration and disease" [8]. This non-stop high pressure on the arterial walls and organs of the kidneys, heart, and brain may eventually result in renal failure, heart disease, and stroke, respectively. Hypertension is referred to as the "silent killer" because there are no other signs and symptoms (other than an elevated blood pressure measurement) that are ever experienced, making it appear to be innocuous [8]. Unfortunately, hypertension is referred to as a *condition* or a *problem* rather than as a disease, which detracts from its seriousness. To dilute its consequences even further, it is often underreported as a cause of death. As discussed by Kaplan:

> *"...It should be noted that the role of hypertension is probably underestimated from morbidity and mortality statistics, which is largely based on death certificates. When a patient dies from a stroke, a heart attack, or renal failure—all directly attributable to uncontrolled hypertension—the stroke, the heart attack, or the renal failure, but not the hypertension is usually listed as the cause of death."* [9].

By some estimates, controlling hypertension could add at least fifteen years to expected life [9]. This fact alone may persuade the reader that hypertension is a disease because it ends life prematurely.

One major problem in managing hypertension is to root out the underlying cause of elevated blood pressure (BP). Several mechanisms induce hypertension, making its diagnosis and treatment non-obvious. The common forms of hypertension are staged in accordance to age, but the reader should not consider a diagnosis to be purely age-dependent. Other factors, such as sympathetic nervous activity also play into the equation. However, based on the measurement of systolic and diastolic pressures alone, the three common forms of hypertension are: (1) Isolated Systolic Hypertension in young adults, (2) Essential Hypertension, and (3) Isolated Systolic Hypertension in older adults.

More than 70 million (30%) adults in the United States now have hypertension. In 2004, prevalence was 28.9%, up from 24.4% in 1990. The World Health Organization (WHO) reports that prevalence is just about equal in developing nations and overall, worldwide hypertension results in over seven-million premature deaths (Table 2.1), accounting for 4.5% of global disease types [6, 10].

While high prevalence rates are disheartening, increased prevention may change this situation. Hypertension is associated with 62% of strokes and 49% of ischemic heart disease (IHD) cases and the WHO estimates that current treatment standards result in a 40% reduction in stroke risk and a 15% reduction in myocardial infarct risk when hypertension is treated [6, 10].

1.2.1 Arterial Stiffening: Aging and Atherosclerosis

Managing arterial health is an important aspect of CVD prevention. The arteries are the conduits that supply blood oxygen and nutrients to all tissues and organs in the body. These greater vessels are arranged in a manner to deliver blood efficiently, governed by principles of least work [11, 12]. This principle is thwarted when certain disease processes or fatigue (from aging) ensue, changing the mechanical properties of the vessels walls to initiate various forms of hypertension.

Arterial stiffening is strongly associated with CVD risk. It increases pressure wave reflections in the major systemic arteries and heart, which elevates systolic blood pressure and decreases diastolic pressure. Early wave reflections increase left ventricular load (LVL) causing the heart to work harder to deliver blood, while reducing myocardial oxygen levels—starving the metabolic needs of the heart. This wave phenomenon and its consequences will be discussed further in the next chapter.

Table 1.1: Worldwide Leading Causes of Preventable Deaths in 2001

Preventable Cause of Death	***Number of premature deaths resulting (millions per year)***
Hypertension	7.8
Smoking tobacco	5.0
High cholesterol	3.9
Malnutrition	3.8
Sexually transmitted diseases	3.0
Poor diet	2.8
Overweight and obesity	2.5
Physical inactivity	2.0
Alcohol	1.9
Indoor air pollution from solid fuels	1.8
Unsafe water and poor sanitation	1.6

Source: Global burden of disease and risk factors [13].

1.2.2 Mechanisms of Arterial Stiffening

Arterial stiffening is positively correlated to aging. The aorta is highly compliant due to high elastin-to-collagen content, which reduces the speed of forward and reflecting pressure waves [14]. With age, elastin content decreases, and the properties of the stiffer collagen result in earlier wave reflections back to the heart in systole. Unfortunately, the degradation process is not reversible, and elastic content cannot be restored [15, 16], however, the degeneration process can be delayed with early intervention [9].

Atherosclerosis is a disease of the large and medium sized arteries, which also results in stiffening. Atherosclerosis is primarily an intravascular disease and characterized by the accumulation of lipids in the intimal lining, which decrease arterial caliber [15]. Inflammation processes also participate in the disease's progression, causing these lipids to calcify, forming hard thrombotic plaques and creating fibrotic lesions on arterial walls. Atherosclerosis is dominant in western societies and growing in prevalence. Unlike arterial aging, however, atherosclerosis is preventable. If left untreated, the result is stiffening of the aorta and major arteries and increased pressure wave reflections in systole, resulting in hypertension.

Aging and atherosclerosis are both causes of stiffening arteries [17]. Therefore, measuring arterial stiffness gives valuable insight into vascular disease progression—although it is regarded as an independent hemodynamic measurement, it is inter-related to pressure [14]. Stiffness measured in conjunction with blood pressure further stratifies CVD risk further and stiffness measurements are gaining acceptance in the cardiovascular community [18]. However, stiffness measurements are not the current standard of care;

measurement devices are in their infancy, and normal ranges have not yet been established—personalized trending may be required.

1.2.3 Screening and Trending Technologies in Hypertension

Due to the high prevalence of hypertension, simple approaches are required for evaluating patients quickly and often. Identification of hypertension begins with measurements of elevated BP. Brachial cuffs are the largest class of screening devices, but they only quantify pressure at the arm, not the heart [18]. Central hemodynamic measurements better represent cardiovascular loads on the heart and are an important emerging class of measurements [9]. Aortic BP and arterial stiffness measurements have recently gained clinical acceptance to manage hypertension [19, 20] and are poised to become mainstream measurements. Since blood pressure and arterial stiffness are inter-related, both are discussed here to explain how arterial stiffness measurements may best be used in the broader picture of hypertension management.

1.3 Arterial Stiffness Measurement Devices

As mentioned previously, arterial stiffness measurement devices are an emerging class of adjunct devices used to isolate the underlying causes of hypertension when used in conjunction with blood pressure. Stiffness is a parameter used to assess arterial aging and/or the degree of atherosclerosis. The method is quite useful in the diagnosis and treatment of Isolated Systolic Hypertension (ISH) as stiff arteries are the hallmark cause in both younger and older populations. Treatments include the use of vasoactive antihypertensives that act to reduce arterial stiffness and attenuate the reflected pulse wave in systole (a change that may go undetected when measuring brachial blood pressure alone) [21]. Current approaches to assess arterial stiffness require a skilled technician to perform the measurements, and techniques range from highly complex to fairly straightforward [22].

Arterial stiffness measurements have great predictive benefits for certain forms of cardiovascular disease (CVD) detection [14]. Such measures, in particular pulse wave velocity (PWV), reflect the true cumulative damage on the artery wall—which can be summarized as a total exposure measure, compared to blood pressure or circulating biomarkers such as lipids, which may only be a snapshot in time. Nilsson summarized the predictive effect of PWV compared to the Framingham Risk Score (FRS), which is the current gold standard for predicting CVD risk, see Figure 1.2 [23]. The FRS takes into account age, gender, total and HDL cholesterol, smoking history, and blood pressure. As shown below, the FRS with multiple inputs carries the same predictive utility as PWV, which is a single measurement. When PWV and FRS are combined, the CVD predictive value increases significantly and represents the highest prognostic value currently known. Therefore, routine measures of arterial stiffness should become common to improve CVD risk detection in the greater population.

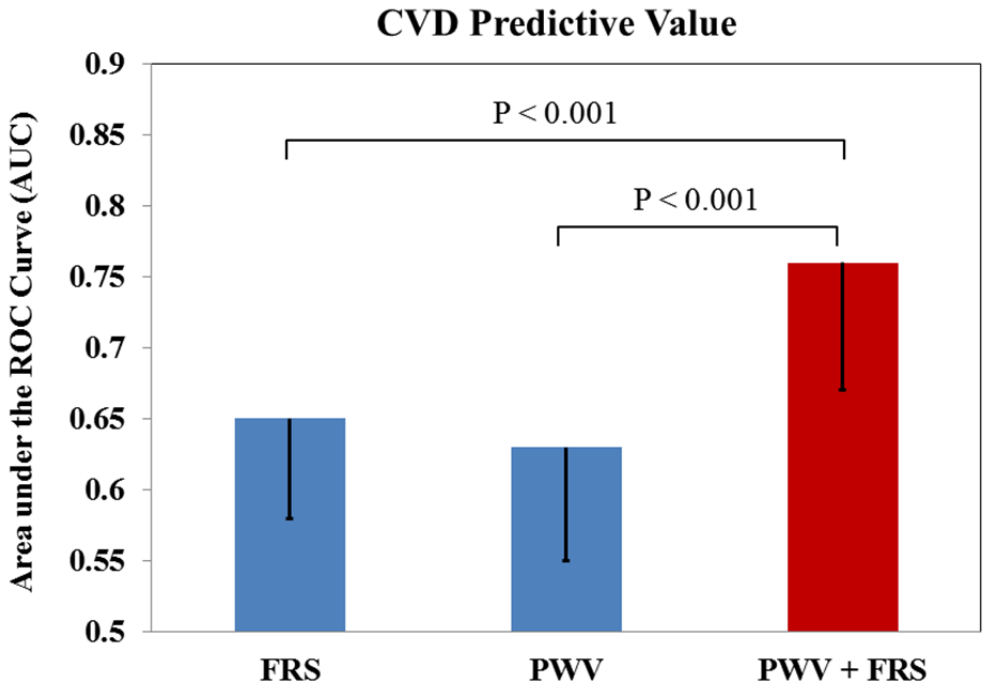

Figure 1.3: Cardiovascular disease predictive value of the Framingham Risk Score (FRS), pulse wave velocity (PWV), and combined benefit of both. Redrawn after [23].

1.3.1 Direct Stiffness Measurements

The direct measurement of stiffness is carried out by measuring arterial distension resulting from a change in internal pressure, giving an instantaneous measurement of stress and strain. The method requires both catheterization and medical imaging (e.g., ultrasound) at the region of interest to image vessel wall displacement [14]. Echo data may be acquired transesophageally or outside the body depending on the region of interest. While direct pressure-displacement measurements are obtained, the notable drawbacks to this method include limited accessible sites for the ultrasound measurement, requirement for a trained sonographer, high cost, and the small amount of arterial anatomy characterized. This method is not considered applicable to broad use in characterizing hypertension.

1.3.2 Pulse Wave Velocity

The most common method to assess vascular stiffness is to measure the pulse transit time (PTT) or pulse wave velocity (PWV) along an artery, giving an average stiffness value between the two measurement locations [24]. While this measurement may be performed invasively or non-invasively, the latter form is most common. Stiffer arteries will have shorter PTT, or conversely, higher PWV. The derivation of stiffness to velocity will be discussed in detail in Chapter 2. Catheterization along two points of an artery can also be used to obtain the PTT; however, if the arteries are superficial, the two pressure pulses may be obtained outside the body, which is the preferred approach. A list of commercial devices to measure vascular stiffness as compared to this work is summarized in Table 1.3.

Carotid-femoral PWV (cf-PWV) is the non-invasive gold standard for arterial stiffness and the AtCor Medical SphygmoCor CPV arterial tonometer is the most prominent system used in large scale clinical studies [19]. cf-PWV provides a reasonable estimate of aortic stiffness since both the carotid and superficial femoral arteries are reasonably close to the ascending and descending aorta. The method requires a technician to locate both of the arterial pulses in an asynchronous manner and current devices will report an "unsatisfactory" measurement if the heart rate differs by five beats per minute between the carotid and femoral measurements. Respiratory sinus arrhythmia (RSA) and/or baroreflex responses from carotid applanation are common factors that can lead to these "large" differences in heart rate [14]. Atherosclerotic plaque rupture in the carotid artery from applanation is also regarded as a risk factor for the cf-PWV method and caution should be exercised in these patient populations.

Table 1.2: Vascular Stiffness Measurement Devices

Classification / Type	**Invasive?**	**Advantages**	**Disadvantages**	**Cost**
Ultrasound & Pressure Catheter	Yes	- Direct stiffness measurement obtained	- Invasive - Region mapped limited to accessibility of US-probe - Technician required	High
Pressure Catheter (PTT/PWV)	Yes	- Imaging not required	- Invasive - Technician required	Medium
Carotid-Femoral PWV	No	- Non-invasive gold standard	- Heart rate dependent - Technician required - Potential carotid thrombus	Medium
Brachial-Ankle PWV	No	- Automated system - No Carotid Applanation - No Superficial Arterial Applanation	- Obtrusive. multiple cuffs	Medium
Standing PWV (from this dissertation)	No	- Acquired while standing on a weighing scale - No wearable sensors needed - Unobtrusive, compact - Removal of WCH and masked hypertension effects	- Device sensitive to motion artifacts from excess body movement	Low

Brachial-ankle PWV (ba-PWV) is an alternate method intended to improve upon ease-of-use issues surrounding cf-PWV [25]. In this approach, pressure cuffs are simultaneously applied to the brachial and ankle arteries, thereby eliminating the need to locate a superficial artery for applanation and do not require the carotid artery. Both arteries are further away from the ascending and descending aorta which may at first appear to be a disadvantage. However, the degree of atherosclerosis and CV risk is still highly correlated to the PWV indices obtained [26], so the method offers reasonable clinical utility. The Colin/Omron VP1000 is an example of a commercially available system.

1.3.3 Concluding Remarks on Arterial Stiffness Measurement Devices

Noninvasive PWV will likely remain the mainstream arterial stiffness technique for the larger patient population as an adjunct to blood pressure measurements. There are significant opportunities to reduce cost and simplify the measurement process with alternative sensing approaches. Current stiffness measurements require technicians and skill to operate properly. The aim of this thesis is to develop and validate an affordable PWV measurement system for personal use, with no need for a trained operator. Unlike the BP measurement systems reviewed, there are no vascular stiffness devices that are suitable for home use. Since BP is best measured when outside the clinic to understand changes in blood pressure, it would be advantageous to also measure vascular stiffness at home, which could be trended with BP changes to better understand CV risk.

1.4 Ballistocardiography and Photoplethysmography for Personal Monitoring of Vascular Stiffness

In light of the preceding information, there is a need to non-invasively measure both blood pressure and vascular stiffness to identify the underlying cause of hypertension and for better titration of antihypertensive medications.

Two non-invasive measurement technologies are incorporated for personal monitoring of vascular stiffness, embodied within a bathroom scale. This standing stiffness measurement is obtained using ballistocardiography (BCG) and photoplethysmography (PPG) to determine the ascending aortic pressure pulse timing and the pressure timing at the feet, which is the site of major pressure reflections [14]. Both measurements are obtained automatically, which removes the requirement of a technician.

The main contributions of this thesis includes new theory describing BCG and a novel PWV measurement system integrated into a weighing scale platform, supported with clinical studies to validate standing arterial stiffness measurements. New biomechanical theory is developed to determine plausibility of the BCG as a measure of the ascending aortic pressure pulse timing. This theoretical framework has been missing in ballistocardiographic literature, yet it is essential to determining whether or not correlations in data should be valid. The field of ballistocardiography has suffered greatly from an excess of data without a clear understanding of what produces the signal in the first place. A significant contribution to the origins of the BCG signal uses computer-based simulations of fluid-solid interactions in arteries.

With a theoretical framework established for ascending aortic pressure waves, a device was constructed to measure the BCG by standing, using previous contributions by members of our group, with the addition of a dual-channel PPG sensor developed to validate the BCG signal as a suitable ascending aortic pressure signal. This combined system was tested in the clinical setting across subjects ranging in age from 18 to 80 years old.

1.5 Summary—Understanding the Cause and Effect Relationships in Hypertension

In summary, blood pressure devices used in the home are preferred to clinical measurements with ABPM as the best candidate to identify true blood pressure. HBPM using automated cuffs can estimate true BP as well, when enough measurements are collected over the course of a week. Unfortunately, peripheral pressure devices are limited in their capability to detect small changes in pressure and prognose CV risk when compared to central pressure measurements counterparts—and are deemed inferior to manage hypertension. Since central measurements are not currently available in the home setting, peripheral BP measurements will continue to be the standard of care as they are insensitive to WCH and masked hypertension effects observed in the clinic. Arterial tonometry PWA may be better suited for clinical use than cuffs, but the technique may still be prone to the same stress responses experienced with CBPM.

PWV is the most straightforward approach to measuring vascular stiffness, supplementing BP measurements. However, these technologies are far less developed than BP devices, with no viable options for home monitoring. PWV will likely be the next hemodynamic measurement adopted broadly when improved devices become available, thereby allowing hypertension to be better managed.

BIBLIOGRAPHY

[1] (2011). *"Mortality" from encyclopedia britannica online*. Available: http://www.britannica.com/EBchecked/topic/393100/mortality

[2] J. C. Riley, *Rising life expectancy: A global history*. Cambridge ; New York: Cambridge University Press, 2001.

[3] J. C. Riley, "Bibliography of works providing estimates of life expectancy at birth and estimates of the beginning period of health transitions in countries with a population in 2000 of at least 400,000," ed: Gapminder Foundation, 2010.

[4] C. P. Lee, G. M. Chertow, and S. A. Zenios, "An empiric estimate of the value of life: Updating the renal dialysis cost-effectiveness standard," *Value in Health,* vol. 12, pp. 80-87, 2009.

[5] P. J. Neumann, A. B. Rosen, and M. C. Weinstein, "Medicare and cost-effectiveness analysis," *New England Journal of Medicine,* vol. 353, pp. 1516-1522, 2005.

[6] WHO, "Global atlas on cardiovascular disease prevention and control," 2011.

[7] A. Minio, E. Arias, K. Kochanek, S. Murphy, and B. Smith, "Deaths: Final data for 2000," *National vital statistics reports,* vol. 50, pp. 1-119, 2002.

[8] M. F. O'Rourke, "Hypertension is a myth," *Australian and New Zealand Journal of Medicine,* vol. 13, pp. 84-90, 1983.

[9] N. Kaplan and R. Victor, *Kaplan's clinical hypertension*, Tenth ed. Philadelphia: Lippincott Williams & Wilkins, 2010.

[10] J. A. Whitworth and I. S. o. H. W. G. World Health Organization, "2003 world health organization (who)/international society of hypertension (ISH) statement on management of hypertension," *Journal of hypertension,* vol. 21, pp. 1983-92, 2003.

[11] C. D. Murray, "The physiological principle of minimum work: II. Oxygen exchange in capillaries," *Proceedings of the National Academy of Sciences of the United States of America,* vol. 12, pp. 299-304, 1926.

[12] C. D. Murray, "The physiological principle of minimum work: I. The vascular system and the cost of blood volume," *Proceedings of the National Academy of Sciences of the United States of America,* vol. 12, pp. 207-14, 1926.

[13] A. D. Lopez, C. D. Mathers, M. Ezzati, D. T. Jamison, and C. J. L. Murray, "Global and regional burden of disease and risk factors, 2001: Systematic analysis of population health data," *The Lancet,* vol. 367, pp. 1747-1757, 2006.

[14] W. W. Nichols, M. F. O'Rourke, and D. A. McDonald, *Mcdonald's blood flow in arteries: Theoretic, experimental, and clinical principles*, 6th ed. London: Hodder Arnold, 2011.

[15] Y. C. Fung, *Biomechanics : Circulation*, 2nd ed. New York: Springer, 1997.

[16] Y. C. Fung, *Biomechanics : Mechanical properties of living tissues*, 2nd ed. New York: Springer-Verlag, 1993.

[17] X. Wang, J. C. K. Jr, A. D. Struthers, and G. Z. Feuerstein, "Assessment of arterial stiffness, a translational medicine biomarker system for evaluation of vascular risk," *Cardiovascular Therapeutics,* vol. 26, pp. 214-223, 2008.

[18] The CAFE Investigators, for the Anglo-Scandinavian Cardiac Outcomes Trial Investigators, C. S. Committee, Writing Committee, B. Williams, P. S. Lacy, S. M. Thom, K. Cruickshank, A. Stanton, D. Collier, A. D. Hughes, H. Thurston, and M. O'Rourke, "Differential impact of blood pressure-lowering drugs on central aortic pressure and clinical outcomes: Principal results of the conduit artery function evaluation (CAFE) study," *Circulation,* vol. 113, pp. 1213-1225, 2006.

[19] M. E. Safar, "Arterial aging - hemodynamic changes and therapeutic options," *Nature Reviews in Cardiology,* vol. 7, pp. 442-449, 2010.

[20] M. R. Nelson, J. Stepanek, M. Cevette, M. Covalciuc, R. T. Hurst, and A. J. Tajik, "Noninvasive measurement of central vascular pressures with arterial tonometry: Clinical revival of the pulse pressure waveform?," *Mayo Clinic Proceedings,* vol. 85, pp. 460-472, 2010.

[21] S. Glasser, D. Arnett, G. McVeigh, S. Finkelstein, A. Bank, D. Morgan, and J. Cohn, "The importance of arterial compliance in cardiovascular drug therapy," *The Journal of Clinical Pharmacology,* vol. 38, pp. 202-212, 1998.

[22] S. DeLoach and R. Townsend, "Vascular stiffness: Its measurement and significance for epidemiologic and outcome studies," *Clinical Journal of the American Society of Nephrology,* vol. 3, pp. 184-192, 2008.
[23] P. M. Nilsson, P. Boutouyrie, and S. Laurent, "Vascular aging: A tale of eva and ADAM in cardiovascular risk assessment and prevention," *Hypertension,* vol. 54, pp. 3-10, 2009.
[24] W. Nichols, S. Denardo, I. Wilkinson, C. McEniery, J. Cockcroft, and M. O'Rourke, "Effects of arterial stiffness, pulse wave velocity, and wave reflections on the central aortic pressure waveform," *Journal of Clinical Hypertension,* vol. 10, pp. 295-303, 2008.
[25] J. Sugawara, K. Hayashi, T. Yokoi, M. Y. Cortez-Cooper, A. E. DeVan, M. A. Anton, and H. Tanaka, "Brachial-ankle pulse wave velocity: An index of central arterial stiffness?," *Journal of Human Hypertension,* vol. 19, pp. 401-406, 2005.
[26] A. Yamashina, H. Tomiyama, T. Arai, K.-i. Hirose, Y. Koji, Y. Hirayama, Y. Yamamoto, and S. Hori, "Brachial-ankle pulse wave velocity as a marker of atherosclerotic vascular damage and cardiovascular risk," *Hypertension Research,* vol. 26, pp. 615-622, 2003.

2 Background

"They say three weeks in the lab will save you a day in the library every time."

-R. Stanley Williams of Hewlett Packard Labs, on their discovery path leading to the missing memristor

The pressures experienced by the heart are a leading indicator of overall cardiovascular disease (CVD) risk. Conventional blood pressure (BP) measurements taken at the arm, however, provide only modest accuracy (sensitivity and specificity) in detecting any underlying problems that may exist. The mechanical structure of the arterial tree is a key contributor for the differences observed between central and peripheral pressures. Unfortunately, current medical school education rarely teaches about these biomechanical influences—so key concepts are introduced in this chapter. With this background, the motivation for measuring pulse wave velocity will become apparent.

Once familiar with these concepts, an important noninvasive measurement technique called *ballistocardiography* is introduced. Previous members of our lab have demonstrated the usefulness of such a device for *cardiac* monitoring. In this thesis, we aim to demonstrate the diagnostic value of ballistocardiography in *vascular* monitoring, motivated by the background physiology presented in this chapter.

2.1 Classical Understanding of Blood Pressure in Hypertension

2.1.1 The Cardiac Cycle

The Wiggers timing diagram in Figure 2.1 depicts the classic relationship and interactions between left-ventricular (LV) pressure, LV volume, and aortic pressure for one cardiac cycle. Beginning left-to-right, in diastole, the left atrium pumps blood into the left ventricle until the mitral valve closes ending the diastolic filling. This End-Diastolic-Volume (EDV) in the LV stretches cardiac muscle fibers, thereby setting the amount of contractility for cardiac ejection (Frank-Starling effect). The action potential propagates from the atrioventricular node to the ventricles to begin isovolumic contraction increasing LV pressure—this is the beginning of the systolic phase.

Isovolumic contraction continues and then ends once ventricular pressure exceeds aortic pressure and the aortic valve opens. Systolic ejection begins; the left ventricle is still contracting, pressure is continuing to rise, based on the propagation of the action potential, however contraction is no longer isovolumic—the heart is now coupled to the aorta (e.g. LV and aortic pressure are equal during ejection);

blood is flowing into the arterial tree. The compliant aorta distends in response to cardiac ejection until peak systolic pressure is attained. Systolic pressure then decreases; the aortic valve closes when LV pressure falls below aortic pressure, which ends systole. During diastole, the heart is decoupled and does not sense arterial pressure. Isovolumic relaxation then occurs, allowing LV filling to begin again starting the next cardiac cycle. During diastole, the coronary artery is perfused with blood, which replaces oxygen and nutrients metabolized by the heart. In hypertension, these pressures increase and may be indicative of problem elsewhere such as an organ or artery. A host of CV diseases may follow if blood pressure is not managed properly.

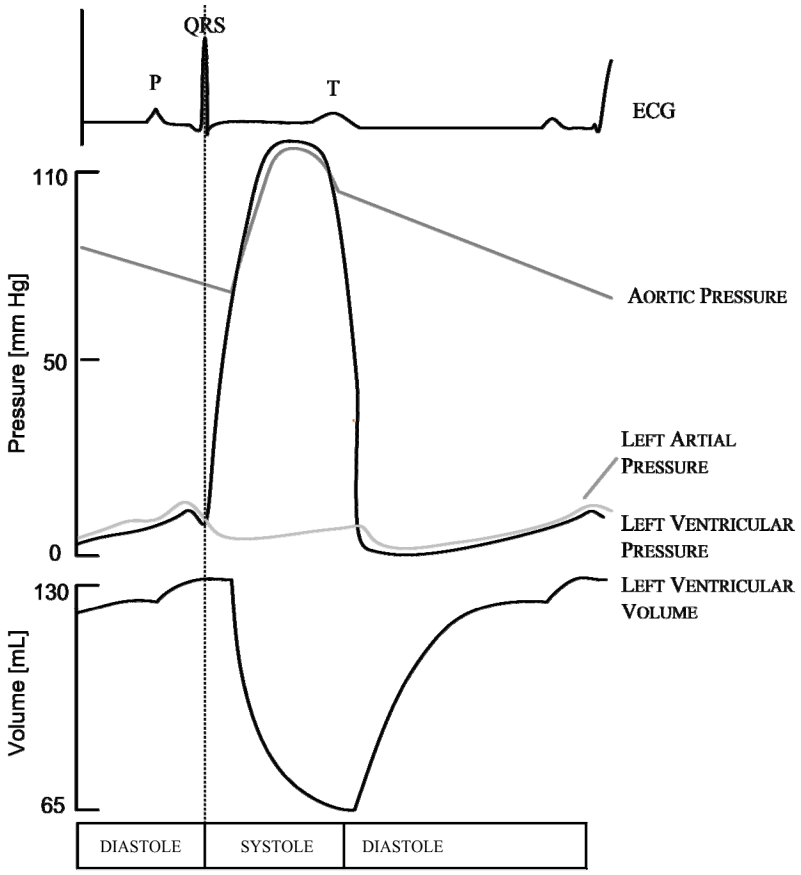

Figure 2.1: Cardiac Cycle Timing Diagram

2.1.2 Arterial Blood Pressure Measurements in Hypertension

Current guidelines recommend measuring arterial blood pressure with a cuff applied to the brachial artery [1]. Proper training is required for both patient and practitioner to obtain accurate values. The patient should be in proper position, sitting upright in a chair with feet flat on the ground (crossing the legs may raise systolic pressure 2-8 mmHg), and rested for at least five minutes. Clinicians are trained to use the auscultatory technique comprised of an arm cuff connected to a mercury sphygmomanometer, and a stethoscope to listen carefully for the first and fifth phases of the Korotkoff sounds as the cuff is carefully deflated. Automated cuffs using the oscillometric methods are recommended for the home or office use, but only if independently validated meeting standard protocols [1, 2].

Elevated blood pressure (BP) leads to health risks with pressures beginning at 115/75 mmHg. The Seventh Report of the Joint National Committee on Prevention, Detection, Evaluation, and Treatment of

High Blood Pressure (JNC 7) provides the following classifications (Table 2.1) defining normal pressure as <120 and <80 mmHg. An algorithm [3] is included in the JNC-7 report with different treatment recommendations for Stage 1 and Stage 2 hypertension.

Table 2.1: Classification of Hypertension (JNC-7)

BP Classification	Systolic BP (mmHg)	Diastolic BP (mmHg)
Normal	< 120	< 80
Prehypertensive	120-139	80-89
Stage 1 Hypertension	140-159	90-99
Stage 2 Hypertension	≥ 160	≥ 100

Stage 1 treatments recommend starting with a thiazide-type diuretic for most (water pill). They may also consider an angiotensin-converting-enzyme inhibitor (ACEI), angiotensin receptor blocker (ARB), beta-blocker (BB), calcium channel blocker (CCB), or combination. Stage 2 treatments are two-drug combinations starting first with the thiazide-type diuretic and the second as ACI, or ARB, or BB, or CCB. Once treatment begins, different medications are tried/added and/or dosages adjusted until the target BP is met. After the goal BP is achieved and stable, patient visits can be scheduled for 3 to 6-month intervals. If hypertension exists along with another condition such as heart failure, diabetes, chronic kidney disease, recurrent stroke prevention, etcetera—additional drug guidelines are then prescribed [1].

Unfortunately, the algorithm is purely a trial and error process. Over seventy types of antihypertensive drugs are currently approved—each acting on the cardiovascular system in a slightly different way. Comorbidities and side-effects can further add to the complication of optimizing treatment. Regrettably, there are no routine and reliable noninvasive measurements available to obtain *aortic* blood pressure—brachial arterial pressure measurements are more accurate at the present time. The brachial artery is only twelve inches away from the aorta, but curiously, the pressure differences between these two sites are quite different as explained in the next two sections.

2.2 Blood Pressure Measurements

2.2.1 Brief History of Blood Pressure Measurement

BP measurements at the brachial artery are the current practice, and the method has remained virtually unchanged for the past century [4]. However, there is a renewed interest in applanation methods that existed long before brachial measurements in order to measure the entire pulse waveform, not just the systolic and diastolic values [5]. The key difference now is that peripheral applanation measurements can be mathematically transformed into a central pressure waveform, enabling non-invasive central measurements.

2.2.2 Brachial Blood Pressure Measurements

Despite attempts by several inventors dating back to 1711, the first reliable measurement of blood pressure was demonstrated in 1896, credited to Scipione Riva-Rocci for the development of the mercury sphygmomanometer [4]. An air bladder cuff was placed around the arm and inflated to constrict circulation in the brachial artery, and the air-line of the cuff connected to a mercury-filled glass manometer to measure the systolic pressure of the arm. The method was not perfected until 1905, when the Russian surgeon Nikoli Korotkoff observed that both systolic and diastolic pressures could be measured using both the Riva-Rocci device and a stethoscope, by listening for characteristic sounds of blood passing through an artery while the cuff was slowly deflated [4]. This *auscultatory* method proved effective in measuring systolic and diastolic BP and became the standard of practice still used in today's healthcare setting. Panasonic introduced the first digital *oscillometric* blood pressure monitor in 1974, where the column of mercury is replaced with a pressure sensor, in the monitor away from the cuff [6]. The digital oscillometric method does not require an acoustic sensor being placed over the brachial artery; therefore, the placement of the cuff is not critical and can be performed by the patient.

2.2.3 Sphygmogram Pressure Measurements

Prior to the auscultatory technique's widespread adoption, sphygmogram devices were used to measure the shape of the entire radial pressure pulse waveform—recording the pulse onto paper. The method was inspired by palpation, an ancient technique known by many cultures—to sense healthy and diseased patterns through touch [7]. Frederick Mahomed classified the recorded radial waveforms (e.g., quantifying the "hard pulse" that clinicians were trained to detect), which advanced the field significantly [8]. In parallel, the auscultatory method also advanced quickly and became the preferred method to understand cardiovascular condition. Life insurance companies found immediate benefit in systolic and diastolic values over palpation to set premiums, which helped to institutionalize the auscultatory method [9, 10]. Sphygmogram devices were subsequently abandoned as tools in clinical medicine. However, after decades of studying the central pressure waveform using catheters [11], a resurgence is underway to re-introduce the radial technique—this time to record it to understand the central arterial pressure wave. This will be discussed further in the central blood pressure section.

2.2.3.1 Clinical Blood Pressure Measurement Bias

Clinical blood pressure monitoring (CBPM) is traditionally performed using the manual or automated auscultatory methods, serving as the clinical gold standard for diagnosing hypertension. CBPM is highly effective in emergency and urgent care but only modestly effective in the diagnosis [12] and on-going management of hypertension [13]. Patients interacting with health care professionals often experience "fight or flight reactions," leading to biases in blood pressure commonly referred to as white coat hypertension (WCH) and masked hypertension—an artificially raising or lowering of blood pressure, respectively [14]. True blood pressure is difficult to establish in the clinical setting due to these stress responses, so diagnosis and management is best performed elsewhere.

2.2.3.2 Home Blood Pressure Measurement

Home blood pressure monitoring (HBPM) eliminates clinically-induced bias; it is more reproducible and accurate, leading to better diagnoses of hypertension and predictions of CV risk [15]. Only brachial HBPM methods are recommended, however. Radial and finger blood pressure monitoring devices are not recommended as their accuracy and reproducibility are highly variable due to the cuff location height difference from the heart, which induces a pressure offset [16]. To estimate true blood pressure, current guidelines recommend a minimum of twelve HBPM readings be taken, twice a day for one week [17].

Ambulatory blood pressure monitoring (ABPM) provides continuous BP readings throughout the day, giving the best estimate of true blood pressure. ABPM devices resemble portable BP cuffs and ABPM and provide valuable trending information, which can be correlated to antihypertensive administration and effect, activity, sleep patterns, and periods of stress [18]. The United Kingdom has recently revised its BP guidelines [19] to use ambulatory monitoring as the primary method to diagnose hypertension, while clearly demonstrating it cost-effectiveness [20].

While HBPM and ABPM methods progress in their accuracy and reproducibility, there are new findings in improved CVD risk stratification and hypertension management emerging from large scale clinical studies that are setting the stage for the use of central blood pressure measurements.

2.2.4 Central Blood Pressure

One of the most misunderstood facts about blood pressure in the clinical community is that blood pressure is not constant throughout the body. As mentioned previously, several readings taken at home are required to estimate true BP; however, this was for brachial artery pressure. Central blood pressure is a measure of the ascending aorta pressure, giving insightful information about left ventricular pressure in systole and coronary perfusion in diastole. In recent years, central BP measurements have generated much interest in the clinical community. Several major clinical trials have been completed; all concluded that the measurement of central pressures is superior to that of peripheral measurement—including ABPM previously described [21]. Since the major organs are located close to the aorta, central pressures provide stronger indication of the loads on the heart, kidneys, and brain—and CVD risk can be further stratified.

New metrics have been developed to explain the central pressure pulse, and this field is known as Pulse Wave Analysis (PWA) [22]. Catheterization of the aorta serves as the gold standard to measure the central pressure waveform. Due to the invasiveness of catheterization, significant work has been done to "estimate" the central pressure waveform by measuring a peripheral waveform in a non-invasive manner, then mathematically reconstructing the central pressure waveform [23]. Applanation tonometry is a method utilizing an external pressure transducer applied against the radial artery, and used in conjunction with a generalized transfer function for indirect estimation of the central pressure waveform [5]. The SphygmoCor PWA system (by AtCor Medical) is currently recognized as the noninvasive central pressure

gold standard. The method has been validated against catheterization and is FDA-approved for sale in the United States and worldwide.

Table 2.2: Blood Pressure Monitoring Devices

Classification / Type	Location	Invasiveness	Advantages	Disadvantages
Mercury Column Sphygmomanometer	Peripheral / Brachial Artery	Minimal	- Gold Standard for BP Measurement	- Requires timer, stethoscope, and trained operator. Deflation rate must be controlled
Automated Cuff	Brachial Artery	Minimal	- Automated for personal use	- One week of measurements required to estimate true blood pressure
Ambulatory Cuff	Brachial Artery	Minimal	- Identifies "true blood pressure" - Eliminates white-coat hypertension - 24-hour recordings	- Nighttime measurements generally wake up user every 30 minutes
Finger Arterial Blood Pressure (Penaz)	Fingertip	Minimal	- Continuous Measurements - Cuff height compensation - Estimates Cardiac Output and Ejection Fraction	- Obtrusive setup - Numbing of fingertips with prolonged use
Pressure Catheter	Aorta, Ventricles	Invasive	- Records Central Pulse Wave (gold standard)	- Invasive - Skilled technician required - Medical imaging required to locate measurements site
Arterial Tonometry	Radial Artery	Minimal	- Estimates Central Aortic Pressure Pulse	- Requires skilled technician for applanation - Brachial artery measurement needed for calibration

2.3 Hemodynamic Factors Affecting Blood Pressure Measurements

Here, a brief introduction is given describing mechanisms responsible for pressure differences in the arterial tree. The concept of wave reflections has been long known, dating back to animal studies performed by William Harvey in 1649, where strong reflections were observed when occluding arteries. Unfortunately, this pressure wave theory is still omitted from most modern textbooks leaving the medical community unaware of these concepts. The relevance of arterial stiffness measurements will become more apparent once this arterial wave phenomenon is explained.

2.3.1 Wave Propagation in Arteries

Since arterial walls are deformable, there will be a finite velocity of propagation of a pulse wave. Conceptually, the arterial wave speed c_0 is analogous to the speed of sound first studied by Isaac Newton. When a material (e.g. air) of density ρ is uniformly compressed, the material will resist this change. Let the bulk modulus, *K,* define this resistance as the ratio of the infinitesimal uniform pressure increase, *dP*, to the relative decrease in volume, *V/dV*.

$$K = -V\frac{dP}{dV} \tag{2.1}$$

The speed at which this compression can occur is the *wave speed* of the material, c_0, which are related to the material resistance K and density ρ as

$$c_0 = \sqrt{\frac{K}{\rho}} \tag{2.2}$$

$$c_0 = \sqrt{V\frac{dP}{\rho dV}} \tag{2.3}$$

The derivation of Equation 2.3 was done by Thomas Young in 1809. A pressure-volume relationship governs the wave speed of any material. For arteries, this equation can be transformed further by making additional assumptions—the first being that the fluid inside the artery is incompressible ($dV_{\text{fluid}} = 0$), thus the artery is the only material compressing, not the fluid it contains. For a thin wall tube of radius R, the waves speed then becomes

$$c_0 = \sqrt{\frac{\pi R^2}{2\pi\rho R}\frac{dP}{dR}} \tag{2.4}$$

$$c_0 = \sqrt{\frac{R}{2\rho}\frac{dP}{dR}} \tag{2.5}$$

where for a change in internal pressure, *dP,* the artery will deform by amount *dR*. For a similar pressure pulse, a compliant artery such as the aorta of radius *R* would have a slower wave speed with higher vessel deformation and vice versa. The Moens-Korteweg wave speed equation [24] can be derived from Equation 2.5, to express the vessel wall resistance in terms of Young's Modulus, *E,* and vessel wall thickness, *h*

$$c_0 = \sqrt{\frac{Eh}{2R\rho}} \tag{2.6}$$

Therefore, the arterial wave speed can be related to the vessel geometry and its material stiffness. Pathologies such as arterial aging increase the wave speed due to elastin damage and furthermore from atherosclerosis—where inter-lumen plaques calcify on the arterial wall.

2.3.2 Wave Reflections in the Arterial Tree

As discussed in the previous section, wave propagation exists along the arterial tree. Consequently, the *amplitude* and *timing* of these reflections become problematic in hypertension when they return too quickly, which increases CVD risk. The arterial tree is comprised of a series of branching tubes and the heart is the driver of the circulation throughout. The pressure wave increases in amplitude as it

travels from the heart, through large and smaller arteries, but is quickly attenuated when it reaches the arteriole and capillary beds, see Figure 2.2.

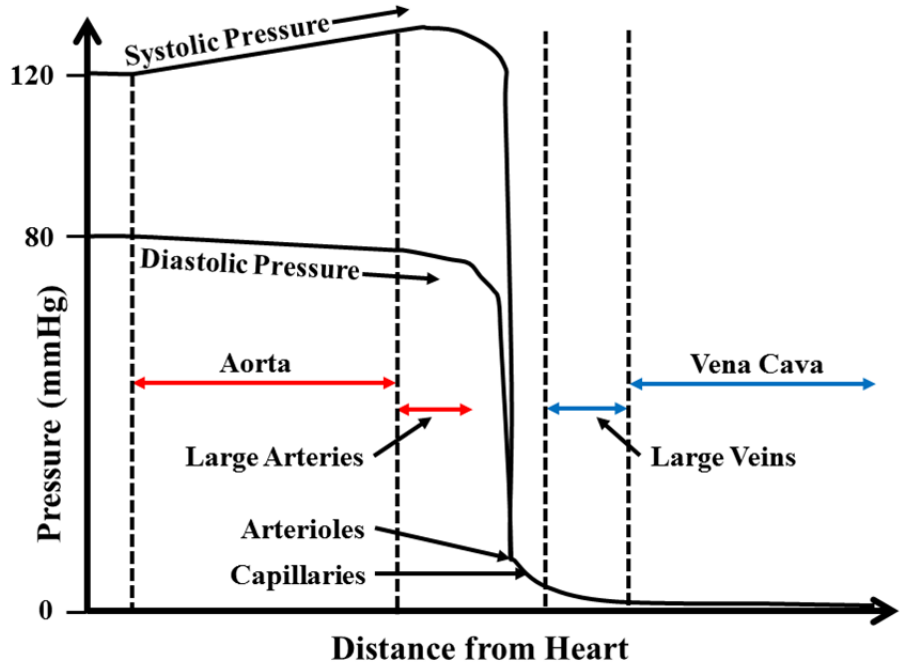

Figure 2.2: Diagram illustrating the wave behavior of the arterial tree. Systolic and pulse pressure continue to increase up until the arteriole/capillary beds, where pulsations cease—with steady flow through the capillaries. The high-resistance arterioles are considered to be the major site of wave reflection in the circulation. Redrawn from [16].

There is minimal pressure wave reflection in large branches as the incident pressure wave travels, since the cross-sectional area is nearly preserved. However, wave reflections will develop when the lumen cross-sectional area changes at sites such as junctions (e.g. bifurcations). The iliac branch point is one such site for wave reflections. While studying aortic input impedance using multisensory catheterization techniques Murgo et al. (1980) confirmed that wave reflections originating at the iliac bifurcation returned to the heart to produce peak systolic loads in the central pressure waveform [11]. However, the major site of wave reflections (largest return amplitudes) occurs at the arteriole bed. The area increase from the arterioles to the capillary beds is so large that pulsatile flow rapidly changes to near steady flow where gas and fluids are exchanged in the tissue beds (Figure 2.2). These multiple reflecting sites along an artery and its ending capillary beds add together, creating one large reflecting wave returning to the heart.

2.4 Central Blood Pressure and Cardiovascular Disease Risk

With wave phenomena in mind, let us revisit the aorta pressure waveform which was introduced originally in Figure 2.1. Ascending aortic pressure (herein referred to as *central pressure*) can be understood conceptually by decomposing the pulse into (1) an incident wave leaving the heart and (2) an

aggregate reflected wave returning from all downstream arterial locations back to the heart. The central pressure waveform is the arithmetic sum of these two waves, Figure 2.3. The timing and amplitude of these superimposed waves produce different effects in systole and diastole.

2.4.1.1 Systole and Left Ventricular Load

Panels A and B in Figure 2.3 shows the central pressure pulse for a normal, healthy person. At beginning systole, the aortic valve opens coupling the ventricle to the aorta, initiating the incident pressure wave. During systole, a small porting of the reflecting wave returns adding to the incident wave (black line, Panel B). Systolic blood pressure is the peak value. In this case peak systole is the same as the incident pressure.

Panel C show the same incident wave produced by the heart, but instead has a reflecting wave returning earlier in systole due to a higher arterial wave speed. The two waves add together to form a larger peak systolic value. The difference between the incident systole and peak systole is known as the *augmented pulse pressure* (ΔPP, in mmHg), Panel D. At this point, the ventricles must work harder to overcome the wave reflection to complete systole; the change in left ventricular load (ΔLVL) represents the additional work, Panel E.

Arterial stiffness is thus responsible for the timing of the returning wave and the degree of augmented systolic pressure. With age, augmented pressure continues to rise, producing Isolated Systolic Hypertension (ISH). In time, the left ventricular wall will thicken to reduce stress on the myocardium, decreasing its pumping efficiency and stroke volume. Unfortunately, faster wave reflections not only threaten to damage the ventricles in systole—they also promote myocardial infarction risk in diastole.

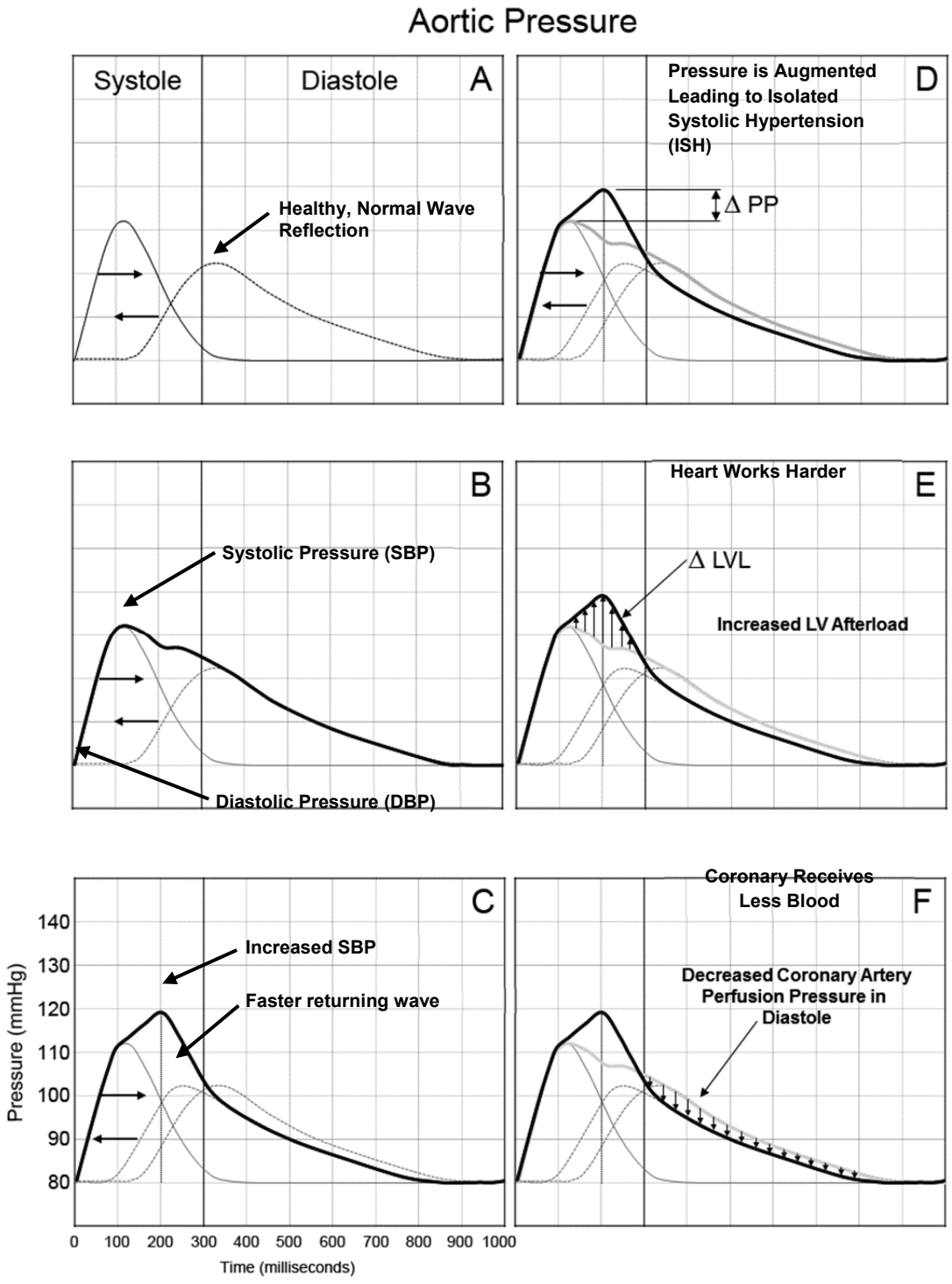

Figure 2.3: Effect of wave reflections in the aortic pressure wave. Case 1, normal wave reflection does not impact systolic blood pressure (Frames A and B). Case 2, a faster returning wave augments systolic pressure (Frame C and D), which increases left ventricular load (Frame E), and decreases diastolic pressure and coronary perfusion.

2.4.1.2 Diastole and Coronary Perfusion

The aortic valve closes to begin diastole, when LV pressure drops below aortic pressure. At this point ascending aortic flow ceases in the forward direction and reverse flow begins. The coronary artery begins to supply oxygenated blood to the myocardium; beginning diastolic pressure is therefore the coronary filling pressure of the heart, not systolic. Low coronary pressure and flow may lead to ischemia. As shown in Figure 2.3, Panel F, the faster returning wave that increased systolic pressure also resulted in lower coronary filling pressure. Therefore, increased arterial wave speeds may also introduce cardiovascular risks related to myocardial infarct.

2.4.2 Arterial Stiffness Measurements

As described in the introduction, results from several large scale clinical studies have concluded that CVD risk increases with increased arterial stiffness. Pulse wave velocity (PWV) is the simplest method to characterize the stiffness along an artery. The first chapter highlighted examples of such devices, including our standing PWV system developed during this thesis. This system utilizes ballistocardiography and photoplethysmography to measure the start and end points along the arterial tree. Currently, ballistocardiography is not widely known or used in clinical cardiology, so a brief introduction to the measurement is presented here.

2.5 Ballistocardiography

Ballistocardiography (BCG) is a noninvasive measurement of dynamic forces produced by the cardiovascular system. An action-reaction force is generated when the heart contracts and ejects blood into the arterial tree. This oscillation can be measured externally when the body is made still and placed on a compliant platform—with a force sensor connected to either the body or platform. A brief history of the BCG field is presented below, with background relevant to measuring arterial stiffness.

2.5.1 Brief History of the BCG

2.5.1.1 Recoil-Era Systems

In 1877, Gordon stood on a spring weighing scale and observed periodic movement of the readout needle. He then proceeded to take his pulse and found the oscillation to be synchronous with his heartbeat and was accredited with the discovery of the ballistocardiogram [25]. Gordon's first recordings were obtained from a person standing erect with perfect stillness. Later on, he improved the measurement method by constructing a swinging bed, suspended by four ropes. However, the recordings between the scale and bed platforms looked quite different; these differences were later classified as the high-frequency BCG and ultra-low frequency BCG, respectively [26]. Gordon's work gathered some attention and a few of his experiments were published in Leonard Landois' Textbook of Human Physiology. Landois himself became interested and built an upright system to measure these movements; publishing the first clinical observations in patients with aortic regurgitation differences in the tracings.

Unaware of these previous works, Yandell Henderson, at Yale, published a communication in 1905 describing a suspended swing bed very similar to Gordon's design to measure beat volume [27]. A 9 kg table was suspended by four steel wires permitting movement in only one direction. A set of levers was used to magnify the table displacement by a factor of one hundred and the oscillation was recorded on a smoked drum. Unfortunately, the natural frequency of the suspended bed was very low and coincided with respiratory signals which were ten times larger than the circulatory, so subjects were instructed to stop breathing to obtain a record. Seeking a better solution, Henderson instructed his subjects to blow long and steady breaths into a whistle, which removed the respiration signal. Below is Henderson's first simultaneous recording of the carotid artery pressure pulse with the recoil oscillation, Figure 2.4. Note the upstroke of the carotid pulse coincides with the first descent of the displacement recoil pulse (beat C).

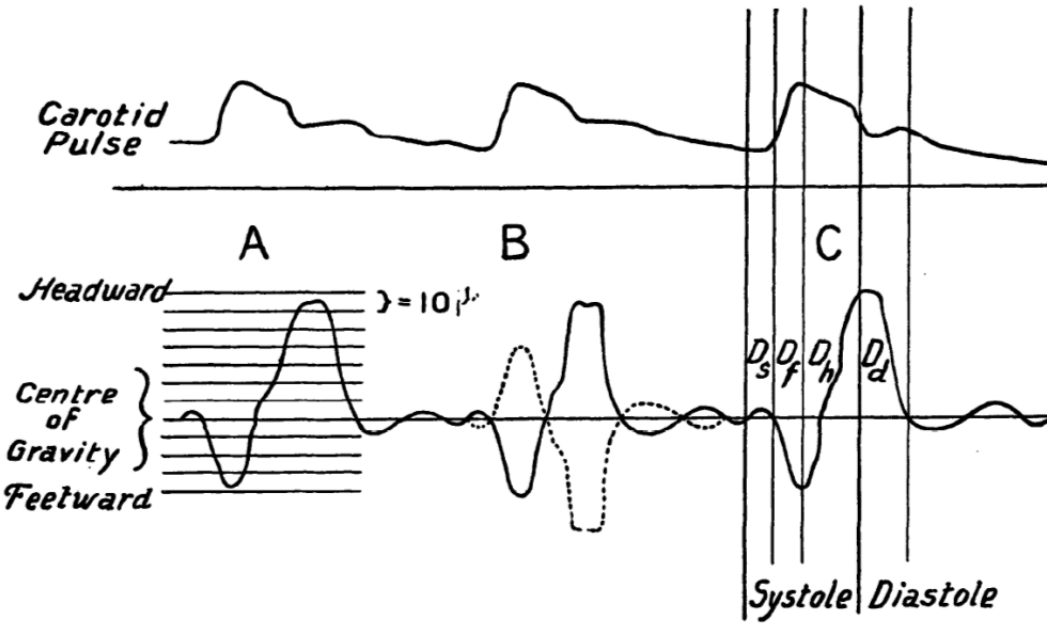

Figure 2.4: Recoil curve recorded by the Henderson apparatus in relation to the carotid artery pulse [27].

2.5.1.2 Starr-Era Ballistocardiography

In 1939, Starr et al. developed and published on a modified suspension bed platform that yielded high quality recordings [28, 29]. Rather than allowing the bed to swing freely like Henderson's, the end of the Starr bed was constrained with a steel spring. This small modification increased the natural frequency of the swing bed to a point where respiration effects were tolerable with normal breathing. Starr's apparatus was named the ballistocardiograph (BCG) and the shape of the BCG waveform was described based on several healthy subject recordings—the normal standard BCG shown in Figure 2.5.

The ECG R-wave precedes the BCG, denoted by the arrow in Figure 2.5. Starr described five intervals as: isovolumetric contraction at the onset of systole (H), start of ventricular ejection of blood (I), reversal of blood in the aortic arch (J), deceleration of blood in the abdominal aorta (K), and diastolic filling (L-N). The diastolic phase description was disputed by Omer Inan (Stanford University) in his thesis, and will be discussed in the modern ballistocardiography section [30]. Nevertheless, there is consensus for the other waves. Starr's seminal paper described a calculation to determine stroke volume (SV) based on the BCG. His noninvasive calculation of SV was compared to SV found by the ethyl iodide method, having a high correlation ($r^2 = 0.74$). Therefore, Starr proposed that the BCG was suitable to determine cardiac output, as well as detecting other CV pathologies [28, 29]. Starr's work inspired a new field and several new ballistocardiographs were invented. Problematically, there were large differences in recorded BCG waveforms, due to the different mechanical responses of each apparatus. For example, Figures 2.4 and 2.5 show strikingly different BCGs for two suspended bed designs, since their natural frequencies are significantly different—0.2 Hz versus 9 Hz, respectively. As a result, hardware standardization was needed so BCGs could be classified.

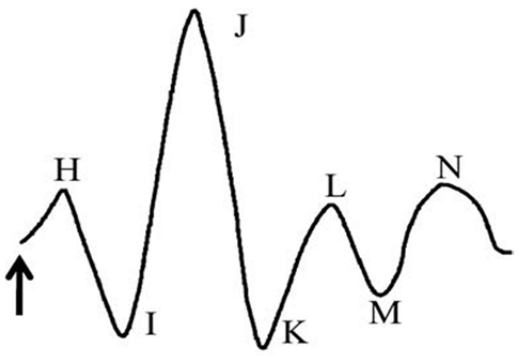

Figure 2.5: One beat of the normal standard acceleration BCG, after [1]. The arrow on the left side indicates the timing of the ECG R-wave.

2.5.1.3 Mechanical Differences in Ballistocardiograph Designs

The mechanical vibration characteristics between BCG designs were complex to characterize and calibrate, but an eloquent description was given by Burger regarding the differences in BCG apparatus designs [31]. For suspension beds, there are no lateral forces opposing the swing motion; therefore, the movements of the bed result only from the changing blood distribution (center of gravity) inside the body and are therefore a displacement measurement. On the other hand, if the lateral motion of the swing bed is restricted by some kind of binding (stronger than the center of gravity displacement), then something else is being measured. If this binding is a spring then a force is measured instead, since the displacements are related to the spring's compression and extension, like the Starr bed. Noordergraaf characterized several systems and developed the ultra-low, low, and high classification scheme—later adopted by the American Heart Association, see Table 6.1 [26, 32, 33]. Investigators now had a simple means to describe their instrument when reporting on new designs and/or clinical findings.

Table 2.3: Classification of Ballistocardiogaphs

Source: After [26]	
Type **A**	*Ultra low-frequency BCG*. Natural frequency of the loaded BCG low with respect to the heart frequency of about 1 Hz. Damping critical or weaker.
Type **B**	*Low-frequency BCG*. Natural frequency of the loaded BCG 1 to 2 Hz. Damping critical or more than critical.
Type **C**	*High-frequency BCG*. Natural frequency high with respect to the highest frequencies of interest. Damping critical or weaker.

The classifications also described the main design tradeoffs. Low-frequency designs (A & B) required fine control of the subject's respiration; otherwise it would mask the BCG signal (e.g. Gordon and Henderson beds). However with controlled respiration, these low-frequency beds would have higher displacements which are easier to amplify. Conversely, high-frequency designs (C) had minimal respiratory interferences so normal breathing could be permitted. But the drawbacks of high-frequency designs included smaller bed displacements which required higher amplification. In addition, the body-to-bed coupling weakens with higher excitation frequencies, such that the moving tissue layer in-between could become a noise artifact in the BCG.

With all these design considerations, Noordergraaf became particularly interested in the ultra-low frequency measurement because the bed swung freely; the body was rigidly coupled, which led to the purest form of the BCG signal. However, to confirm this hypothesis, he needed a "perfect" BCG signal to compare against. This perfect signal was mathematically derived and matched well to his empirical measurements.

2.5.1.4 Physical Models of the Ballistocardiogram

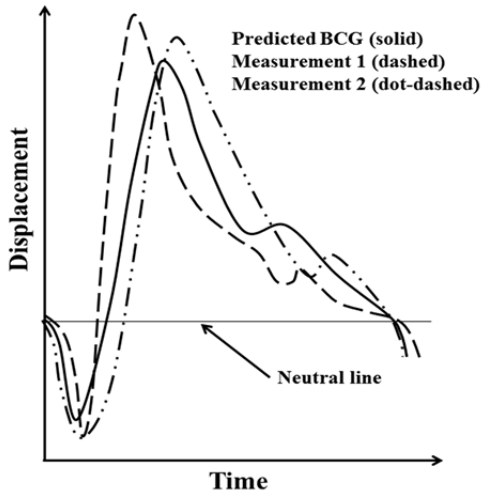

Figure 2.6: Noordergraaf's predicted displacement BCG (solid line) and two ultra low-frequency BCG measurements (broken lines), redrawn after [2].

Theoretical simulations of the BCG's movements are rare. 60 years of clinical BCG research elapsed before the first publication on physical models. Abraham Noordergraaf derived the ultra-low frequency BCG curve, treating the arterial tree as a network of elastic tubes where he mapped the changes in vessel caliber [26]. Using a hypothetical pressure pulse, he distended the arteries along the tree and calculated volumetric changes in vessel caliber to determine the blood's center-of-mass position relative to a neutral point.

The theoretical displacement BCG is very similar to the measurements with the ultra-low frequency bed. Noordergraaf did not label the peaks and valleys for the displacement curve with H, I, J, K, etcetera—since the Starr BCG was a force. The displacement curve would have to be differentiated twice into force before labels could be applied.

Later, in 1956, the American Heart Association (AHA) formed a committee to recommend BCG terminology due to all the various designs [33]. As shown on the right-side panel, the high-frequency force BCG (I) and ultra-low frequency displacement BCG (IV) look quite different. Relative to the carotid pulse start, the I-waves are coincident in time for displacement and force BCGs, but not with the Dock direct-body (II) and low frequency designs (III), where the I-waves occur later relative to the carotid pulse. The J-waves occur at similar times for displacement and force BCGs; however, the BCGs are no longer comparable between J-M. The AHA guidelines also described the later waves (L, M, N) as diastolic filling, however, this thesis will not consider these waves in the analysis since one modern view is that they are systolic resonances.

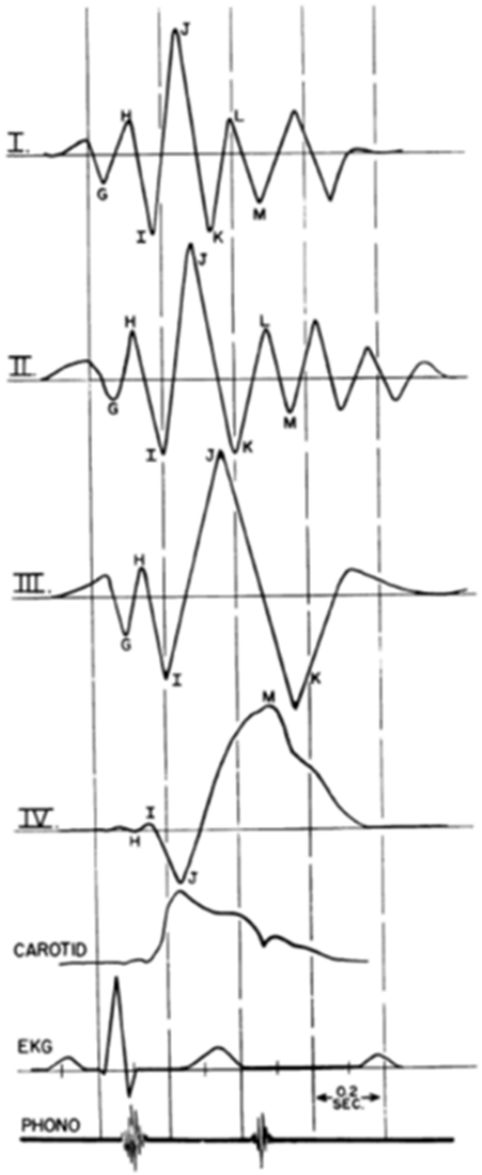

Figure 2.7: Official Displacement BCG Nomenclature recommended by the American Heart Association Committee on Ballistocardiographic Terminology. (I) High frequency BCG, (II) Direct body BCG, (III) Low frequency BCG, and (IV) Ultra-low frequency BCG. Used with permission, [14].

2.5.1.5 End of an Era

The BCG was investigated heavily from the 1930's to 1970's, and researchers sought to demonstrate its clinical utility as a noninvasive cardiac output measurement, and to diagnose several CVD pathologies—but the method was deemed unreliable for routine clinical use and was subsequently abandoned in favor of electrocardiography (ECG) and echocardiography. Cardiac output was more readily attainable with Doppler echo with basic knowledge of the aortic diameter; which was comparatively simpler (and more direct) to obtain than the mechanical tuning required for the BCG. However, as a diagnostic, BCG was more sensitive than ECG in detecting coronary artery disease (CAD), but less specific. In a retrospective analysis, Inan compiled results from several studies occurring between 1940-1960 for total of 1,019 patients with ages ranging 20-80 years; 618 with CAD and 401 healthy [30]. For simultaneous ECG and BCG measurements, sensitivities were 72.9% and 89%, respectively—specificities were 95.8% and 80.9%, respectively. Nevertheless, newer technologies were favored over BCG because they were more reliable and practical in clinical medicine.

2.6 Modern Ballistocardiography

BCG research almost vanished from the late 1980's and 1990's, but interest has recently been renewed, Figure 2.8. Its disappearance can be traced back to (1) a lack of standard measuring techniques, leading to different signals as discussed above; (2) a lack of understanding of the physiological origin of the signal; (3) focus on diagnostic performance in clinical cardiology which required high accuracy, calibration and reliability; and (4) disruptive technologies.

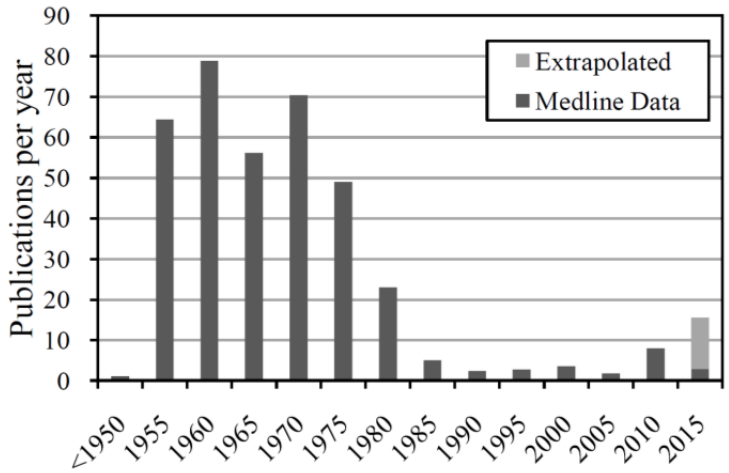

Figure 2.8: Publication rate of BCG-related research over the past 100 years (Source: Medline. Search keywords: ballistocardiogram and derivative, excluding specifically EEG, MRI, and fMRI papers). Used with permission [34].

Thirty years later however, advancements in sensing, signal processing, and computing power have become technology enablers to revitalize BCG research [34]. As a result, newer efforts have focused on improving the practicality and ease-of-use of BCG devices without a trained medical professional. The

most notable new devices have been (1) piezoelectric strain sensing (EMFi) in chairs and beds, (2) static-charge-sensitive-beds (SCSB), (3) wearable accelerometers, and, (4) modified commercial weighing scales. A thoughtful review for these technologies has been done by Inan in his thesis [30]. Here, updates are given for newer publications on these systems, to supplement the previous review.

2.6.1 Pulse Wave Velocity Using EMFi-Sensor-Based Chairs

Koivistoinen *et al*., developed a BCG chair using electromechanical film (EMFi) pressure sensors placed on the seat and backrest, in 2004. With this setup, the BCG was measured from the seat and sternal accelerations (also known as the seismocardiogram, SCG) were measured from the backrest sensor.

Between 2008 to 2011, Alametsa, from the same research group, performed a series of multi-sensor studies using EMFi sensors taped to the carotid, radial, and ankle arteries, while sitting on the chair BCG, where he characterized timings and signal amplitudes [35-38]. In one study, he characterized signals for one subject (41 year old, male) over a two-year duration who was taking statin medications (Simvastatin, 40 mg). He rationalized that the BCG should be useful to estimate pulse transit times (PTT). In doing so, he observed a pulse wave velocity ($PWV_{BCG\text{-}ankle}$) decrease from 4.35 m/s to 4.33 m/s and concluded that BCG was useful to determine PWV. In a retrospective analysis, we determined that PWV change was non-significant; there were no changes in PWV as claimed, Figure 2.9 [35]. Furthermore, Simvastatin has been shown to not affect PWV with long-term use in a larger clinical study. During a 12-month randomized study with 88 subjects, Ichihara showed a PWV decrease with Simvastatin at 3-months but it returned to basal PWV levels by 12-months (N = 22 subjects). However, Fluvastatin had an average PWV decrease of 1.5 m/s which was sustained after 12-months [39]. This long-term study may explain the non-result in Alametsa's study. In a more recent work, Alametsa characterized the repeatability of BCG-PWV measurements, comparing it to systolic and diastolic blood pressure changes in 48 males over a two-week time course. He correlated Week 0 PWV to Week 2 PWV finding a strong correlation ($r^2 = 0.759$), which he concluded that arterial stiffness repeatability was more

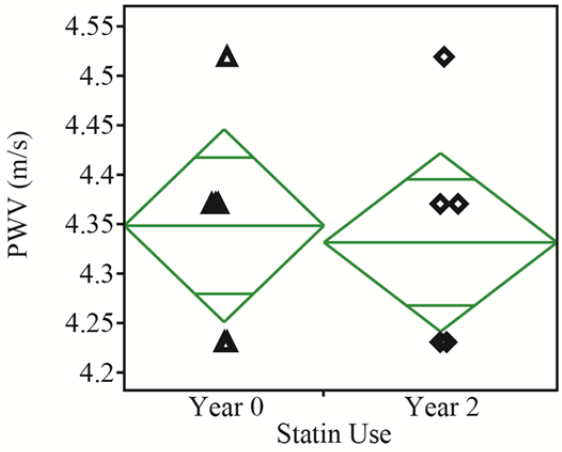

Figure 2.9: Re-analysis of BCG-Ankle Pulse wave velocity change for one subject taking statin medications (Simvastatin) over a two-year period. The diamonds represent the mean and 95% confidence intervals. When the two diamonds do not overlap, the two groups are significantly different.

consistent than blood pressure repeatability. Also, he found no correlation of PWV to blood pressure, but made observational conclusions that the healthy subjects in his pool appeared to have less variability than those with high blood pressure and known cardiovascular disease. Changes in PWV lacked a correlation back to a carotid reference timing, although it was measured during the study. Without a carotid reference, nor a measured decrease from the statin study, it is unclear whether the chair BCG was capable of measuring arterial stiffness.

2.6.2 Modified Commercial Weighing Scales

The first idea to use an electrical weighing scale to measure the BCG was disclosed in 1990 by Jim Williams of Linear Technology in an Application Note (AN-43) on bridge circuit design. Modern weighing scales are electronic, using strain gauges in a bridge arrangement—replacing mechanical spring scales. Williams was working on an ultra-precise scale to measure weight loss due to perspiration for a physiological monitoring project, accurate to 4.5 grams. While characterizing the scale he noticed a heart-induced oscillation and recognized it as the BCG. He published his analog circuit design and a photo of the BCG recording in the application note.

Inspired by his work, our lab pursued a similar BCG scale design. A scale platform would offer the benefits of practicality, which the BCG generally suffered from. Furthermore, if the signal could be obtained reliably simply by standing on the platform, the need for a trained operator would be removed. Omer Inan, et al., (Stanford University) modified the Williams circuit design and started work characterizing the signal quality; publishing an initial paper on the robustness when signal processing is utilized to increase the signal-to-noise ratio (SNR—with normal standards for BCG amplitude and timing, referenced to the electrocardiogram (ECG). The scale is classified as the high-frequency BCG that measures force, since the subject stands on a platform and the displacements are resisted by four spring-like strain gauges.

2.6.2.1 Cardiac Output Changes & Pacemaker Tuning Measured on a BCG Scale

Inan and Etemadi (Stanford University) then performed studies to investigate relative cardiac output (RCO) change, using echocardiography as a gold standard. A metric was developed to describe the BCG power (e.g. timing and amplitude) representing the contractility and stroke volume of the heart. During exercise recovery studies, the cardiac output change and BCG power change was highly correlated ($r^2 = 0.85$, $N = 10$, $p < 0.001$). This study demonstrated the potential impact in monitoring RCO for heart failure patients at home, since the BCG signal contains information about cardiac ejection. In another study, Inan characterized the BCG sensitivity for optimal tuning of biventricular pacemakers. Optimal atrio-ventricular and inter-ventricular timings will vary patient to patient. The IJ amplitude represents the maximum cardiac ejection force and for six subjects, statistical differences were observed between sub-optimal and optimal tunings.

2.6.2.2 Preejection Period Changes Measured on a BCG Scale

Etemadi conducted a study in healthy subjects to investigate the relationship between BCG timing and the preejection period (PEP) changes. This work was motivated by an initial study showing that the RJ timing of the BCG changes significantly during the Valsalva maneuver. Decreased contractile behavior is an important factor in many diseases such as heart failure and myocardial hypertrophy. Pursuant to this, PEP and RJ timings were measured in healthy volunteers during Valsalva maneuvers which were also highly correlated ($r^2 = 0.86$, 10 subjects). The regression slope was close to unity (1.05), which shows convincingly that the BCG tracks well to contraction changes.

2.7 Thesis Aims

Based on the BCG scale works, the BCG should be useful in PWV measurements despite the conflicting data reported using the chair-based EMFi sensing. The classic BCG description given by Starr and the AHA suggest that the I- and J-waves are related in time to the ventricular ejection of blood into the aorta arch and carotid artery (see Figure 2.7). These I- and J-waves are systolic timings by definition. Therefore, the early BCG timings should correlate to carotid pulse arrival time, since BCG timing changes are so closely linked to PEP timing changes as demonstrated by Etemadi. However, empirical correlations and intuition are not sufficient to establish fact. Two correlated factors merely have statistical agreement, or "scientific-truth." Physical theories are therefore necessary to support the claims. As a result, this thesis has the following aims to validate the use of BCG in pulse wave velocity measurements:

1. To develop a physical model to justify whether BCG forces are related to aortic arch pressures as first described by Isaac Starr.
2. To investigate clinically, the timing characteristics of the BCG related to the carotid artery.
3. To investigate clinically, the stability of a BCG-based PWV system, particularly in its anticipated intended use configuration.

BIBLIOGRAPHY

[1] A. V. Chobanian, G. L. Bakris, H. R. Black, W. C. Cushman, L. A. Green, J. L. Izzo, Jr., D. W. Jones, B. J. Materson, S. Oparil, J. T. Wright, Jr., and E. J. Roccella, "The seventh report of the joint national committee on prevention, detection, evaluation, and treatment of high blood pressure: The JNC 7 report," *JAMA: The Journal of the American Medical Association,* vol. 289, pp. 2560-72, 2003.

[2] T. G. Pickering, J. E. Hall, L. J. Appel, B. E. Falkner, J. Graves, M. N. Hill, D. W. Jones, T. Kurtz, S. G. Sheps, and E. J. Roccella, "Recommendations for blood pressure measurement in humans and experimental animals," *Hypertension,* vol. 45, pp. 142-161, 2004.

[3] P. Verdecchia and F. Angeli, "The seventh report of the joint national committee on the prevention, detection, evaluation and treatment of high blood pressure: The weapons are ready," *Revista Espanola de Cardiologia,* vol. 56, pp. 843-7, 2003.

[4] Y. L. Shevchenko and J. E. Tsitlik, "90th anniversary of the development by nikolai s. Korotkoff of the auscultatory method of measuring blood pressure," *Circulation,* vol. 94, pp. 116-118, 1996.

[5] M. R. Nelson, J. Stepanek, M. Cevette, M. Covalciuc, R. T. Hurst, and A. J. Tajik, "Noninvasive measurement of central vascular pressures with arterial tonometry: Clinical revival of the pulse pressure waveform?," *Mayo Clinic Proceedings,* vol. 85, pp. 460-472, 2010.

[6] E. Balestrieri and S. Rapuano, "Calibration of automated non invasive blood pressure measurement devices," in *Advances in biomedical sensing, measurements, instrumentation and systems*. vol. 55, S. C. Mukhopadhyay and A. Lay-Ekuakille, Eds., ed: Springer Berlin Heidelberg, 2010, pp. 281-304.

[7] R. G. Sinclair, "High blood pressure--ancient, modern and natural," *Journal of the Royal College of General Practitioners,* vol. 18, pp. 207-13 contd, 1969.

[8] M. O'Rourke, "Frederick akbar mahomed," *Hypertension,* vol. 19, pp. 212-217, 1992.

[9] B. Symonds, "The blood pressire of healthy men and women," *Journal of the American Medical Association,* vol. 80, pp. 232-236, 1923.

[10] E. A. Lew, "High blood pressure, other risk factors and longevity: The insurance viewpoint," *The American journal of medicine,* vol. 55, pp. 281-94, 1973.

[11] J. Murgo, N. Westerhof, J. Giolma, and S. Altobelli, "Aortic input impedance in normal man: Relationship to pressure wave forms," *Circulation,* vol. 62, pp. 105-116, 1980.

[12] T. G. Pickering, G. D. James, C. Boddie, G. A. Harshfield, S. Blank, and J. H. Laragh, "How common is white coat hypertension?," *JAMA: The Journal of the American Medical Association,* vol. 259, pp. 225-228, 1988.

[13] H. Celis, E. D. Hond, and J. A. Staessen, "Self-measurement of blood pressure at home in the management of hypertension," *Clinical Medicine & Research,* vol. 3, pp. 19-26, 2005.

[14] T. Pickering, W. Gerin, J. Schwartz, T. Spruill, and K. Davidson, "Franz volhard lecture: Should doctors still measure blood pressure? The missing patients with masked hypertension," *Journal of hypertension,* vol. 26, pp. 2259-2267, 2008.

[15] T. G. Pickering, N. H. Miller, G. Ogedegbe, L. R. Krakoff, N. T. Artinian, and D. Goff, "Call to action on use and reimbursement for home blood pressure monitoring: Executive summary: A joint scientific statement from the american heart association, american society of hypertension, and preventive cardiovascular nurses association," *Hypertension,* vol. 52, pp. 1-9, 2008.

[16] W. W. Nichols, M. F. O'Rourke, and D. A. McDonald, *Mcdonald's blood flow in arteries: Theoretic, experimental, and clinical principles*, 6th ed. London: Hodder Arnold, 2011.

[17] N. Kaplan and R. Victor, *Kaplan's clinical hypertension*, Tenth ed. Philadelphia: Lippincott Williams & Wilkins, 2010.

[18] S. Mann, M. W. Millar Craig, and E. B. Raftery, "Superiority of 24-hour measurement of blood pressure over clinic values in determining prognosis in hypertension," *Clinical and experimental hypertension. Part A, Theory and practice,* vol. 7, pp. 279-281, 1985.

[19] *Hypertension. Clinical management of primary hypertension in adults. This guideline partially updates and replaces NICE clinical guideline 34,* CG127, 2011.

[20] K. Lovibond, S. Jowett, P. Barton, M. Caulfield, C. Heneghan, F. D. R. Hobbs, J. Hodgkinson, J. Mant, U. Martin, B. Williams, D. Wonderling, and R. J. McManus, "Cost-effectiveness of options

for the diagnosis of high blood pressure in primary care: A modelling study," *The Lancet,* vol. 378, pp. 1219-1230, 2011.

[21] The CAFE Investigators, for the Anglo-Scandinavian Cardiac Outcomes Trial Investigators, C. S. Committee, Writing Committee, B. Williams, P. S. Lacy, S. M. Thom, K. Cruickshank, A. Stanton, D. Collier, A. D. Hughes, H. Thurston, and M. O'Rourke, "Differential impact of blood pressure-lowering drugs on central aortic pressure and clinical outcomes: Principal results of the conduit artery function evaluation (CAFE) study," *Circulation,* vol. 113, pp. 1213-1225, 2006.

[22] M. O'Rourke, "Time domain analysis of the arterial pulse in clinical medicine," *Medical and Biological Engineering and Computing,* vol. 47, pp. 119-129, 2009.

[23] M. Karamanoglu, M. F. O'Rourke, A. P. Avolio, and R. P. Kelly, "An analysis of the relationship between central aortic and peripheral upper limb pressure waves in man," *European Heart Journal,* vol. 14, pp. 160-167, 1993.

[24] J. C. Bramwell and A. V. Hill, "The velocity of the pulse wave in man," in *Proceedings of the Royal Society of London. Series B, Containing Papers of a Biological Character*, 1922, pp. 298-306.

[25] J. W. Gordon, "Certain molar movements of the human body produced by the circulation of the blood," *Journal of Anatomy and Physiology,* vol. 11, pp. 533-6, 1877.

[26] A. Noordergraaf, "Physical basis of ballistocardiography," Doctoral Dissertation, Utrecht University, s'Gravenhage, Netherlands, 1956.

[27] Y. Henderson, "The mass-movements of the circulation as shown by a recoil curve," *American Journal of Physiology,* 1905.

[28] I. Starr, A. J. Rawson, H. A. Schroeder, and N. R. Joseph, "Studies on the estimation of cardiac output in man, and of abnormalities in cardiac function, from the heart's recoil and the blood's impacts; the ballistocardiogram," *The American Journal of Physiology,* vol. 127, pp. 1-28, 1939.

[29] I. Starr and H. A. Schroeder, "Ballistocardiogram. II. Normal standards, abnormalities commonly found in diseases of the heart and circulation, and their significance," *Journal of Clinical Investigation,* vol. 19(3), pp. 437–450, 1940.

[30] O. T. Inan, "Novel technologies for cardiovascular monitoring using ballistocardiography and electrocardiography," Ph.D Dissertation, Electrical Engineering, Stanford University, 2009.

[31] H. C. Burger and A. Noordergraaf, "Physical basis of ballistocardiography. II : The quantities that can be measured with different types of ballistocardiographs and their mutual relations," *American heart journal,* vol. 51, pp. 127-139, 1956.

[32] J. R. Braunstein, "A proposed nomenclature and convention for recording the ballistocardiogram," *Circulation,* vol. 7, pp. 927-928, 1953.

[33] W. R. Scarborough, S. A. Talbot, J. R. Braunstein, M. B. Rappaport, W. Dock, W. F. Hamilton, J. E. Smith, J. L. Nickerson, and I. Starr, "Proposals for ballistocardiographic nomenclature and conventions: Revised and extended: Report of committee on ballistocardiographic terminology," *Circulation,* vol. 14, pp. 435-450, 1956.

[34] L. Giovangrandi, O. T. Inan, R. M. Wiard, M. Etemadi, and G. T. A. Kovacs, "Ballistocardiography -- a method worth revisiting," *Proceedings of the IEEE Engineering in Medicine and Biology Society (EMBC), Boston,* pp. 4279-82, 2011.

[35] J. Alametsä, J. Viik, and A. Palomäki, "Arterial elasticity measurements with ankle pulse width velocity and ballistocardiography," presented at the 4th European Conference of the International Federation for Medical and Biological Engineering, 2009.

[36] J. Alametsa and et al., "Ballistocardiography in sitting and horizontal positions," *Physiological Measurement,* vol. 29, p. 1071, 2008.

[37] J. Alametsä, A. Palomäki, and J. Viik, "Short and longer term repeatability of ballistocardiography in a sitting position with emfi sensor," *Medical and Biological Engineering and Computing,* vol. 49, pp. 881-889, 2011.

[38] J. Alametsa, A. Varri, J. Viik, J. Hyttinen, and A. Palomaki, "Ballistocardiogaphic studies with acceleration and electromechanical film sensors," *Medical Engineering & Physics,* vol. 31, pp. 1154-65, 2009.

[39] A. Ichihara, M. Hayashi, Y. Koura, Y. Tada, Y. Kaneshiro, and T. Saruta, "Long-term effects of statins on arterial pressure and stiffness of hypertensives," *J Hum Hypertens,* vol. 19, pp. 103-109, 2004.

3 Modern Theory of Ballistocardiography

3.1 Introduction

Physical models describing the timings and amplitudes of the BCG waveforms have rarely been attempted. Investigating the behavior of the BCG clinically in large populations is simpler than solving second-order partial differential equations that describe blood flow in arteries—usually under restrictive assumptions permitting solutions to be found. Because of this, very limited viewpoints have been presented as to what causes the BCG. Therefore, the classical viewpoints remain the current accepted view.

In the past decade, computational toolsets have been developed to accurately model pressures, flows, and vessel deformations of the systemic circulation. These simulation techniques are now commonly used in research for stent design, and virtual surgical planning to remove stenoses, or to assess potential bypasses or endographts. These hemodynamic simulation tools had not yet been used to model the BCG. The research described in this chapter covers the initial development of a modern theory, to model BCG-like forces using finite element method (FEM) approaches.

3.2 Background and Theory

3.2.1 Physical Modeling of the Ballistocardiogram

And mentioned in the previous chapter, the discovery of the BCG signal was attributed to Gordon in 1877 [1], but seminal studies launching the BCG field did not occur until 1939, when Starr published BCG cardiac output studies using spring-mass dampened beds [2, 3]. Unfortunately, two decades of clinical BCG research elapsed before formal investigations of its physical understandings commenced. Physical models were pursued in the late 1950's to address concerns with measurement system reliability, since the BCG field was lacking in standardization of hardware designs [4].

Most notably, Noordergraaf and Burger developed physical models to understand mechanical transfer functions for various ballistocardiographs [5-12], where a hardware classification system later emerged to describe BCG signals based on the type of device used (e.g. the ultra-low, low, and high frequency BCG) [4]. With their models, they concluded that left ventricular ejection patterns and arterial distensibility had clear relationship to predicted center-of-mass changes [13, 14]. Noordergraaf's model was retrospectively examined during this thesis with the aim of explaining how pulse wave velocity (PWV) was related to BCG forces. PWV was included in his model as an input, but only to explain when an

arterial segment would distend and what the subsequent blood volume change was. The model was not constructed in a manner to quantify three-dimensional forces; rather it was a one-dimensional displacement model. Therefore, no information could be readily determined to directly relate PWV to forces. Understanding this BCG force transduction process is therefore necessary to reveal potential clinical utility, which is the primary goal set forth in this thesis. The key realization here is that FEM hemodynamic simulation toolsets should be suitable to model BCG-like forces by analyzing the interface surface between the fluid and solid. The force interactions between the fluid and solid are referred to as the *traction*.

A novel theory for the BCG signal genesis is presented in this chapter, called Central Aortic Force (CAF). A key feature of this method is the ability to directly relate *traction* and *pulse pressure propagation*—which uncovers whether whole-body BCG measurements are appropriate for localized arterial stiffness measurements.

This chapter begins with an overview of modern FEM approaches used to solve hemodynamic problems. This FEM background was then expanded to explain a novel theory on how to model forces to investigate BCG signal genesis. The multi-domain approaches used required high computational effort, but yielded informative three-dimensional (3D) results that cannot be attained by hand calculation. Meta-analysis was then performed between simulations and clinical results in literature (to address statistical power) to quantify effect size observed for BCG timings and amplitude. Finally, the mathematical and physical theories governing these simulation results were distilled into a practical theory, which can be taught in a straightforward manner to the clinical community.

3.2.2 Physical Explanations of the Ballistocardiogram

"The mutual forces of action and reaction between two bodies are equal, opposite and collinear." Newton's Third Law of Motion was used to describe the BCG in the seminal works on physical models, but the resulting interpretations were dependent upon the free-body diagram chosen to depict these force interactions. For example, Noordergraaf's center-of-mass (COM) model was conceived as a displacement model by mapping the changing blood distribution during the cardiac cycle [5]. This model consisted of a segmented arterial tree, where the volumetric changes of each segment were used to trace the COM change as displacement over time (Figure 3.1). The second derivative of the COM displacement was the acceleration (and force) used to predict the BCG waveform.

BCG free-body diagrams may be constructed in other ways—the exact construct used is a matter of semantics based on the desired interpretation. For example, to make a physiological case relating the BCG to arterial stiffness, cardiovascular forces could be analyzed in relation to the vessel wall (e.g. a surface analysis) instead of the changing blood volume based upon Bramwell and Hill's description of the velocity of the pulse wave in man:

"…the pulse wave must be considered as travelling, like a ripple on moving water, relatively to the fluid in which it occurs. The arterial wall merely exerts an elastic constraint upon the surface of the fluid, and in the simplified theory of the transmission of the wave…the inertia of the wall, and the tissues outside it, exert no influence on the velocity of the wave."

This description considers blood as incompressible, with an elastic wall constraining the fluid. Pulsatile cardiac ejection creates a step response at the input, propagating a shock wave along the wall. The velocity of this forward travelling wave is proportional to the stiffness and dimensions of the vessel wall using the original Moens-Korteweg pulse wave velocity (PWV) equation

$$PWV = \sqrt{\frac{Eh}{2\rho R}} \qquad \text{(Moens-Korteweg)} \qquad (3.1)$$

where E is the elastic modulus, h the vessel wall thickness, ρ the blood density, and R the vessel radius [15]. Alternatively, PWV may be expressed with the Bramwell and Hill form by using a series of substitutions to express the velocity in terms of the pressure-volume characteristics of the vessel

$$PWV = \sqrt{\frac{dP \cdot V}{\rho \cdot dV}} \qquad \text{(Bramwell-Hill)} \qquad (3.2)$$

where dP is the changing pressure, and dV the changing vessel volume [16].

These PWV expressions highlight an interesting discussion point about physical derivations, namely, that their clinical usefulness is starkly different. The Bramwell-Hill equation is used more often clinically, since pressure catheters and medical imaging directly measure the changing pressure and vessel diameter—which are easily performed in live subjects. Conversely, the elastic modulus is the slope measured in a tensile test (post-mortem?) for the Moens-Korteweg case, and vessel wall thickness is more difficult to measure than vessel diameter.

Likewise, differing physical models of the BCG can introduce nuances in their clinical interpretations. The BCG is a force, and there are multiple approaches to model cardiovascular (CV) forces emanating from the body. For example, the COM approach shows that the change in volume (dV) leads to a changing distributed mass, thus a change in center-of mass displacement—with the second derivative of displacement describing the cardiovascular force (Figure 3.1, left). Alternatively, CV forces can be modeled as surface phenomena at the vessel wall due to pressure and shear stresses caused by blood flow (Figure 3.1, right).

Molar CV forces have been investigated extensively using volumetric models, however, no works have attempted to model BCG forces based on surface interactions. Theoretically, either modeling

approach used should yield similar forces; however, subsequent interpretations regarding the origins of forces may vary since the analysis domains (volume vs. surface) are different.

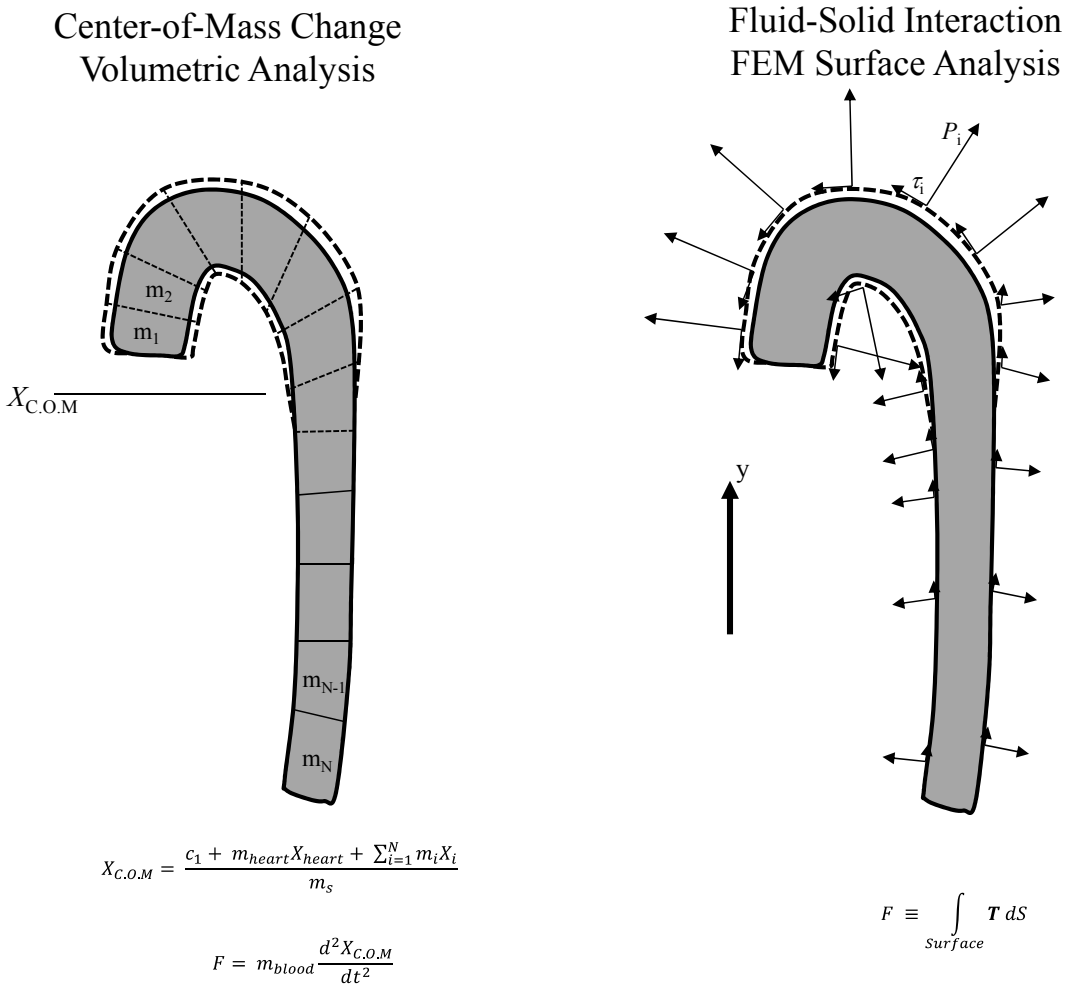

$$X_{C.O.M} = \frac{c_1 + m_{heart}X_{heart} + \sum_{i=1}^{N} m_i X_i}{m_s}$$

$$F = m_{blood}\frac{d^2 X_{C.O.M}}{dt^2}$$

$$F \equiv \int_{Surface} \boldsymbol{T}\, dS$$

Figure 3.1: Two approaches used to develop BCG physical models. Center of Mass (C.O.M) volumetric changes of blood (left, Noordergraaf and Burger), and surface-derived forces due to pressure and shear stress (right, this work).

3.2.2.1 Generation of Surface Forces on the Vessel Wall

A surface free-body diagram can be constructed to examine cardiovascular forces acting at the vessel wall boundary, where blood flow imparts the action force and reaction forces are imparted by the elastic vessel wall (Figure 3.2). For example, the infinitesimal surface area dS on the vessel wall is perpendicular to the normal surface vector **n** and the force pairs interacting here are defined as the traction **T** (a tensor), where the fluid traction $\vec{t}^{f}$ is equal to the solid traction $\vec{t}^{s}$. In the fluid domain, a pressure gradient $dP=P_{out}-P_{in}$ induces blood flow with velocity profile v(r). At dS, there are in-plane forces due to shear stress (τ) in the opposing direction to blood flow and perpendicular forces due to pressure *P*(z).

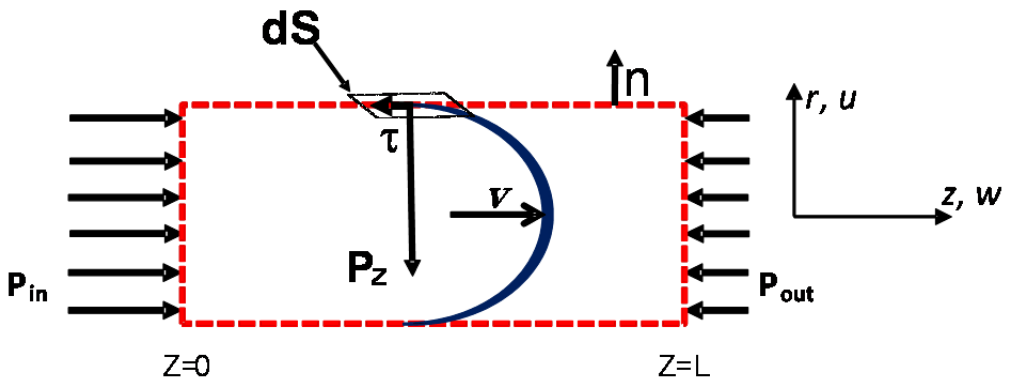

Figure 3.2: Free body diagram of an artery with blood flow. The vessel wall is where action-reaction forces can be studied at the fluid-solid interface.

The action force or *fluidic traction* $\vec{t}^{\,f}$ is thus

$$\vec{t}^{\,f} = [-p\mathbf{I} + \boldsymbol{\tau}]\vec{n} \tag{3.3}$$

where (*P*) is the pressure scalar multiplied by the identity tensor **I**, and summed with the shear tensor and this quantity is then projected onto ***n*** to become a vector perpendicular to **dS**. The expression may be simplified further, for a Newtonian fluid as

$$\vec{t}^{\,f} = [-p\mathbf{I} + 2\mu\mathbf{D}]\vec{n} \tag{3.4}$$

where **D** is the rate of deformation tensor and is related to the gradient of the velocity field **v**.

$$\mathbf{D} = sym(\nabla\vec{v}) = \tfrac{1}{2}(\nabla\vec{v} + (\nabla\vec{v})^T \tag{3.5}$$

and the gradient in cylindrical coordinates is

$$\nabla \equiv \hat{r}\frac{\partial}{\partial r} + \hat{\theta}\frac{1}{r}\frac{\partial}{\partial\theta} + \hat{z}\frac{\partial}{\partial z} \tag{3.6}$$

then, after some algebra, the fluid traction for steady flow in a rigid tube simplifies to

$$\vec{t}^{\,f} = \begin{bmatrix} -p(z) & 0 & \frac{dp}{dz}\frac{r}{z} \\ 0 & -p(z) & 0 \\ \frac{dp}{dz}\frac{r}{z} & 0 & -p(z) \end{bmatrix} \cdot \vec{n} \tag{3.7}$$

The traction midway along the vessel (e.g. z = L/2) is

$$\vec{t}^{f}(R,0,\ 0.5L) = \begin{bmatrix} -\frac{(P_0+P_L)}{2} & 0 & \frac{dp}{dz}\frac{R}{2} \\ 0 & -\frac{(P_0+P_L)}{2} & 0 \\ \frac{dp}{dz}\frac{R}{2} & 0 & -\frac{(P_0+P_L)}{2} \end{bmatrix} \begin{bmatrix} 1 \\ 0 \\ 0 \end{bmatrix} = \begin{bmatrix} -\frac{(P_0+P_L)}{2} \\ 0 \\ \frac{dp}{dz}\frac{R}{2} \end{bmatrix} \tag{3.8}$$

The preceding solution depicts an example of tensor relationships applied to fluid-solid interaction problems. Scalar, vector, and matrices easily add together when tensors are used. However, this particular steady-flow solution is incomplete for a BCG model, lacking two important properties enabling the pulse wave transmission. First, a pulsatile solution of the Navier-Stokes equation is necessary to represent the cardiac cycle. Secondly, the vessel wall cannot be rigid; otherwise the pulse wave speed would be infinite, so a deformable-wall pulsatile relationship is required to study obtain appropriate values for pressure and velocity profile for the constitutive relationship in Equation 3.3.

3.2.2.2 Pulsatile Flow in a Rigid Tube

The Womersley solution for unsteady, unidirectional flow in a vessel can be described mathematically if the $v_r = v_\theta = 0$ and $v_z = v_z(r,t)$ when using cylindrical coordinates (Figure 3.3). The pulsatile pressure gradient may be expressed using known periodic functions of the form F=f(t+T) to represent the cardiac cycle. This permits the use of Fourier series to obtain the unsteady velocity profile as a function of time, where the convergence of the solution depends upon the sums of modes to obtain a general solution. The time-varying periodic pressure with amplitude *A* using complex notation is

$$\frac{\partial P}{\partial z} = Ae^{i\omega t} \tag{3.9}$$

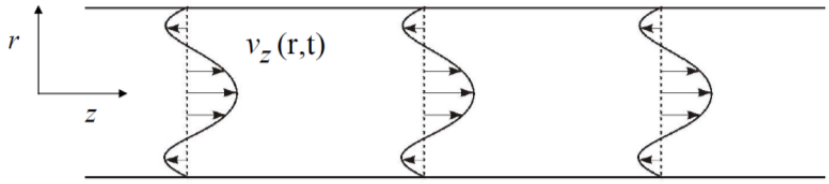

Figure 3.3: Depiction of the velocity profile vz when subjected to a periodic pressure gradient, along a rigid cylindrical tube.

Let $w = v_z$ and thus, the Navier-Stokes relationship in the axial direction becomes

$$\frac{\partial^2 w}{\partial r^2} + \frac{1}{r}\frac{\partial w}{\partial r} - \frac{1}{\nu}\frac{\partial w}{\partial t} = -\frac{A}{\mu}e^{i\omega t} \tag{3.10}$$

and is a partial differential equation in space and time, with viscosity μ. A separable solution may be found using the substitution

$$w = ue^{i\omega t} \tag{3.11}$$

which cancels the $e^{i\omega t}$ terms to become

$$\frac{\partial^2 u}{\partial r^2} + \frac{1}{r}\frac{\partial u}{\partial r} - \frac{i\omega}{\nu}u = -\frac{A}{\mu} \tag{3.12}$$

Equation 3.12 is the Bessel form of the equation with known solutions. Thus, the solution for axial velocity becomes

$$u = \frac{A}{i\omega\rho}\left\{1 - \frac{J_0[r\sqrt{(\omega/\nu)}i^{3/2}]}{J_0[R\sqrt{(\omega/\nu)}i^{3/2}]}\right\} \tag{3.13}$$

where $J_0(xi^{3/2})$ is a Bessel function of the first kind of order zero. Bessel functions are also known as cylinder functions, as they are the solutions found to Laplace's equation in cylindrical coordinates, which is the geometry of interest in Womersley flow. Applying the substitution, the velocity *w* then becomes

$$w = \frac{AR^2}{i\mu\alpha^2}\left[1 - \frac{J_0(\alpha y i^{3/2})}{J_0(\alpha i^{3/2})}\right] e^{i\omega t} \tag{3.14}$$

where y = r/R and

$$\alpha = R\sqrt{\frac{\omega}{\nu}} \tag{3.15}$$

α is the Womersley number, a non-dimensional parameter analogous to the Reynolds number, describing the relative behavior between the transient inertia and viscous forces. The Womersley number in a human is ~22 in the proximal aorta and ~4 in the femoral artery, so the velocity profile is plug-like and flattened-parabolic, respectively [15].

The velocity profile can be obtained at any point along the vessel axis when a periodic pressure gradient is specified. The cardiac pressure pulse is generally periodic (e.g. a constant heart rate may be assumed) but is not a pure sinusoid, so the pressure gradient must be approximated as sums of modes using Fourier analysis. Euler's formula may be used to decompose the harmonics of the systolic and diastolic phase

$$e^{-i\omega t} = \cos\omega t + i\sin\omega t \tag{3.16}$$

The pressure gradient is written as the function

$$-\frac{\partial p}{\partial z} = \sum_{n=0}^{N} A_n e^{in\omega t} \tag{3.17}$$

One mode can be considered

$$-\frac{\partial p}{\partial z} = Ae^{i\omega t} \tag{3.18}$$

And recalling that the solution obtained in Equation 3.14 for the axial velocity is separable of the form

$$v_z(r,t) = w(r)e^{i\omega t} \tag{3.19}$$

a general solution can then be obtained using superposition. Once a solution is obtained for v_z, the flow rate Q and wall shear stress τ_w can be calculated

$$Q(t) = 2\pi \int_0^R v_z(r,t) r dr \tag{3.20}$$

$$\tau_w(t) = \mu \left.\frac{\partial v_z}{\partial r}\right|_{r=R} \tag{3.21}$$

The preceding derivation illustrated how to obtain solutions for pulsatile flow by assuming periodic functions. This solution can then be applied to the constitutive relationship in Equation 3.3 to obtain traction but, this solution is limited to rigid wall cases.

3.2.2.3 Pulsatile Flow in an Elastic Tube

Womersley also derived solutions to pulsatile flow in elastic tubes, which is necessary to observe pulse wave transmission. Storage of blood in the artery delays flow downstream and the pulse wave speed (PWV) depends on the material properties of the artery. Wave phenomena cannot be modeled without a radial solution to blood flow. Wall deformation occurs when $v_r \neq 0$ and therefore, the radial velocity of the fluid at the boundary is equal to the velocity of the distending wall when the continuum is extended to the solid domain. In this section, the key properties of elastic flow are described, to establish the characteristics of flow that are related to the traction.

Letting $u=v_r$ and $w=v_z$, the Navier Stokes equations for radial and axial flow in a deformable cylinder are

$$\frac{\partial u}{\partial t} + \left(u\frac{\partial u}{\partial r} + w\frac{\partial u}{\partial z}\right) = -\frac{1}{\rho}\frac{\partial p}{\partial r} + \nu\left[\frac{\partial^2 u}{\partial r^2} + \frac{1}{r}\frac{\partial u}{\partial r} - \frac{u}{r^2} + \frac{\partial^2 u}{\partial z^2}\right] \text{ (radial direction)} \tag{3.22}$$

$$\frac{\partial w}{\partial t} + \left(u\frac{\partial w}{\partial r} + w\frac{\partial w}{\partial z}\right) = -\frac{1}{\rho}\frac{\partial p}{\partial z} + \nu\left[\frac{\partial^2 w}{\partial r^2} + \frac{1}{r}\frac{\partial w}{\partial r} + \frac{\partial^2 w}{\partial z^2}\right] \text{ (axial direction)} \tag{3.23}$$

and rotational flow (swirling) can be neglected ($v_\theta=0$). The continuity equation is thus

$$\frac{\partial u}{\partial r} + \frac{u}{r} + \frac{\partial w}{\partial z} = 0 \quad \text{(conservation of mass)} \tag{3.24}$$

The differential equations again are in both space and time. Assuming a periodic pressure as before, and applying linear assumptions for separation of variables, and long-wave assumptions[1]

$$\frac{R}{L},\ \frac{\bar{w}}{c} \ll 1 \tag{3.25}$$

the radial and axial velocities can be solved using Bessel functions similar to the previous section. The general solutions are thus

$$p(r,z,t) = p_0 + k_s(z - z_0) + He^{i\omega\left(t-\frac{z}{c}\right)} \tag{3.26}$$

$$u(r,z,t) = \frac{Hi\omega R}{2\rho c^2}\left[\frac{r}{R} - M\frac{2J_1\left(\frac{\Lambda r}{R}\right)}{\Lambda J_0(\Lambda)}\right]e^{i\omega\left(t-\frac{z}{c}\right)} \tag{3.27}$$

$$w(r,z,t) = \frac{k_s}{4\mu}(r^2 - R^2) + \frac{H}{\rho c}\left[1 - M\frac{J_0\left(\frac{\Lambda r}{R}\right)}{J_0(\Lambda)}\right]e^{i\omega\left(t-\frac{z}{c}\right)} \tag{3.28}$$

$$\Lambda = i^{\frac{3}{2}}\alpha \tag{3.29}$$

where H and M are integration constants and are determined when the fluid and wall velocities are matched as a compatibility condition. The axial velocity w has a steady and oscillatory term, where the steady term is given by Poiseulle's solution with constant pressure gradient k_s, and the radial velocity is purely oscillatory. Axial flow will continue after the oscillatory contribution becomes zero, which is similar to aortic flow in diastole.

Womersley's elastic theory was invoked for the simulations in this thesis. Rigid wall simulations are simpler to solve numerically, but are deemed unsuitable for the BCG theory developed. Rigid wall simulations result in infinite pulse wave velocities—therefore, the effect of wave reflections cannot be investigated.

3.2.2.4 Elastodynamic Reaction Forces of the Solid Domain

Solutions to Womersley elastic tube flow result in a non-zero fluid velocity at the vessel wall and the conventional non-slip assumption is no longer valid—therefore, momentum transfer will occur between

[1] The length of the propagating wave (L) is much longer than the vessel radius R, and the wave speed c is much higher than the average longitudinal velocity w within the tube.

the fluid and solid resulting in deformation. This momentum transfer must be balanced against the material response of the vessel wall—the *solid* traction therefore must be equal to the *fluidic* traction, acting in the opposite sense (action-reaction principle).

$$\vec{t}^{solid} = \vec{t}^{fluid} \tag{3.30}$$

and the kinematic condition must also be invoked (continuity of velocities):

$$\vec{v}^{solid} = \vec{v}^{fluid} \tag{3.31}$$

The vessel thus deforms based on the material response specified. Large arteries exhibit viscoelastic behavior across large deformations, but under small deformations can be treated as linear elastic—which is less computationally intensive to solve, still permitting wave propagation. Cauchy's equation of motion for linear elasticity of a thin-walled tube of thickness *h* is

$$\rho^s \frac{\partial^2 \vec{u}}{\partial x^2} = \vec{B}_0 + \nabla \cdot \mathbf{T} \tag{3.32}$$

where **u** is the displacement vector (not to be confused with *u* in the fluid equations) for the radial and longitudinal directions. **T** is the Cauchy stress tensor and the divergence of this stress tensor describes the material deformation response of the solid. B_0 is the per unit volume body force associated with the pressure and shear forces exerted by the fluid. The radial and longitudinal body forces are

$$B_r = \frac{p}{h} \tag{3.33}$$

$$B_z = -\frac{\tau}{h} = -\frac{\rho\nu}{h}\left(\frac{\partial u}{\partial z} + \frac{\partial w}{\partial r}\right)\Big|_{r=R} \tag{3.34}$$

Cauchy's equation of motion couples the fluid via the body force, traction, and velocity conditions to produce a Fluid-Solid Interaction (FSI) response. An in-depth derivation of the fluid and solid coupling can be found in [17, 18] for the interested reader.

3.2.3 Finite Element Methods to Simulate Cardiovascular Forces

The preceding section described the physical mechanisms and assumptions used to model cardiovascular pressures and shear stresses, but solutions are incomplete without an algorithm to numerically solve the FSI problem. The Multidomain Hemodynamic method was utilized in this dissertation to simulate cardiovascular forces [19]. This Finite Element Method (FEM) approach simulates realistic pressures and flows in deformable artery meshes, constructed from medical imaging obtained from patients. An overview of the Multidomain Method is presented here and the limitations of these simulations are pointed out with respect to understanding theoretical BCG-like forces.

3.2.3.1 Overview of the Multidomain Method for FSI Problems

The Multidomain Method for cardiovascular biomechanics is a hybrid simulation approach using both a FEM mesh of human vessels and lumped parameter boundary conditions (BC) to simulate downstream flow impedances (Figure 3.4). The BC can then be adjusted, thus allowing the FEM mesh to simulate different flows and deformations. Wall motion is solved for in the Multidomain Method to understand wave propagation, contrasting the original volumetric analysis developed by Noordergraaf and Burger, where the PWV was prescribed to obtain the solution [5] .

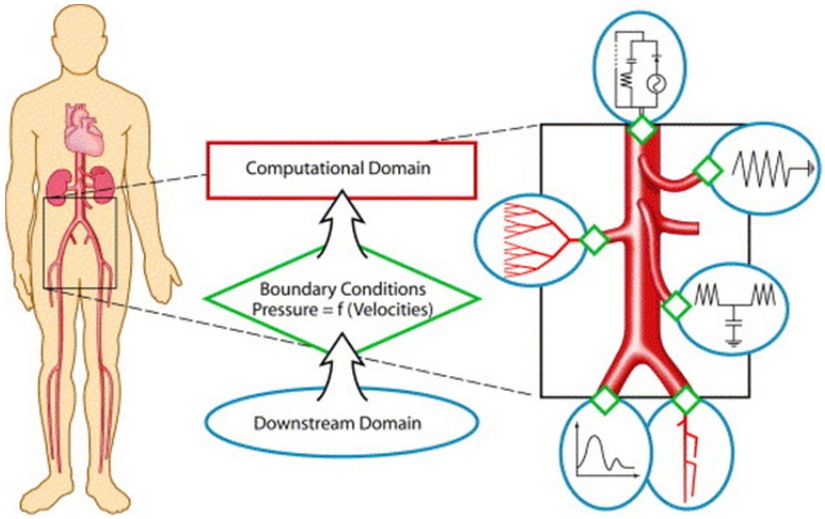

Figure 3.4: Diagram of the Multidomain Method after [20]. Finite Element simulations of blood flow are performed using arterial geometry derived from medical imaging. Lumped parameter boundary conditions are specified at the inlet and outlets to define impedances resulting in realistic pressures and flow distributions. Used with permission [19].

3.2.3.2 Fluid-Solid Interaction Algorithm

The open-source SimVascular software was developed at Stanford University to solve 3D hemodynamic problems [21]. The FSI algorithm is iterative, see Figure 3.5, solving for deformable flow equations to obtain wall traction, and then updating the vessel geometry based on the elastodynamics response.

First, an inlet condition is prescribed for the pressure pulse. At the start of flow, a shape function for the velocity profile is enforced (e.g., parabolic or plug flow) at the inlet to stabilize the solution. Newer methods utilize time-varying elastance functions to mimic the response of the heart [22]. Pressure and velocity are solved in the fluid domain and then resulting wall traction is computed. The fluid and solid domains are coupled together with a compatibility conditions described earlier using the Coupled Momentum Method for Fluid-Solid Interactions (CMM-FSI) algorithm [17, 18]. The vessel wall geometry then updates based on the traction to complete the time step. The algorithm repeats until the cardiac cycle is completed. The outlet faces on the arterial models have boundary conditions (BCs) enforced to represent the impedance of the smaller branching arteries, arterioles and capillary beds. Windkessel and resistive

models are common BCs used [20]. The model is limited by the spatial resolution of the finite element mesh, the time step between each loop iteration, and available computational power. The FSI algorithm development efforts have exceeded a decade to realize validated code, with several doctoral dissertations awarded. The interested reader is directed to the dissertations of [20] for impedance boundary conditions, [18] for CMM-FSI algorithm development, and [23] for lumped heart models—to fully appreciate the complexity and rigor required to solve modern CFD problems. The SimVascular cardiovascular simulation software was developed under the direction of Professor Charles A. Taylor of Stanford University, and is part of the greater NIH Center for Biomedical Computation at Stanford, supported by NIH Research Grant U54 GM072970.

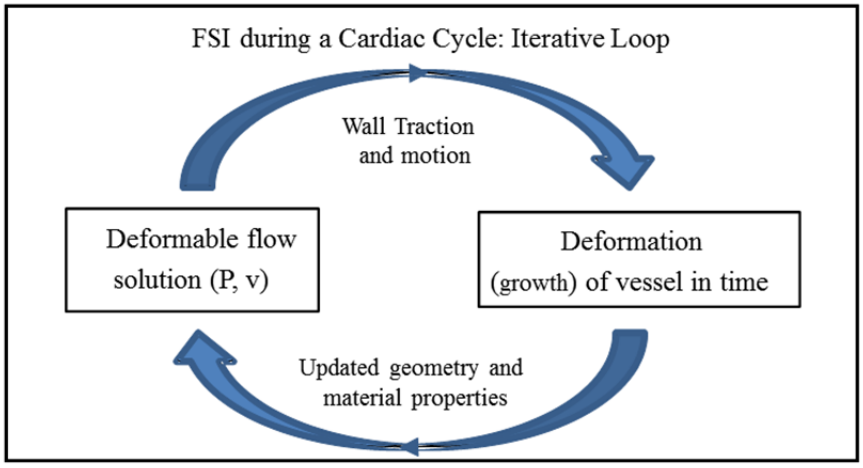

Figure 3.5: Iterative algorithm for fluid-solid interaction problems. Redrawn after [17].

3.2.3.3 Definition of Central Aortic Forces

A theory and toolset was presented to describe surface forces based upon fluid-solid interactions in deformable arteries—now, a definition of molar cardiovascular forces is introduced. Since the BCG is a whole body measurement in the headward-footward direction, let the domain be the entire arterial tree. The molar cardiovascular force (defined here as the Central Aortic Force or CAF) is thus the sum (integral) response of all the individual traction values on the surface FEM mesh in three-dimensions, over the cardiac cycle, per the algorithm discussed. CAF_y is the projection of CAF onto the conventional BCG measurement axis [4]. The integral expression is:

$$CAF_y \equiv \left[\int_{SA\_aorta} \vec{t}^{\,s} dS\right] \cdot \vec{n}_y \tag{3.35}$$

CAF_y is the internal CV force, whereas the BCG is the force measured outside the body. Additional theory may be required to relate CAF_y and BCG—for example; the differences between these quantities may be due to mechanical coupling of the vasculature to the body. CAF and BCG are not identical quantities.

3.3 Multi-Domain Simulations of CAF in a Healthy Individual under Rest and Exercise Conditions

3.3.1 Goals and Objectives

The goal of this simulation is to develop a quantitative model of Central Aortic Forces using the Multidomain Method, to study how BCG-like forces are generated. At present, the computational effort is high and limits the number of physiological conditions that can be simulated, so the results will be compared to clinical BCG data (meta-analysis) for interpretation.

3.3.2 Materials and Methods

3.3.2.1 Patient-Specific Vascular Anatomy

The principles of studying traction at the fluid solid interface were examined using human anatomy, obtained by medical imaging, and rendered into geometry that can be used for CFD simulations (Figure 3.6). The aortic mesh contained over 700,000 nodes to represent both the fluid and solid domains. Each node on the surface can be treated with the same free body diagram depicted in Figure 3.2 with normal vectors emanating in the direction orthogonal to the surface of the vascular model. The Multidomain algorithms solves for each node in the fluid and solid domain, yielding the velocity profile, pressure, and vessel distention. The anatomy and derived mesh used was limited due to the required computer processing time, and due in-part to the rarity of full-body angiographies performed in routine medical imaging.

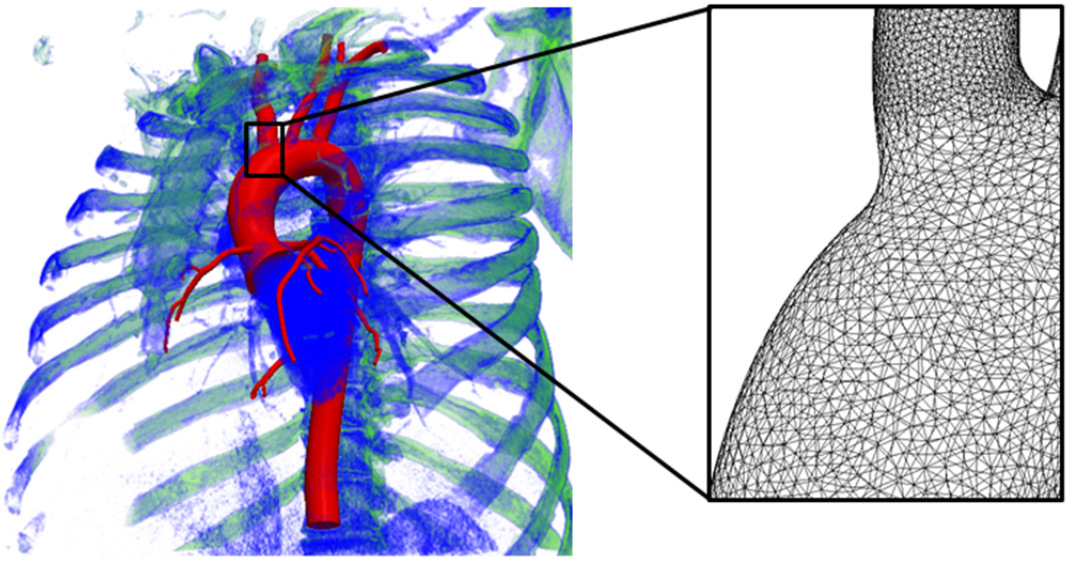

Figure 3.6: Computed Tomography (CT) image of an adult male, with patient specific anatomy of the aorta derived from medical imaging, rendered into a finite element mesh with over 700,000 elements.

3.3.2.2 Subject-Specific Thoracic Aorta Modeling

The computer model used in the first simulations was constructed from cardiac-gated computer tomography (CT) data of a 36-year-old healthy subject as shown in Figure 3.6. The model started from the root of the aorta, ended above the diaphragm, and included major coronary arteries (left anterior descending, left circumflex, and right coronary arteries) and major upper branch vessels (right subclavian, left subclavian, right vertebral, left vertebral, right carotid, and left carotid arteries).

Blood flow was modeled using the incompressible Navier-Stokes equations, and the motion of the vessel wall using the elastodynamics equations [17]. A stabilized finite element method was used to compute pressure and velocity fields in the three-dimensional model of the aorta with coronary arteries and major upper branch vessels. A fixed fluid mesh and small displacements of the vessel wall was assumed [17].

3.3.2.3 Boundary Conditions for Inlet and Branching Outlets

Appropriate boundary conditions were assigned to compute physiologically realistic velocity and pressure fields in the computational models. A lumped parameter heart model was coupled to the inlet of the three-dimensional thoracic aorta model to compute left ventricular pressure and aortic pressure and flow, by considering the interactions between the heart and arterial system [22]. Left ventricular pressure and volume were related using a time varying elastance function scaled from a normalized elastance function [22]. The coronary outlets were coupled to lumped parameter coronary vascular models whereas the outlets of the upper branch vessels and the descending thoracic aorta are coupled to three-element Windkessel models to represent the coronary vascular beds and the upper and lower extremities absent in the computational model, respectively. The parameter values of the heart, coronary, and Windkessel models were set to approximate measured heart rate, cardiac output (CO), and pulse pressure of the subject. Finally, an augmented Lagrangian method was used to enforce a shape of the velocity profiles of the inlet and the outlets with retrograde flow [24].

3.3.2.4 Physiological Parameters for Rest and Exercise Conditions in Healthy Subject Model

The blood vessel walls were modeled with a linear elastic material assumption with Poisson's ratio of 0.5, a wall density of 1.0 g/cm^3, and a uniform wall thickness of 0.1 cm. The Young's modulus of the vessel walls was chosen to be $6.26 \cdot 10^6$ $dynes/cm^2$ so that the aortic deformations match the measured wall deformations of the CT data. The measured CO of the subject was 5.0 L/min with a heart rate of 60 bpm. To simulate a light exercise condition, the heart rate was doubled to 120 bpm and the downstream resistance of the descending thoracic aorta was reduced to 33% of its resting value, to send more flow to the extremities. This resulted in a CO of 10.3 L/min. The computed brachial pressure of the subject ranged from 78 to 124 mmHg for the resting condition and 78 to 149 mmHg for the exercise condition. The stroke volume increased from 83 cc at rest to 86 cc during exercise. The maximum contractility of the left ventricle maintained the constant value of 2.0 mmHg/cc.

3.3.3 Results

3.3.3.1 Determination of Central Aortic Forces in Healthy Subject Model

The surface mesh of the model was extracted from the volumetric finite element mesh. Next, the traction values were integrated over the surface area of the aorta to compute CAF for each time step using Equation 3.35. CAF_y was then extracted from CAF to estimate the magnitude of the force in the BCG measurement axis. The longitudinal pressure and wall shear stress tractions were decomposed from CAF to obtain CAF_y (Figure 3.7).

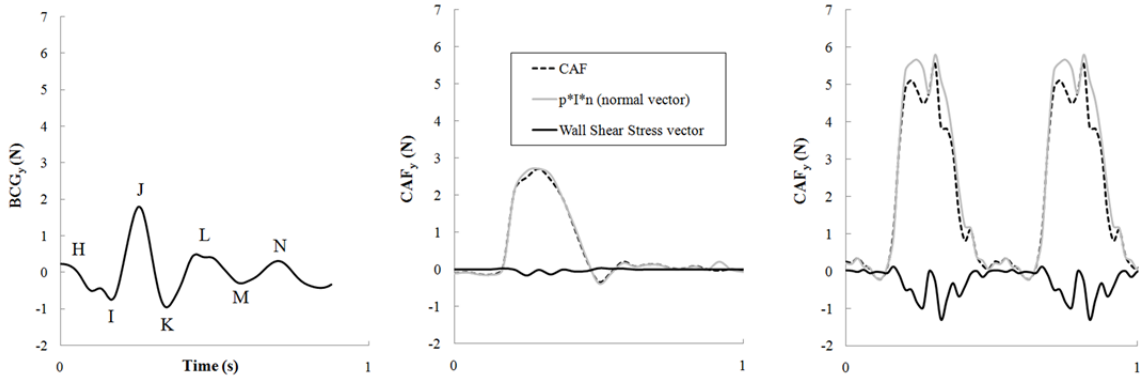

Figure 3.7: Typical resting BCG measurement (left). Simulation results of forces produced during rest (center) and exercise (right). The pulse pressure difference increased the stroke volume from 83 to 86 mL, and doubled CAF peak amplitude.

3.3.3.2 Comparison of Central Aortic Forces to the Ballistocardiogram

The comparison of CAFy to BCG is limited to data obtained from calibrated BCG recording systems (several works report BCG values with arbitrary units, such as volts or A/D counts). Furthermore, we limit the analysis to BCG measurements in the longitudinal axis, which are often confused with ballistic measurements in the transverse axis (sternal vibrations). The peak force amplitudes of the BCG and CAF_y both occur in early-to-mid systole. The BCG IJ amplitude is the peak amplitude compared to the CAF_y peak amplitudes.

Male subjects in the seminal 20 year study conducted by Starr reported BCG amplitudes of approximately 2.8-4.2 N, recorded on the Starr table-based system [25]. Female BCG amplitudes were approximately 1.4-2.7 N. More recent work on bathroom scale BCG systems by Inan, et. al, report resting IJ amplitudes of 1.82-2.95 N for males, and 0.83-2.41 N resting values in female subjects [26]. In both studies cited, the recordings were obtained from displacement-based BCG measurement systems and were calibrated in terms of force. BCG amplitudes as high as 8 N were observed after heavy exercise, in exercise recovery studies [27]. In comparison, the estimated CAF_y amplitudes for rest and mild exercise are within ranges previously measured on calibrated BCG recording systems.

3.3.3.3 CAF and Aortic Pressure Relationship

CAF_y amplitudes resulting from the surface integration were obtained—now CAF_y timing relationships are discussed. Since the pressure traction term is the main component constituting CAF_y. Next, the CAF_y waveform was compared to aortic pressure waveform (Figure 3.8). Aortic pressure ranged from 80 mmHg to 120 mmHg for the resting case, taken at the inlet. Interestingly, CAF_y peak was found to be synchronous with aortic inlet pressure, but its upstroke started ~40 ms after the pressure upstroke. In other words, peak systolic pressure coincides with peak CAF_y force; end systolic pressure coincides with minimum CAF_y.

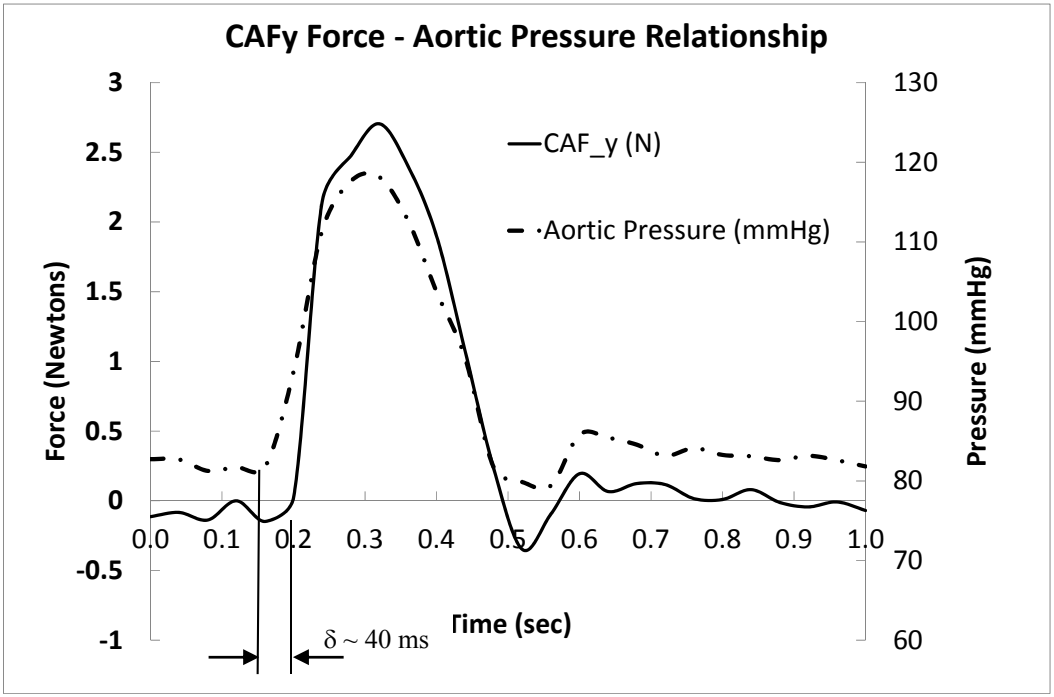

Figure 3.8: Time trace of CAF_y in Newtons (blue trace) and ascending aortic pressure in millimeters of mercury. The CAF_y upstroke is ~40 ms after the pressure upstroke.

3.3.3.4 Aortic Segmentation Analysis of CAF Localization

In order to locate the force, sections of the mesh were analyzed separately, which cannot be measured experimentally. Localized peak force generation was examined by segmenting the thoracic aorta into various pieces and then estimating CAF_y for the individual segments, as shown in Figures 5.9 and 5.10. Three of the four segments included a portion of the arch, and the fourth segment was just the descending portion after the arch. The semi-circle arch segment (which lacked the descending aorta) produced a CAF_y amplitude approximately 110% of the full thoracic model. The quarter-arch segment started at the root of the aorta and ended at the apex. The force was 65% of the full model. The apex-segment, immediately before and after the major upper branch vessels, produced a force 10% of the full model. The descending segment produced forces in the footward direction, which was mostly oscillatory in behavior. Therefore, it

was concluded that the arterial shape asymmetry, in particular the arch, is necessary to produce headward-footward BCG forces and the arch plays an essential role in the generation of peak forces.

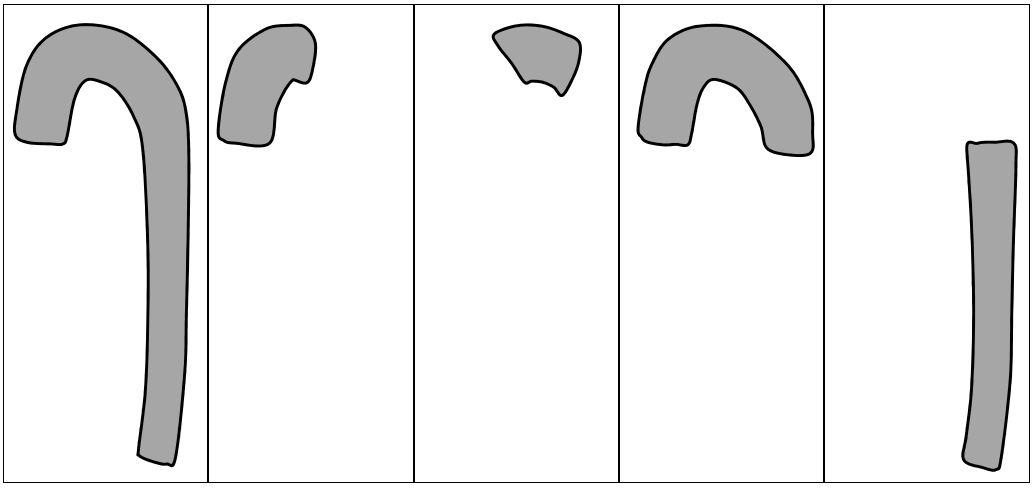

Figure 3.9: Segmentation analysis of the thoracic aorta model to localize peak CAFy forces. Left to right: Whole model, ascending (quarter), crown (apex), arch (semi-circle), and descending aorta (no arch)

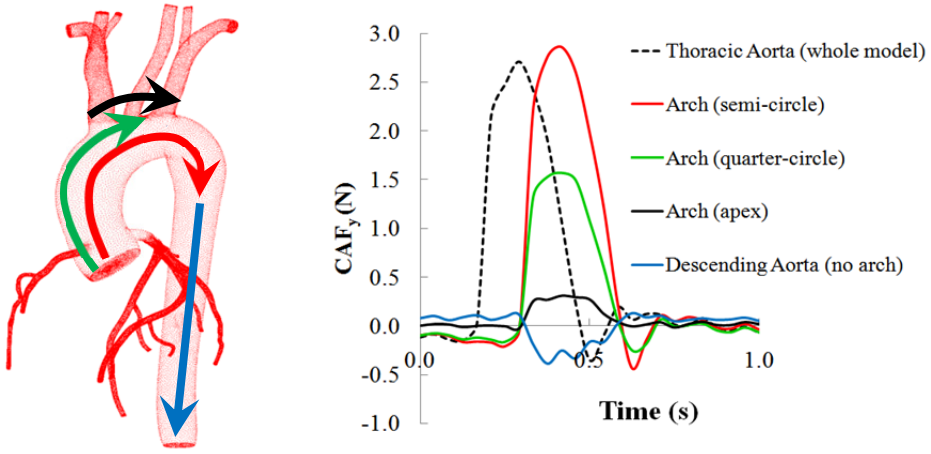

Figure 3.10: Localization of peak CAFy forces in a thoracic aorta model. The semi-circular arch (ascending-crown-proximal descending) is the required anatomy to generate peak forces.

3.3.3.5 Hemodynamic Forces in Three Dimensions

The results for CAF in three dimensions are presented in Figure 3.11. CAF_x (in the sagittal plane) had one large systolic peak with amplitude of 2.75 N, similar to CAF_y. The rise-fall time of CAF_x was 400ms, and the upstroke began 75 ms before the upstroke of CAF_y, but ended at the same time—so the CAF_x pulse was longer than CAF_y. CAF_z (anterior-posterior) did not exhibit single peak behavior; it was mostly oscillatory in behavior through systole and one-half of diastole with 0.75 N peak-to-peak amplitude, in the opposite sense.

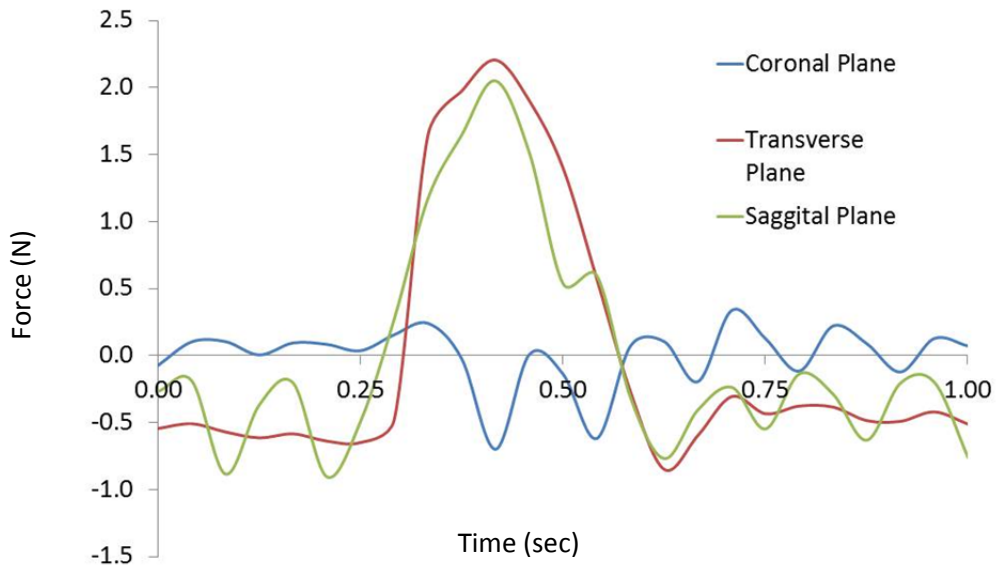

Figure 3.11: Simulation results for Central Aortic Force for the three anatomical planes

3.3.4 Discussion

3.3.4.1 Limitations of Current Simulations

Simulations of BCG-like cardiovascular forces have been performed using the Multidomain methodologies, but the amount of anatomy in the FEM mesh was limited (aorta only). Yet, the simulation yielded results consistent with measured BCG amplitudes—supporting the premise that surface analysis approaches are valid to model the BCG. The amount of vasculature comprising the mesh will increase in time, but available processing time currently restricts modeling the full arterial tree. This barrier will decrease when faster processing becomes available and/or algorithms become more efficient. Additional anatomical structures must be simulated to study the behavior of wave reflections, since reflections are known to originate at the iliac branch and feet, where flow impedances and stiffness change significantly. Wave reflections were generally absent in the models since the aortic pressure wave lacked pressure augmentation in systole (see Figure 3.8). The wave reflection behavior could improve with additional branching sites, such as the iliac bifurcation, which is a major reflecting site. Since this reflection is absent, current interpretations of the data will concentrate on force generation in early systole and wave reflections will not be discussed.

3.3.4.2 CAF_y Amplitude and Localization

Simulated CAF_y amplitudes were consistent with measured BCG IJ amplitudes in literature for at-rest and light exercise conditions [26, 27]. The doubling of pulse pressure accounted for most of the increase in CAF_y amplitude. Stroke volume (SV) change was minimal (83 cc versus 86 cc), yet CAF_y amplitude doubled—suggesting that pressure changes are more significant than mass changes for headward-footward forces. Recalling the definition for body forces in Cauchy's equations of motion

(Equations 5.33 and 5.34), the pressure term in B_r is directly proportional to the force—so a doubling of pulse pressure should double the radial body force. Physiologically, higher stroke volumes increase contractility, via the Frank-Starling effect, which in turn raises peak pressure. BCG amplitude changes observed clinically are therefore consistent with traction models. Comparisons of simulations to the exercise recovery study are deemed acceptable, since treadmill exercise requires more blood flow directed towards the legs, and the simulation decreased the descending thoracic impedance BC by 33% to shunt more blood flow in the same manner.

The CAF_y rise time was delayed by 40 ms compared to the aortic pressure pulse, so force genesis must occur in the early portion of the aorta, by way of reasoning. The subsequent segmentations of the surface mesh confirmed that peak force generation occurs in the semi-circular portion of the arch, and footward forces are produced in the descending aorta, which retards peak force generation. From a geometric viewpoint, the arch contains a significant amount of surface area normal to the BCG y-axis (headward) where radial body forces (B_r) are in-line. Also, the descending aorta decreased CAF_y amplitude because of the shearing body force (B_z) in the longitudinal axis (y), but this forces is negligible since the shear influences are small. Therefore, CAF_y is a pressure-induced signal which is localized to the aortic arch.

The CFD analysis thus predicted force amplitudes consistent with measured BCG amplitudes. Simulation of exercise showed a doubling of the resting CAF_y peak force, also consistent with experimental data. In this case, the increase in pulse pressure accounts for the sharp increase in CAF_y, which relates back to the normal pressure component of traction. CO doubled as well; however, this was mostly due to the imposed doubling of heart rate. While the amplitude of the CAF and BCG forces are similar, (strongly suggesting CAF as a major contributor to the BCG signal), it is obvious from Figure 3.7 that morphologies are not: the CAF_y is mostly monophasic, while the BCG is multiphasic. The typical H wave of the BCG was not present in the CAF signal. This wave has been linked to the heart's movement [10], and since our model does not incorporate the heart (only the inlet flow profile), it is not expected to appear in these simulations. The BCG K-L-M-N waves are not observed in the CAF traces either. This may be due to geometrical limitations of the model (thoracic aorta only), resonance artifacts from under-damped measurement systems, or due to the propagation of CAF forces through the body [28].

3.3.5 Ockham's Razor Applied to Modern Theories of Ballistocardiography

Simpler theories are easier to understand, and are generally better than complex ones. These cardiovascular simulations provide a high degree of quantitation for pressure, wall shear stress, body forces, and vessel deformation—but the mathematical theories introduced are not instructive for general audiences interested in BCG. Noordergraaf was aware of this "razor approach" when describing his physical models, and drew a simple sketch of a fly-fisherman in *Circulation* to illustrate the main point of COM change [11]. Likewise, simplified figures are presented here for the FEM approaches used to

understand surface forces acting on the vasculature—and a "napkin approach" to estimate BCG forces and timings based on this sketch.

3.3.5.1 Geometric Reasoning of BCG Amplitudes

Figure 3.12 depicts the surface boundary of the aorta model with normal surface vectors throughout (Figure 3.12, left), and pressure gradient annotated in color. When examining area projections perpendicular to the y-axis, a difference in surface area can be observed for the semi-circular arch (Figure 3.12, right). As shown, the semi-circular arch region is the main area where net forces act (Figure 3.12, right). Since the outer diameter of the arch has a greater circumference than the inner, there is more surface area on the crown. Therefore, when a pressure pulse acts upon the arch, a net-headward lift will occur, synchronous with the pressure waveform—*force* is equal to *pressure x area*. But, the lift would not begin until the pulse wave traverses the arch.

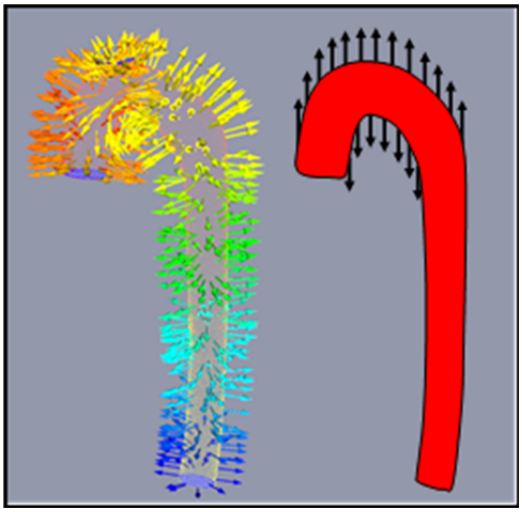

Figure 3.12: Aorta model represented with surface normal vectors n (left) at the fluid-solid interface and simplified representation of aortic lift (right) acting in the headward-footward directions.

If the aorta were straight rather than curved, there would be significantly less force produced since shear stress acting along the wall results in roughly $1/1000^{th}$ the tractive force on a per area basis, compared to pressure. The net-area hypothesis thus provides geometric rationale to use the BCG in vascular stiffness measurements based upon three reasons.

First, the geometric asymmetry of the aorta results in area-mismatch creating lift, and therefore the genesis of the BCG is localized to the aorta arch—thus, timings related to PAT_{arch} (A_{top}-A_{bottom}) may be used as one time point in pulse wave velocity (PWV) measurements. In time, however, reflections in arterial tree will contribute to the overall BCG shape as the pressure pulse propagates beyond the arch. Therefore, the "net-area" behavior is valid only for a short duration in systole—this argument is similar to

those made for measuring pressure and flow in early systole to determine the vascular characteristic impedance before the influence of wave reflections [15].

Secondly, the aorta distends based on Laplace's Pressure Law, so larger pulse pressures should result in more lift. In the rest and exercise simulations, stroke volumes were held nearly constant (83 cc versus 86cc, respectively), but pulse pressure was doubled. By way of numbers (the napkin approach), a 46 mmHg pulse pressure resulted in ~3.3 N of lift which would require 5.38 cm^2 of area-mismatch at peak systole—for the rest condition simulation (Figure 3.7, middle). For light exercise, the 71 mmHg pulse pressure resulted in ~6.16 N of lift and would therefore require 6.62 cm^2 of area-mismatch at peak systole. For rest, pulse pressure increased by 54%, yet CAF_y force increased 86%. By Laplace's Law and Poisson effects, increased systolic pressure will distend the vessel in the radial and axial directions, in turn creating additional area-mismatch to produce additional lift (e.g. 4.89 cm^2 versus 6.02 cm^2), which is expected for compliant vessels.

The idealized aorta model in Figure 3.13 depicted an area-mismatch of 8.57cm^2, using aortic dimensions by Worz [29]. At first glance, the idealized area appears to be 1.4-1.75 time too large (more lift is expected), however—this idealized geometry is within reason when considering pressure amplification, which is of the same order. The simulation BCs on the aorta were based on brachial cuff measurements, which were the amplified pulse pressure. Therefore, lift was coincidentally the same. In summary, the napkin approach agrees with measurements to a first approximation. Other considerations may be required to improve the approximation, for example, including the iliac branch, which has surface geometry that may produce footward forces that reduce peak forces produced by the arch.

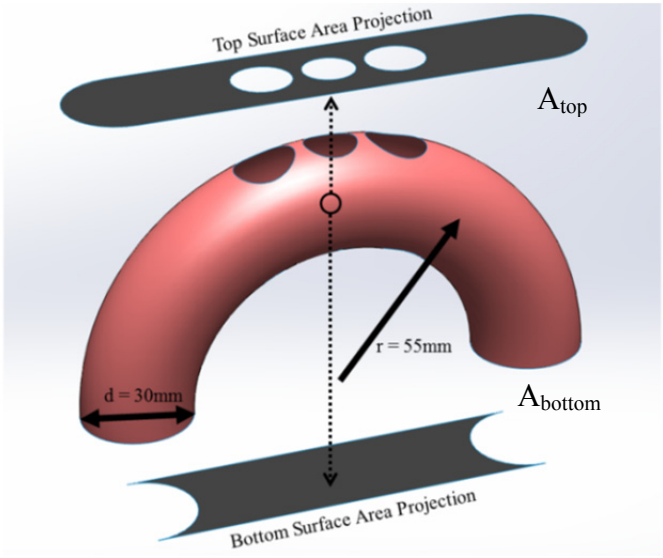

Figure 3.13: Surface-Area-Mismatch illustration of idealized aortic arch geometry is approximately 8.57 cm^2 greater (A_{top}-A_{bottom}) in the top projection.

Lastly, if the first and second assumptions are physically reasonable, then aortic stiffening (from aging) would lead to decreased BCG amplitudes and an earlier onset of the BCG (e.g. the I and J-waves), for healthy subjects. The H-wave is a pre-ejection timing and not considered part of this reasoning, since the aortic valve is still closed and pressure therefore is not coupled to the vasculature. In the 20-year longitudinal BCG study, Starr observed decreasing IJ amplitudes in his patients as they aged and correlated this finding to mortality [25]. Patients in the lower-third of BCG amplitude had the highest incidence of heart disease. His study goal was to report on myocardial health, not vascular stiffness—but it is interesting to consider whether longitudinal degradation of BCG IJ amplitude was also attributable to aortic stiffening. For example, stiffened aortas would not distend as much, producing less lift. Another potential consideration is fast pulse wave arriving earlier at the iliac branch during systole, creating downward forces countering the upstroke. Additional aorta models including the descending portions and iliac branches are needed to examine downstream traction behavior, beyond the distal Windkessel BC at the descending outlet.

3.3.5.2 Simplified Explanation of Initial Upstroke BCG Timings

If the BCG is a pressure-induced signal originating in the arch, then certain timings in the BCG waveform may represent stiffness characteristics of the aortic arch. Several works in the literature have characterized BCG timings with investigators reporting on the coincidence in timings for the onset of the carotid pulse and the onset (I-wave) of the BCG. These findings are interesting, but lack quantitative models to support the observations. The elastic wall theory and simulations presented here may be used to support the following hypothesis of BCG timings.

When examining cardiovascular signal timings, a delay is observed between the upstroke of the BCG and the R-wave [26, 27], which is hypothesized here to be *the pulse arrival time (PAT) to traverse the semi-circular arch*. By way of numbers, an aorta of diameter 30 mm and 55 mm radius of curvature has 220 mm of path length to traverse the arch, Figure 3.13. Aortic pulse wave velocity (PWV) ranges 4 to 6 m/s measured via catheterization [15, 30], which results in respective PTTs of 55 ms and 37 ms to traverse the arch. Preejection period (PEP) timings range from 75 ms to 110 ms [31, 32]. When added the average timings together ($PAT_{arch} = PEP + PTT_{arch}$), the theoretical PAT_{arch} is 138.5 ms. Therefore, the initial upstroke timing of the BCG (I-wave) is similar, if not identical to the calculated PAT_{arch} (Figure 3.14)—and sufficiently close to the $PAT_{carotid}$ to be used as the early timing for arterial stiffness measurements.

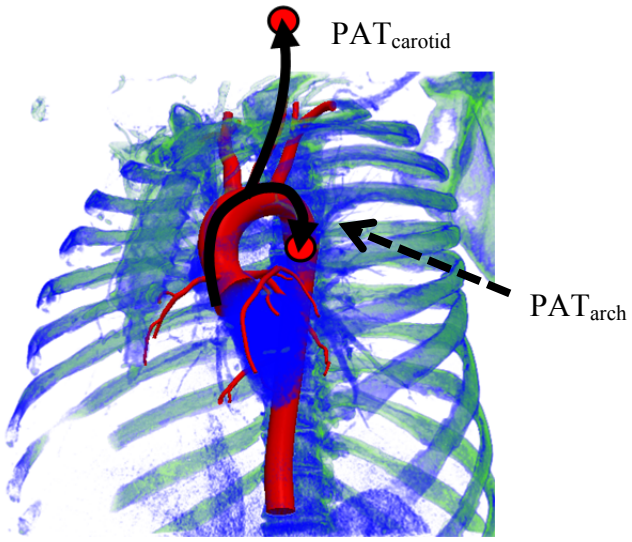

Figure 3.14: Depiction of proposed relationship of the BCG and carotid timings. The PAT timings are similar since the BCG is considered to be a surface pressure-induced signal, as opposed to a change in center-of-mass.

If the I-wave is in fact related to stiffness of the arch, then known patterns of arterial stiffness should reflect in clinical BCG studies. Since the early beginnings of BCG research there has been correlations reported for the I-wave and carotid artery PTTs [4, 33], which can be further explained by the time required to subtend the arch. These works, however, were performed with intent to study cardiac performance; not vascular stiffening. Unfortunately, mainstream BCG research ended (coincidentally) in the era when PWV research was nascent, resulting in missed opportunities to study this in-depth. However, a recent work using chair-BCG systems with electromechanical film EMFi (electromechanical film) sensors has reported similarity in carotid timings in multi-sensor studies for vascular stiffness assessment [34]. The statin study mentioned in the background chapter studied PWV change for subject, measured over two years, but no changes in PWV were observed—when retrospectively analyzing the data. A second two-week study was initiated to study short and longer term repeatability of the system in forty-eight subjects of ages ranging 41 to 65 years to validate the technique. However, this study results did not lead to clinically relevant results [35]. A comprehensive characterization study of the carotid and BCG PAT was therefore performed and summarized in the next chapter, to validate whether the BCG timings were suitable for arterial stiffness measurements.

3.3.5.3 Discussion of Three Dimensional BCG Forces

Few studies have been able to quantify BCG forces in three dimensions. A weightless environment is required to obtain the "ideal" whole-body BCG and unconstrained 3D measurements began with the work of Hixon in 1964. More recently, Prisk, Migeotte, and De Ridder undertook new efforts to improve the understanding of 3D BCG recordings in weightlessness using accelerometers and advanced signal interpretation within the European Space Agency-sponsored B3D (3-D Ballistocardiography in

Microgravity) program, along with ground-based measurement in dry-immersion conditions [36]. Both seminal and recent works recorded significant forces in the left-right axis (perpendicular to sagittal plane) with amplitudes comparable to the longitudinal axis. To date, no explanations have been presented for the left-right forces—nor have they been modeled.

The results for CAF_x (left-right) were unanticipated, but were consistent with triaxial measurements taken in weightlessness. It is interesting that CAF_x begins before CAF_y and ends at the same time and is of the same amplitude (longer pulse). But, CAF_x begins exactly when aortic pressure pulse starts whereas CAF_y starts ~50 ms after the aortic pressure wave, so the lift argument given for CAF_y traversing the arch cannot be reasoned the same for CAF_x. The arch of the aorta is slightly rotated in the left-right plane, which may be the physical mechanism is responsible for force generation and requires further investigation.

3.4 Conclusions

The Multidomain approaches described above provide an alternate methodology to model BCG-like cardiovascular forces. Thus far, partial arterial models were studied to quantify the initial signal genesis suggesting that peak forces are transduced in the aortic arch—with onset beginning after the pulse wave traverses the arch. Left-right forces were also present in the 3D CAF model which has been measured in microgravity studies. Clinically, the data suggests that aortic PAT (determined via the BCG) may be synchronous with the carotid PAT giving a physical rationale to use the BCG as a legitimate proxy to estimate PWV. Clinical studies were performed to validate these models and provided in the following chapters.

BIBLIOGRAPHY

[1] J. W. Gordon, "Certain molar movements of the human body produced by the circulation of the blood," *Journal of Anatomy and Physiology,* vol. 11, pp. 533-6, 1877.

[2] I. Starr, A. J. Rawson, H. A. Schroeder, and N. R. Joseph, "Studies on the estimation of cardiac output in man, and of abnormalities in cardiac function, from the heart's recoil and the blood's impacts; the ballistocardiogram," *The American Journal of Physiology,* vol. 127, pp. 1-28, 1939.

[3] I. Starr and H. A. Schroeder, "Ballistocardiogram. II. Normal standards, abnormalities commonly found in diseases of the heart and circulation, and their significance," *Journal of Clinical Investigation,* vol. 19(3), pp. 437–450, 1940.

[4] W. R. Scarborough, S. A. Talbot, J. R. Braunstein, M. B. Rappaport, W. Dock, W. F. Hamilton, J. E. Smith, J. L. Nickerson, and I. Starr, "Proposals for ballistocardiographic nomenclature and conventions: Revised and extended: Report of committee on ballistocardiographic terminology," *Circulation,* vol. 14, pp. 435-450, 1956.

[5] A. Noordergraaf, "Physical basis of ballistocardiography," Doctoral Dissertation, Utrecht University, s'Gravenhage, Netherlands, 1956.

[6] H. C. Burger and A. Noordergraaf, "Physical basis of ballistocardiography. II : The quantities that can be measured with different types of ballistocardiographs and their mutual relations," *American heart journal,* vol. 51, pp. 127-139, 1956.

[7] H. C. Burger and A. Noordergraaf, "Physical basis of ballistocardiography. III," *American heart journal,* vol. 51, pp. 179-185, 1956.

[8] H. C. Burger, A. Noordergraaf, J. J. M. Korsten, and P. Ullersma, "Physical basis of ballistocardiography. IV : The relative movement of subject and ballistocardiograph," *American heart journal,* vol. 52, pp. 653-673, 1956.

[9] H. C. Burger, A. Noordergraaf, and H. J. L. Kamps, "Physical basis of ballistocardiography. V: The distortion of the ballistocardiogram caused by the movement of the heart inside the body," *American heart journal,* vol. 53, pp. 907-921, 1957.

[10] A. Noordergraaf, "Genesis of displacement of the human longitudinal ballistocardiogram from the changing blood distribution," *American Journal of Cardiology,* pp. 748-756, 1958.

[11] A. Noordergraff, "Further studies on a theory of the ballistocardiogram," *Circulation,* vol. 23, pp. 413-425, 1961.

[12] A. NOORDERGRAAF, "Physical aspects of the "direct" recording of body displacement, velocity, and acceleration by shin-bar ballistocardiographs," *Circulation,* vol. 23, pp. 426-433, 1961.

[13] A. Noordergraaf, P. D. Verdouw, and H. B. K. Boom, "The use of an analog computer in a circulation model," *Progress in Cardiovascular Diseases,* vol. 5, pp. 419-439, 1963.

[14] N. Westerhof, F. Bosman, C. J. De Vries, and A. Noordergraaf, "Analog studies of the human systemic arterial tree," *Journal of Biomechanics,* vol. 2, pp. 121-134, IN1, 135-136, IN3, 137-138, IN5, 139-143, 1969.

[15] W. W. Nichols and M. F. O'Rourke, *Mcdonald's blood flow in arteries, theoretical, experimental and clinical principles*, Fifth Edition ed. New York: Hodder Arnold, 2005.

[16] J. C. Bramwell and A. V. Hill, "The velocity of the pulse wave in man," in *Proceedings of the Royal Society of London. Series B, Containing Papers of a Biological Character*, 1922, pp. 298-306.

[17] C. A. Figueroa, I. E. Vignon-Clementel, K. E. Jansen, T. J. R. Hughes, and C. A. Taylor, "A coupled momentum method for modeling blood flow in three-dimensional deformable arteries," *Computer Methods in Applied Mechanics and Engineering,* vol. 195, pp. 5685-5706, 2006.

[18] C. Figueroa, "A coupled-momentum method to model blood flow and vessel deformation in human arteries: Applications in disease research and simulation-based medical planning," Stanford University Ph.D., Stanford University, United States -- California, 2006.

[19] I. E. Vignon-Clementel, C. Alberto Figueroa, K. E. Jansen, and C. A. Taylor, "Outflow boundary conditions for three-dimensional finite element modeling of blood flow and pressure in arteries," *Computer Methods in Applied Mechanics and Engineering,* vol. 195, pp. 3776-3796, 2006.

[20] I. E. Vignon-Clementel, "A coupled multidomain method for computational modeling of blood flow," Doctor of Philospohy, Mechanical Engineering, Stanford University, 2006.

[21] C. A. Taylor, T. J. R. Hughes, and C. K. Zarins, "Finite element modeling of blood flow in arteries," *Computer Methods in Applied Mechanics and Engineering,* vol. 158, pp. 155-196, 1998.

[22] H. J. Kim, I. E. Vignon-Clementel, C. A. Figueroa, J. F. LaDisa, K. E. Jansen, J. A. Feinstein, and C. A. Taylor, "On coupling a lumped parameter heart model and a three-dimensional finite element aorta model," *Submitted to the Ann. Biomed. Eng.,* 2008.
[23] H. Kim, "Three-dimensional finite element modeling of blood flow in the coronary arteries," Stanford University Ph.D., Stanford University, United States -- California, 2009.
[24] H. Kim, C. Figueroa, T. Hughes, K. Jansen, and C. Taylor, "Augmented lagrangian method for constraining the shape of velocity profiles at outlet boundaries for three-dimensional finite element simulations of blood flow," *Comp. Methods Appl. Mech. Engng.,* 2009.
[25] I. Starr and F. C. Wood, "Twenty-year studies with the ballistocardiograph: The relation between the amplitude of the first record of "healthy" adults and eventual mortality and morbidity from heart disease," *Circulation,* vol. 23, pp. 714-732, 1961.
[26] O. T. Inan, M. Etemadi, R. M. Wiard, L. Giovangrandi, and G. T. Kovacs, "Robust ballistocardiogram acquisition for home monitoring," *IOP Journal of Physiological Measurement,* vol. 30, pp. 169-185, 2009.
[27] O. T. Inan, M. Etemadi, A. Paloma, L. Giovangrandi, and G. T. Kovacs, "Non-invasive cardiac output trending during exercise recovery on a bathroom-scale-based ballistocardiograph," *Physiological Measurement,* vol. 30, pp. 261-274, 2009.
[28] G. Elzinga, N. Westerhof, G. van den Bos, and P. Verdouw, "Transfer of cardiovascular forces through the body," *Medical and Biological Engineering and Computing,* vol. 12, pp. 322-327, 1974.
[29] S. Worz, H. von Tengg-Kobligk, V. Henninger, F. Rengier, H. Schumacher, D. Bockler, H. U. Kauczor, and K. Rohr, "3-d quantification of the aortic arch morphology in 3-d cta data for endovascular aortic repair," *Biomedical Engineering, IEEE Transactions on,* vol. 57, pp. 2359-2368, 2010.
[30] J. Murgo, N. Westerhof, J. Giolma, and S. Altobelli, "Aortic input impedance in normal man: Relationship to pressure wave forms," *Circulation,* vol. 62, pp. 105-116, 1980.
[31] H. J. Montoye, P. W. Willis, G. E. Howard, and J. B. Keller, "Cardiac preejection period: Age and sex comparisons," *Journal of Gerontology,* vol. 26, pp. 208-216, 1971.
[32] M. Etemadi, O. T. Inan, L. Giovangrandi, and G. T. A. Kovacs, "Rapid assessment of cardiac contractility on a home bathroom scale," *Information Technology in Biomedicine, IEEE Transactions on,* vol. 15, pp. 864-869, 2011.
[33] Y. Henderson, "The mass-movements of the circulation as shown by a recoil curve," *American Journal of Physiology,* 1905.
[34] J. Alametsä, J. Viik, and A. Palomäki, "Arterial elasticity measurements with ankle pulse width velocity and ballistocardiography," presented at the 4th European Conference of the International Federation for Medical and Biological Engineering, 2009.
[35] J. Alametsä, A. Palomäki, and J. Viik, "Short and longer term repeatability of ballistocardiography in a sitting position with emfi sensor," *Medical and Biological Engineering and Computing,* vol. 49, pp. 881-889, 2011.
[36] G. K. Prisk, S. Verhaeghe, D. Padeken, H. Hamacher, and M. Paiva, "Three-dimensional ballistocardiography and respiratory motion in sustained microgravity," *Aviation, space, and environmental medicine,* vol. 72, pp. 1067-74, 2001.

4 Clinical Validation of BCG Pulse Arrival Timings

"Verification is proving the equations were solved correctly. Validation is proving the correct equations were solved." -Professor Charles A. Taylor, Stanford University

Does the ballistocardiogram (BCG), measured non-invasively at the feet while standing, contain information about the pulse arrival timings in the arch? A theory was proposed in earlier chapters as a central aim of this work, and this chapter is devoted to investigating whether or not the BCG is an stiffness measure related to the aortic arch, using systems developed by our lab.

Long-term arterial stiffness changes are age-related, caused by elastin degeneration and atherosclerosis over decades—while short-term changes result from vessel wall tension variations, caused by internal volume loading (fluid shifts), or autonomic responses that initiate vasoconstriction/vasodilation. For that reason, long-term patterns were characterized in a cross-sectional age study to characterize stiffening behavior across several decades of life. And shorter-term variations were characterized in a trending study (over four months) to study BCG and carotid timing changes for one subject. Pharmaceuticals that induce vasoconstriction/vasodilation of the muscular arteries were not performed in this thesis due to the risks involved modulating blood pressure in healthy subjects. Nevertheless, the data from these two studies present a compelling case supporting our aim. The BCG physical model timing predictions in the previous chapter were found to be accurate—therefore, BCG *force timings* are in-fact aortic arch *pressure timings*. Now, attention is directed to the results obtained from human subject testing.

4.1 Expected Effects of Age on Pulse Arrival Times

The effects of age on the arterial tree as related to the BCG are discussed in this section. Compliant arteries stiffen over time from (1) mechanical fatigue of elastin in the vessel wall, (2) vascular remodeling (wall thickening), and from (3) atherosclerotic lesions that eventually calcify into hard plaques. Stiffened arteries result in shorter pulse transit times (PTT) which increase pressure wave reflections back to the heart, thereby increasing the left ventricular work required to eject blood from the heart [1]. As a result, the heart tends to weaken over time becoming less contractile, which results in longer preejection periods (PEP). Consequently, there is both an expected decrease and increase in the pulse arrival timing (PAT) with aging, since PAT=PEP+PTT. Therefore, the carotid artery pulse arrival timing (carotid-PAT) was chosen as a reference signal to characterize the BCG as a potential T1 timing. The carotid artery pulse is also the first timing used in for carotid-femoral PWV (cf-PWV) measurements, so the BCG method can be compared to a similar non-invasive measure. We hypothesize that the absolute timings of the BCG and

carotid-PAT will be similar, but not necessarily identical since the carotid artery is of a different branch, compliance, length, and diameter than the aorta.

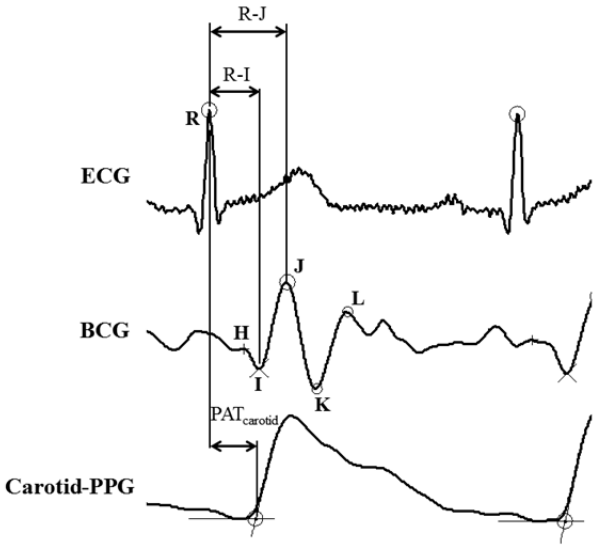

Figure 4.1: Timings extracted from the ECG, BCG, and carotid-PPG signals. Peaks were identified for the ECG and BCG, while the intersecting tangent method was used to the PPG upstroke.

As discussed above, the carotid pulse arrival time ($PAT_{carotid}$) contains two timings (PEP + $PTT_{carotid}$) which can vary independently. Fortunately, arterial stiffness measurements do not require knowledge of PEP since the PEP delay is constant between two measure sites, which cancel out

$$PTT_{cf} = PAT_{femoral} - PAT_{carotid} \tag{4.1}$$

$$PTT_{cf} = (PEP + PTT_{femoral}) - (PEP + PTT_{carotid}) \tag{4.2}$$

$$\therefore\ PTT_{cf} = PTT_{femoral} - PTT_{carotid} \tag{4.3}$$

4.1.1 Method and Materials—Age Study

56 healthy adults participated in the age study, spanning a range of 18 – 79 years old (Stanford IRB 20058). Upon arrival to the study center, each subject was asked to sit down for a minimum of ten minutes to establish a stable resting hemodynamic baseline. Subject demographics were collected inclusive of age, gender, brachial blood pressure, weight, body mass index (BMI), cardiovascular disease / medication history, and anthropometric measurements to determine PWV along different arterial branches.

4.1.1.1 Measurement Setup

ECG electrodes were then placed on the subject's body in a Lead I configuration. The subject was then instructed to stand for two minutes before taking measurements, to reduce transient cardiovascular (CV) changes. The BCG was recorded using a modified scale platform [2] and the carotid pulse was recorded with a reflective PPG sensor, see Figure 4.2. The subject was instructed to stand still for 30-seconds on the scale while recording the ECG, BCG, and carotid PPG signals (each sampled at 1 kHz). The sensors were connected to a 16-bit analog-to-digital (A/D) converter (National Instruments, Austin, TX) and laptop computer—the signals were acquired, stored, and processed using MATLAB® (The MathWorks, Natick, MA). The 30-second recordings were repeated five times for each subject to study variability.

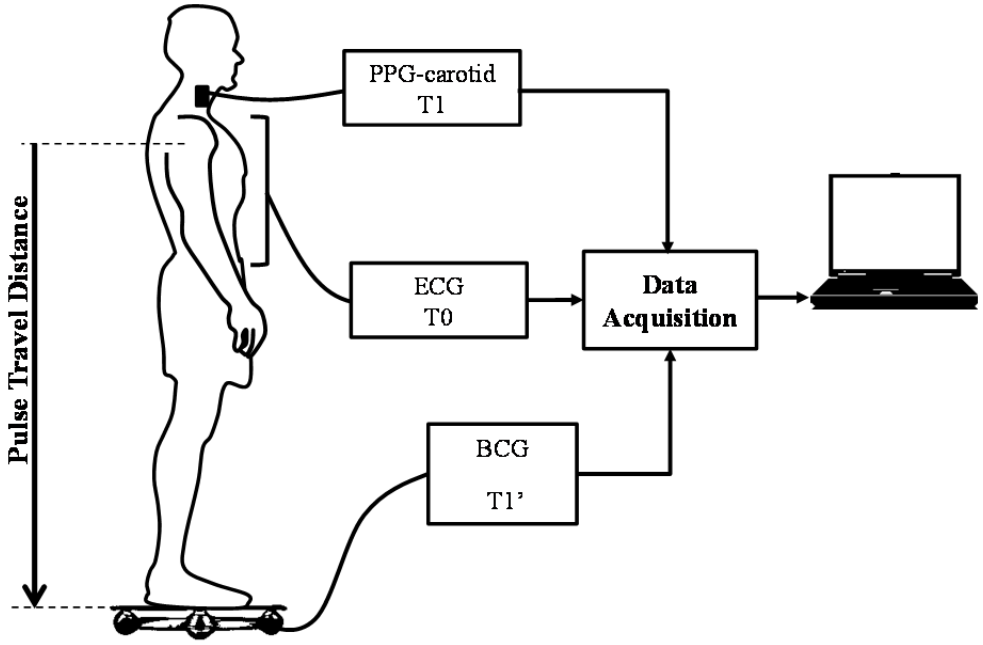

Figure 4.2: System block diagram for the Age Study

4.1.1.2 Signal Processing of Pulse Arrival Timings

To extract the timings, the raw BCG and PPG signals were digitally band-pass filtered (0.5 – 20 Hz, 2 – 30 Hz, and 0.5 – 20Hz respectively) with an IIR filter run in forward and reverse to have zero phase distortion, Figure 4.2. Low frequency baseline wander of the signals were removed using a Savitzky-Golay filter to improve identification of peaks. Next, the ECG R-wave timings were extracted and used for segmenting the BCG and carotid-PPG time trace into individual beats. The BCG ensemble average was computed from the 30-second recordings and used as a template for beat-by-beat feature extraction of BCG timings. The I- and J-waves were extracted from each beat by finding the maximum cross-correlation from the ensemble average, and then by finding local minima and maxima before and after the J-wave. Automatic error checking was included in the algorithm to verify features were correctly identified. For example, if the J-amplitude was greater than I-amplitude, feature extraction would be considered correct.

The carotid pulse arrival timing ($PAT_{carotid}$) was calculated by computing the intersecting tangent point of the rising pulse. The intersection point was obtained using the tangent of local minima (derivative equal to zero) before the upstroke, and the other tangent was computed using the maximum derivative of the upstroke, as shown below. The RI, RJ, and $PAT_{carotid}$ timings were then computed for each beat and stored in a data table for multivariate analysis.

4.1.2 Results

4.1.2.1 Raw RI Interval Timings—Age Study

The beat-by-beat RI intervals (delay adjusted, see Appendix) represent the start timing of the BCG upstroke and were extracted from the patient data set, totaling 10,703 beats for 56 subjects and plotted in a histogram, Figure 4.3.

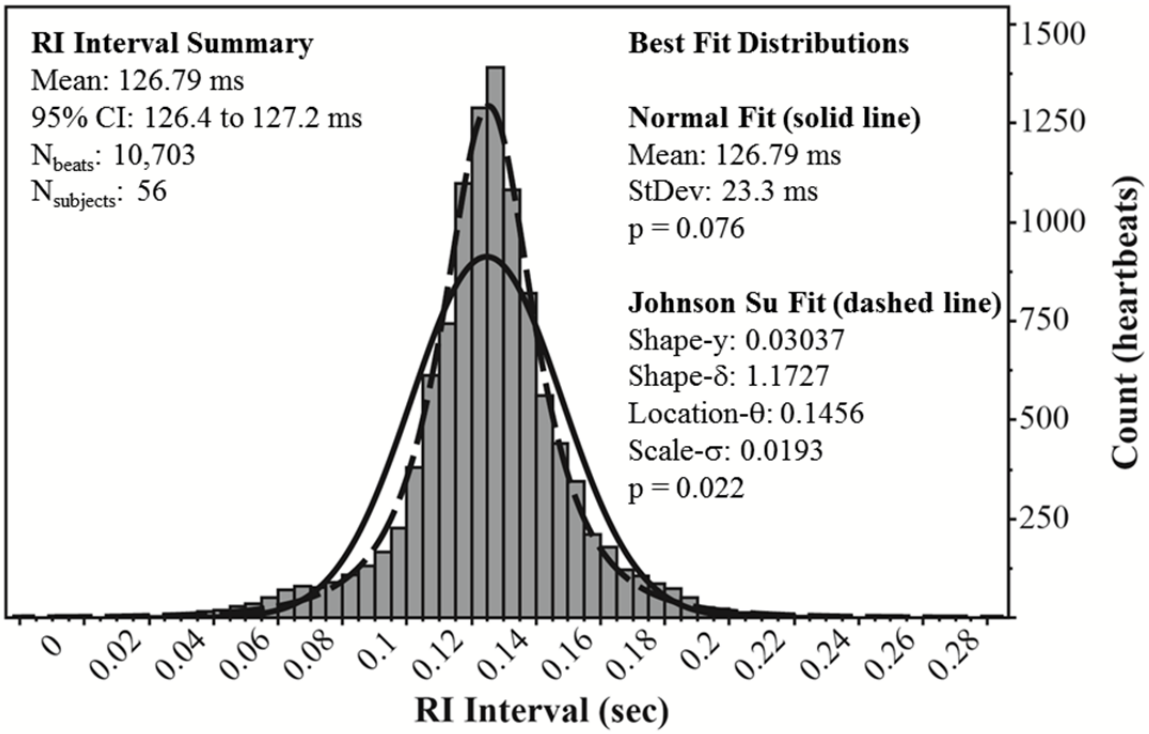

Figure 4.3: Histogram of raw RI interval from the age study, with a best-fit normal distribution (solid line) and best-fit Johnson Su distribution (dashed).

JMP® statistical tools (SAS Institute, Inc., Cary, NC) were used to fit the data using a series of continuous distributions. The purpose of this exercise was to provide an initial assessment of the raw data sampled (as a baseline) before investigating components of variation. The normal fit (solid line) underestimated the probability occurrence of the central distribution—barely failing the Kolmogorov-Smirnov-Lilliefors (KLS) goodness-of-fit test ($p = 0.076$). However, the Johnson Su distribution (dashed line) fit the data well ($p = 0.02$) and was plotted in favor of other higher order fits that were also.

RI Interval Comparison to Theoretical Pulse Arrival Times

For this study, the average RI interval was 126.79 ms with a 95%-confidence interval of 126.4 ms to 127.2 ms. The confidence interval (CI) was calculated as:

$$95\%\ \text{CI} = \bar{x} \pm (1.96 \frac{s}{\sqrt{n}}) \tag{4.4}$$

where 1.96 times the *standard error* represents the confidence bands of the average, $\bar{x}$, standard deviation, s, and number of beats, n. From the previous chapter, a theoretical PAT_{arch} value of 138ms was estimated to compare against BCG timings. However, PAT_{arch} must include the QR interval from the ECG signal, since it is part of the preejection period. The QR was estimated to be 29 ms from the subject population and therefore the final PAT_{arch} (QI interval) is 155.79 ms. Thus, there is a measurable error between theory and reality (QI interval). Therefore, the *Model Error* (calculated as)

$$(\%)\text{Model Error}_{\text{RI Interval}} = \frac{\overline{\text{QI Interval}} - \text{PAT}_{\text{arch}}}{\text{PAT}_{\text{arch}}} \times 100\% \tag{4.5}$$

for the average QI interval (155.79 ms) and the theoretical PAT_{arch} (138 ms) was 12%.

RI Interval Components of Variation—Aging

Returning to the non-normal variability, data stratification techniques were attempted to investigate components of variation for the RI interval. One-way ANOVAs and regressions were performed for the RI interval versus Age, Height, Weight, BMI, and blood pressure, which were found to be non-significant. Since arterial stiffening changes significantly around 55 years old [3, 4], an age-group variable was introduced dividing the study population into two groups (under-55, 55 and over), Figure 4.4. The RI interval differences for the age-group variable was not significant ($p = 0.11$). For the older age group, one other data point appeared to also be an outlier (Figure 4.4 data point at 100 ms, 78 years old). However, further inspection of the raw time traces demonstrated that both the BCG and $PPG_{carotid}$ signal qualities were normal and all timings were correctly extracted by the algorithm, so the data point was left in the analysis.

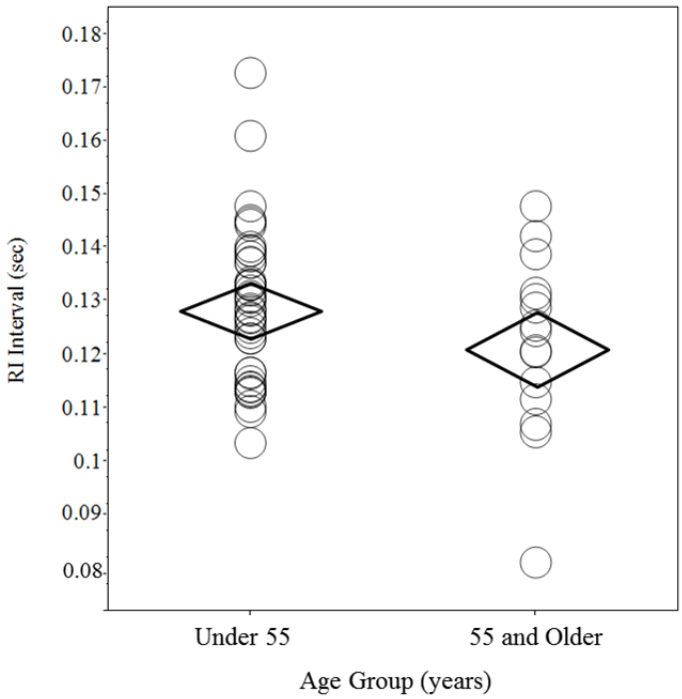

Figure 4.4: Analysis of Means for the RI interval versus younger and older age groups at 55-years old (Mean Difference = 7.3 ms, p = 0.11). The black diamonds depict the visual t-statistic.

4.1.2.2 RJ and IJ Intervals

In similar fashion, the RJ and IJ interval histograms and age-group t-tests are presented below in Figures 7.5 and 7.6.

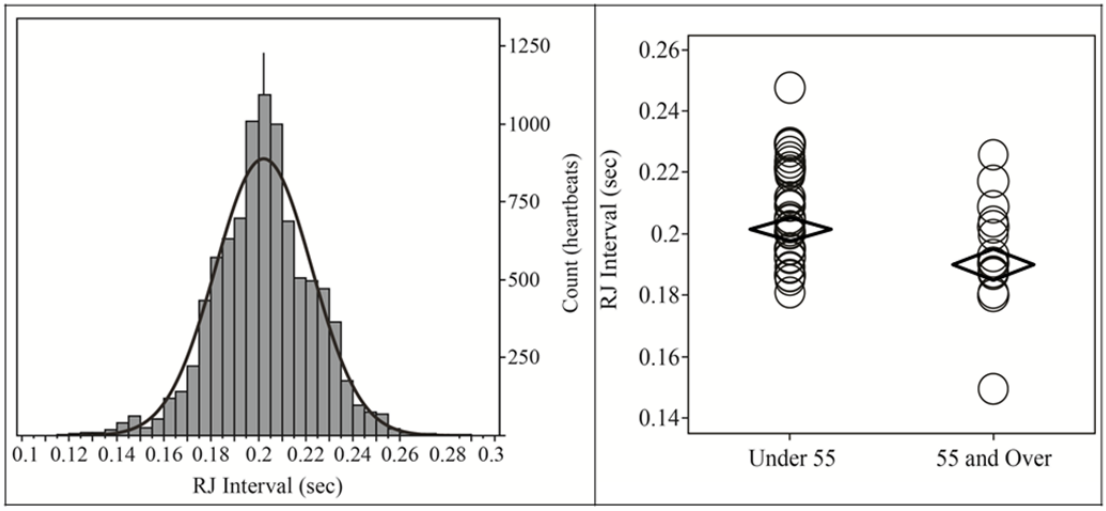

Figure 4.5: RJ Interval Histogram (left) and Analysis of Means for younger and older age group (Mean Difference = 11 ms, p < 0.01). The black diamonds (right) depict the visual t-statistic.

The average RJ interval was 199.7 ms, with a standard deviation of 20.3 ms, passing the KLS fit test for a normal distribution ($p < 0.05$). The 95%CI for the RJ average was 199.3 ms to 200.1ms. The QJ *Model Error* (adjusted for PEP), calculated similar to Equation 4.3, was 65.7%. The age-group was the only significant variable, with an average RJ difference of 11 ms, $p < 0.01$. The 55 and Over age group had shorter RJ intervals. Since the RJ age-group difference was found to be significant, while the RI was not, further analysis was performed for the IJ interval (which is not a preejection timing), see Figure 4.6.

The IJ interval is the rise time response of the BCG and does not include the preejection period. Again, the age-group variable (Figure 4.6, right) was found to be significant ($p < 0.05$) for IJ interval for 6 ms difference. As can be seen, this dataset is free of outliers, which were observed in RI and RJ datasets.

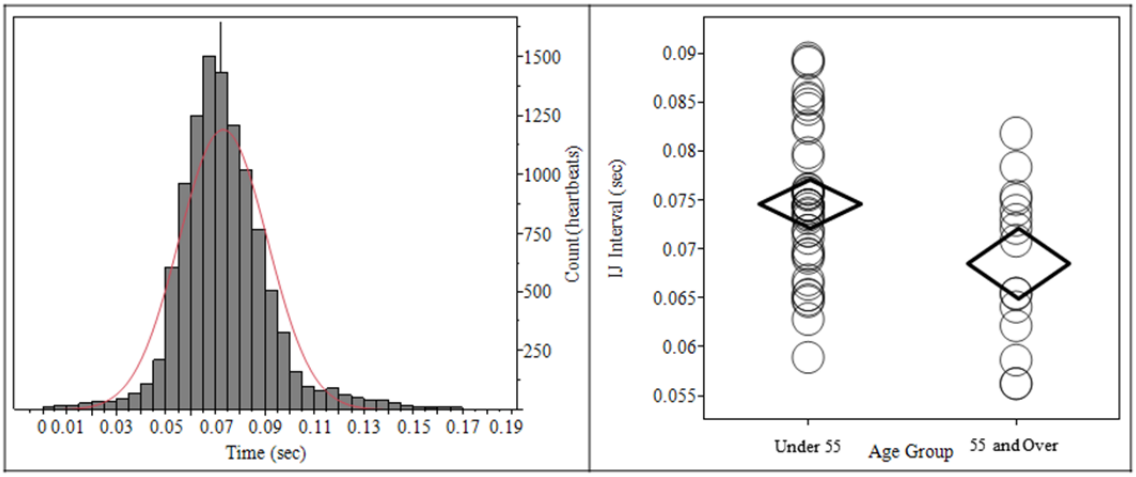

Figure 4.6: IJ Interval Histogram (left) and Analysis of Means for younger and older age group (Mean Difference = 6 ms, $p < .05$, right). The black diamonds (right) depict the visual t-statistic.

4.1.2.3 Raw Carotid Timings

Finally, the carotid-PATs results are presented, Figure 4.7. The average carotid-PAT was 138 ms (left), with a 14 ms time difference across age-groups—decreasing with increasing age. The outlying data point in the older group was the subject ID as identified for RI and RJ.

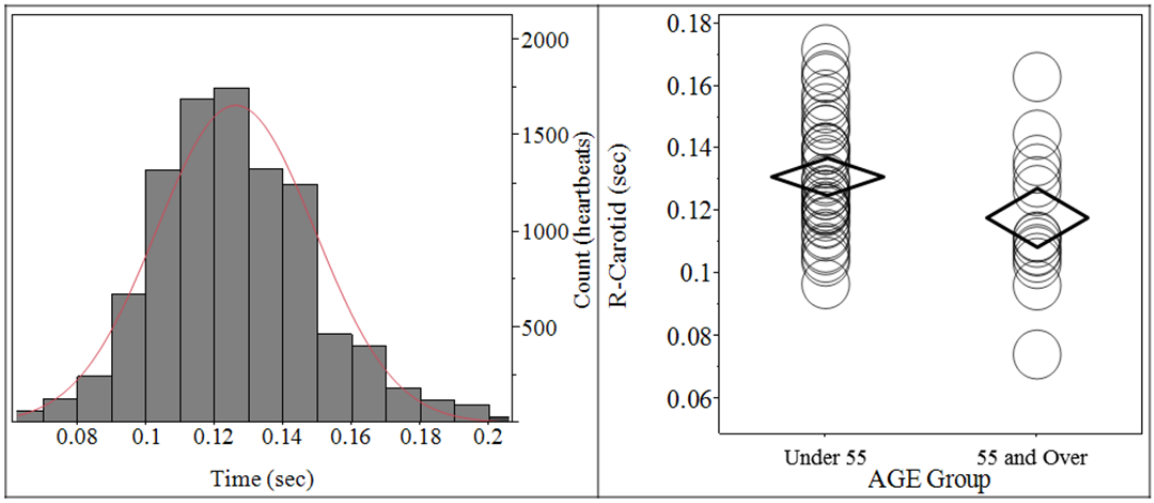

Figure 4.7: R-Carotid Interval Histogram (left) and Analysis of Means for younger and older age group (Mean Difference = 14 ms, $p < .05$). The black diamonds (right) depict the visual t-statistic.

4.1.3 Discussion on Pulse Arrival Time Age Study

The age study highlights two interesting features of the BCG related to arterial stiffness. The discussion is divided into *absolute* and *relative* timings.

First, BCG timings are within reasonable agreement to theoretical timings proposed in the previous chapter. On an absolute scale, QI interval closely matched predicted timings from Central Aortic Force in the longitudinal axis (CAF_y) within 12%. From a validation standpoint, the RI interval for the study group are within reasonable error (*e.g.*, within 10%) to theory to be considered true that RI = PEP + PTT_{arch}.

Second, both carotid and BCG relative timings decreased between the younger and older age groups. This was unexpected since pulse transit time (PTT) accounts for only 30% of the overall pulse arrival time (PAT). The preejection period (PEP) accounts for the other 70% and increases in duration with age as the heart weakens [5]—so the fact that a decrease was observed with age strongly suggests that the BCG contains information about the aortic stiffness. The IJ interval data trends to further support stiffening, since IJ is the rise time of the BCG, it is completely independent of PEP. Otherwise, the BCG timings would have increased in accordance to PEP only—but this did not occur.

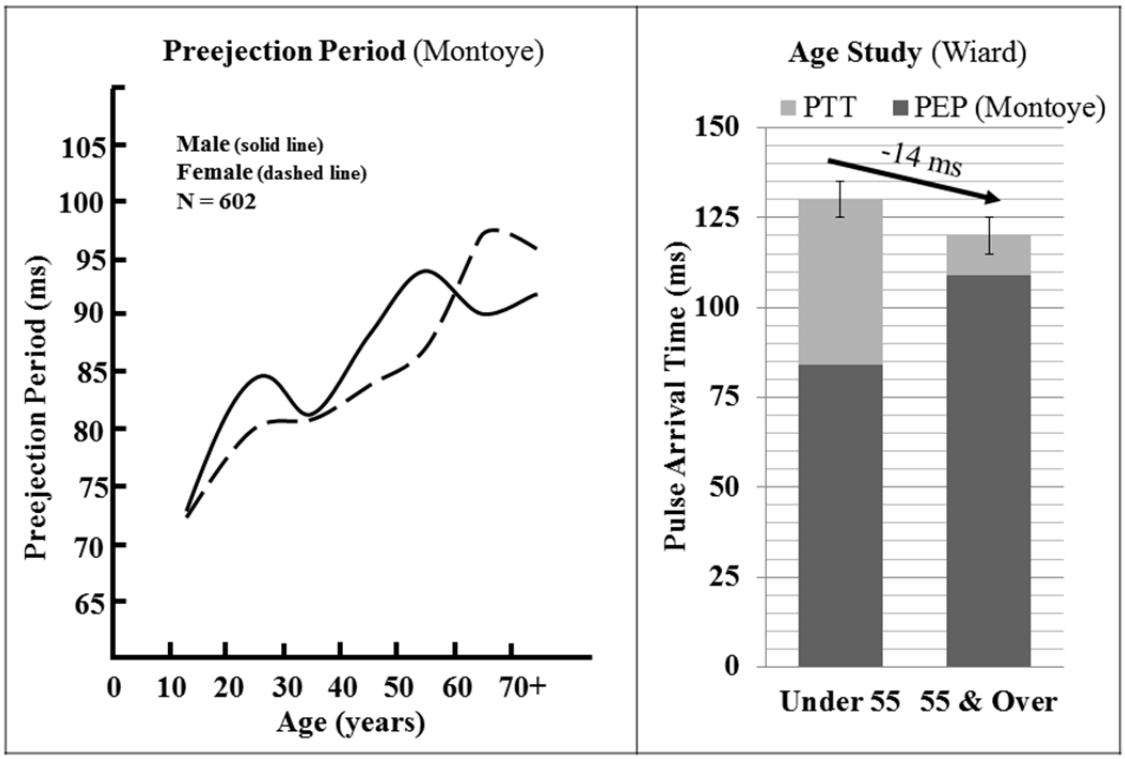

Figure 4.8: Characteristic preejection period (PEP) timings from 602 subjects, after Montoye [5]. PEP increases with age due to a weakening heart (left), while BCG and carotid timings decreased with age (right), indicative of vascular stiffening (PTT decrease).

The carotid-PAT was the reference signal for this study. This timing decreased with age by 14 ms. The carotid is a compliant artery of similar stiffness to the aorta, so the R-carotid timing change would equate to a 2-3 m/s increase in pulse wave velocity ($PWV_{carotid}$), assuming a constant PEP value across age. Physiologically, $PWV_{carotid}$ change is likely larger than 2-3 m/s if actual PEP changes were factored in, however, PEP was not measured in this study. Nevertheless, statistical significance for detecting vascular stiffening in the carotid was still observed.

RI interval changes remained essentially constant across age. The timings decreased with increasing age, but not quite enough to declare statistical differences. Stiffening can still be implicated as the assignable cause for a non-significant outcome. Montoye measured PEP in a large study population for ten years, and quantified a 20 ms average increase in PEP over six decades [5], which was not measured in our study. Since a null response was observed in our data, it can be reasoned that arterial stiffening occurred, which counteracted the expected increase in PEP. Alternatively, to rule out PEP, the null hypothesis could be changed to $H_0 < 20$ ms. In this case, all timing differences (including RI) would be significant which favors arterial stiffening as likely cause.

Statistical significance is one way to interpret the results—practically, the average differences should be inspected with respect to pulse wave velocity changes. When doing so, the RJ interval decreases

11 ms between the young and old age group, which reflects a PWV increase of 1.5 m/s in the aortic arch—or, 3.3 m/s PWV increase when factoring in an additional 20 ms for PEP increase. Similarly for carotid-PAT, a 14 ms PAT decrease equates to a 1.9 m/s PWV increase (or, 4.6 m/s PWV increase, with 20 ms PEP increase). All of these PWV increases would be within reasonable PWV ranges measured in the ascending aorta [6].

From this study, we conclude that the RI interval is within agreement of timings predicted using the physical model. Statistically, RJ intervals differences were more significant than RI for the age-groups. Most likely, this is due to the fact that the BCG signal-to-noise ratio is greater for RJ than RI. From a signal processing perspective, RJ would be the favored and may be used of trending demonstrates so. The RI interval is closer to the predicted timing of the arch, which would give an absolute PWV value closer to the absolute value of the carotid PWV. Therefore, both BCG timings may be important and necessary to trend arterial stiffness.

4.2 Longitudinal Study of BCG Pulse Arrival Timings

From the age study, absolute BCG timings were shown to have similar stiffness behavior as the carotid. And early systolic BCG timings occurred close to when the physical model predicted (e.g. PEP + PTT_{arch}). Therefore, we conclude that the central aortic force model is reasonably accurate—the BCG is the pulse arrival timing in the arch even when measured at the feet on the standing scale platform. Therefore, the early BCG intervals can now be defined as *aortic arch pulse arrival times* $PAT_{arch,I}$ and $PAT_{arch,J}$.

Therefore, we propose that the BCG is an appropriate physiological signal to trend arterial stiffening. In this section, we attempt a longitudinal study to trend changes in arterial stiffness using BCG, by direct comparison to the carotid method. The goal of the study is to demonstrate that the BCG is a suitable alternate to carotid applanation. Additional confidence to initiate this trending study is based on earlier works by our group investigating short-term changes in the BCG timings—which are briefly reviewed below. After this review, a trending study will be demonstrated that supports our stiffening proposal.

4.2.1 Review—BCG and Preejection Period Timings in Short-term Recordings

From previous works our lab has concluded that the BCG can be used in short-term assessments of cardiac timing changes. The seminal work investigated RJ interval changes during the Valsalva maneuver, while subjects stood still on a BCG scale [7]. The RJ interval changed in a manner consistent with contractility changes (Frank-Starling effect) expected from the Valsalva. This preliminary finding led to a more in-depth study, which correlated the BCG to the preejection period (PEP, discussed below).

PEP changes were investigated using impedance cardiography (ICG) which were highly correlated to RJ interval changes ($r^2 = 0.86$, $p < 0.001$) [8]. The study demonstrated, in ten subjects, that short-term cardiac changes could be assessed using ECG and BCG where pulse arrival time (PAT) varies primarily

due to PEP. This PEP study highlighted the usefulness of BCG in the rapid assessment of contractility changes without the need for ICG, where precise electrode placement is required. Physiologically, PEP accounts for 70% of the PAT in the carotid or arch. Therefore, short-term changes in PAT are mostly due to PEP change since vascular stiffening is not likely during this course.

The age-study, however, reveals that carotid and BCG PAT decreases with advancing age which results from stiffening, not PEP. Therefore, trending PEP change with BCG will become confounded when vascular remodeling results. Remodeling rate depend on age, blood pressure, and several variables. Therefore, the BCG needs to be treated as a cardiovascular timing (and not purely a cardiac signal) to avoid confounding in long-term trending. So here, we present an initial study of PAT correlations to BCG timings over several months, to baseline trending capability. The protocol is discussed below.

4.2.2 Methods and Materials—Longitudinal PAT & PTT Trending

The aim of this study is to investigate feasibility of trending arterial stiffness changes using BCG. The carotid pulse arrival time ($PAT_{carotid}$) and carotid-to-toe pulse transit time ($PTT_{carotid\text{-}toe}$) are the arterial stiffness reference signals; measured simultaneously with the BCG, see Figure 4.9. Preejection period (PEP) was not measured in this study, since PEP mathematically cancels when calculating vascular stiffness, per equations 7.1 to 7.3.

One healthy volunteer (male, 33 years old) participated in the trending study, visiting the study center repeatedly for measurements over a four month period. The measurement setup was similar to the age study—the ECG, BCG, carotid-PPG signals were obtained—with the addition of the toe-PPG to determine arterial stiffness across the aorta and muscular arteries in the legs.

Each recording was 30-seconds in length. One recording was performed each day the subject participated. In one case, two recordings were taken in the same day. On this day, the subject noted he was self-administering a prescribed beta-blocker for his standard of care. Therefore, pre- and post-dose recordings were coordinated to measure any cardiovascular changes.

Example time-traces for the longitudinal study are depicted below in Figure 4.10. Note that the pulse arrival times $PAT_{carotid}$ and PAT_{toe} are gated to the ECG R-wave, while pulse transit time to the toe (PTT) is with respect to the I-wave and/or carotid.

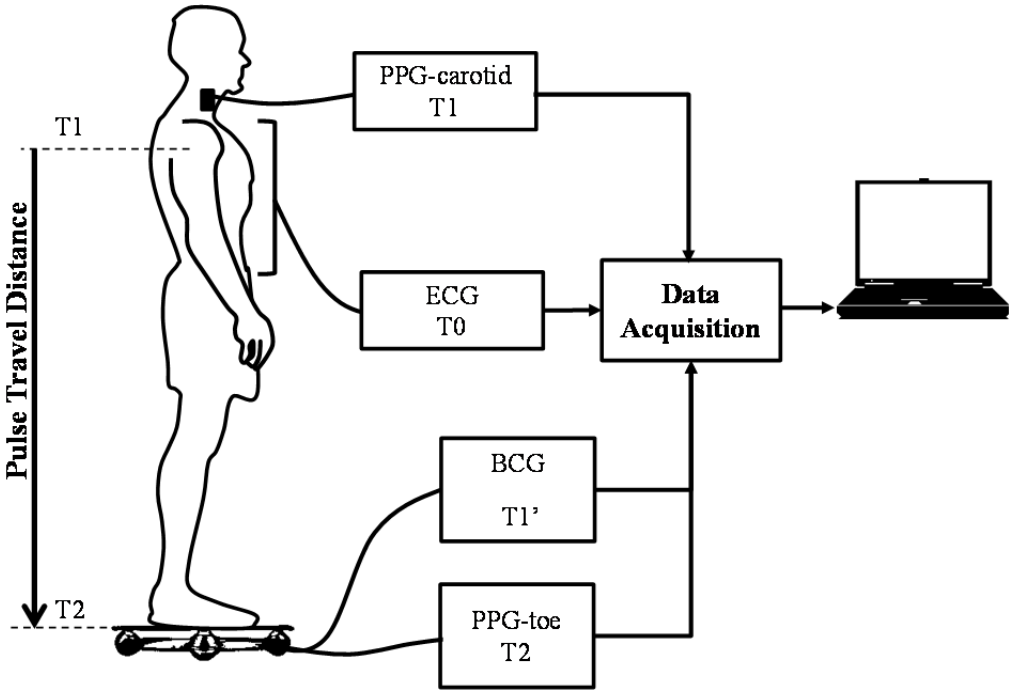

Figure 4.9: System block diagram for the longitudinal study. BCG timings are compared to the carotid starting from the ECG R-wave to trend the first time point (T1). The toe-PPG was also recorded to obtain the T2 timing to calculate the PTT (T2-T1).

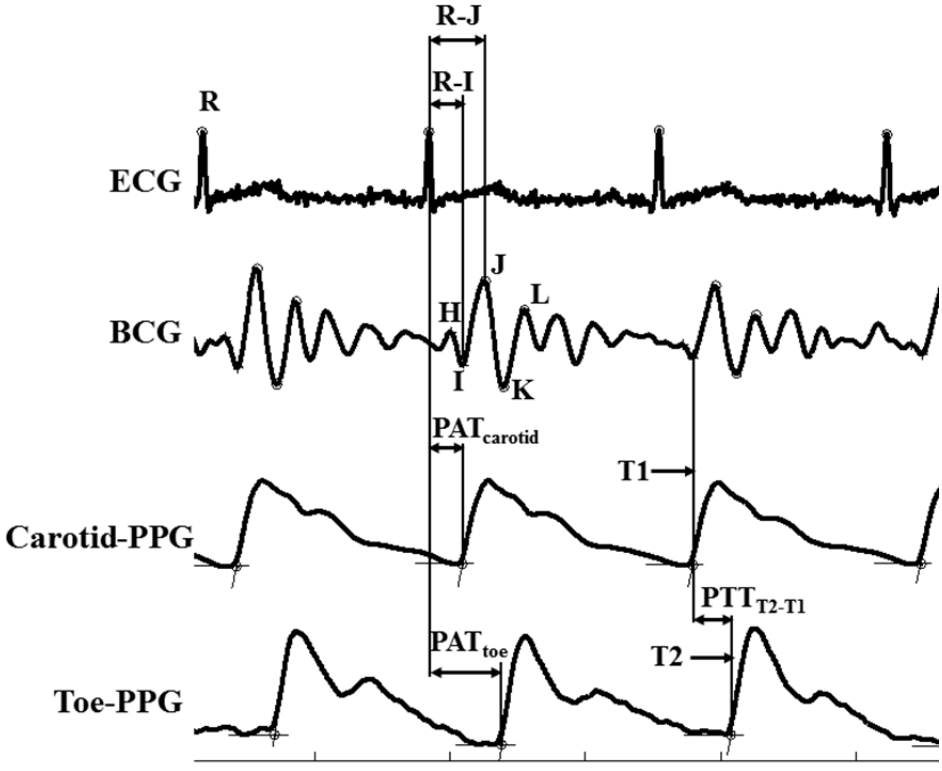

Figure 4.10: Example time traces and definition of pulse timings for the trending study.

4.2.3 Results for Study 2 – Longitudinal Trending

At conclusion, twenty-three recordings were obtained over four months. The raw and averaged timings are presented below: first for T1 timings (Figure 4.11), and then for T2-T1 (Figure 4.12) representing the pulse transit time across the aorta and legs.

4.2.3.1 Raw T1 Timings

The raw T1 timings for the carotid, I-wave, and J-wave extracted from each 30-second recording utilizing signal processing methods described in the hardware chapter, see Figure 4.11. The ECG R-wave is the zero reference representing the ventricular start of systole.

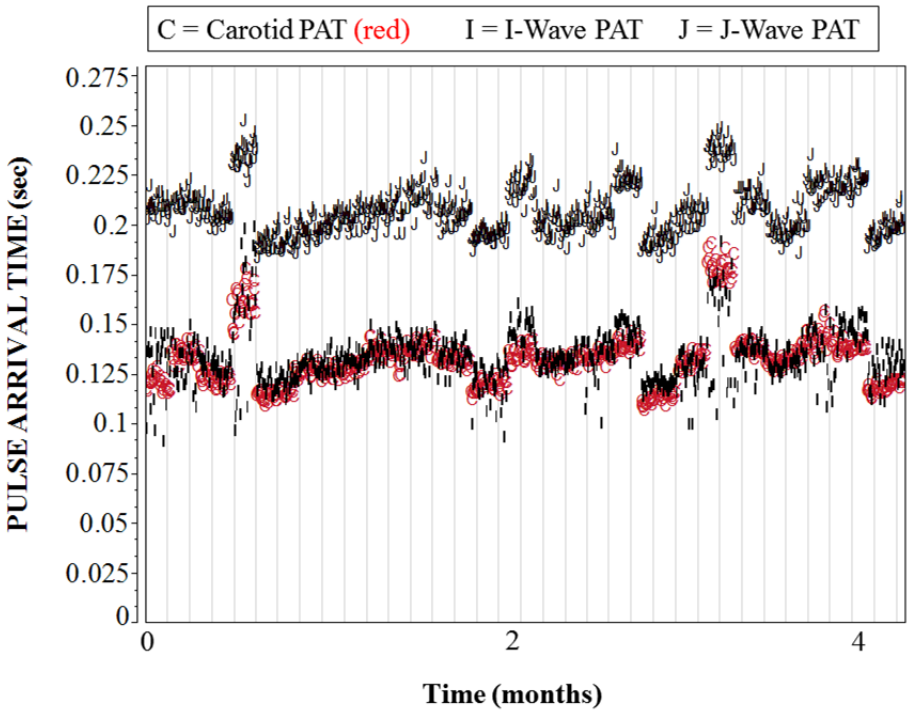

Figure 4.11: Individual T1 timings for the carotid (C), BCG I-wave (I) and J-wave (J) all gated from the ECG R-wave. The vertical lines segment the data between 30-second recordings, over the four month study.

Using the carotid as the gold standard, the average difference from the I-wave/carotid was 1.6 ms ± 12.3 ms (one standard deviation) and the average J-wave difference was 75 ms ± 8.5 ms. The Shapiro-Wilk fit tests were applied since individual I-wave/carotid differences are paired to the same subject. The goodness-of-fit applied the I-wave/carotid differences was approximately normal, however, one-sided skewness (long tail) also existed, while the J-wave/carotid differences were found to be normal. Since asymmetry was only detected for the I-wave/carotid pairs, the increased variability in I-wave/carotid timings was determined to be related to the I-wave timings; not carotid—otherwise skewness would have also been detected in the J-wave/carotid pairs. Reasons for the I-wave/carotid skewness were identified and are explained in the discussion section.

4.2.3.2 Raw Timings for Pulse Transit Times (T2-T1)

Similar signal processing methods were applied to the PPG-toe signal to extract the T2 pulse arrival timing at the toe. Equation 4.1 was then applied to estimate pulse transit times (T2-T1) along the aorta and legs to estimate arterial stiffness for the beat-by-beat timings (Figure 4.12).

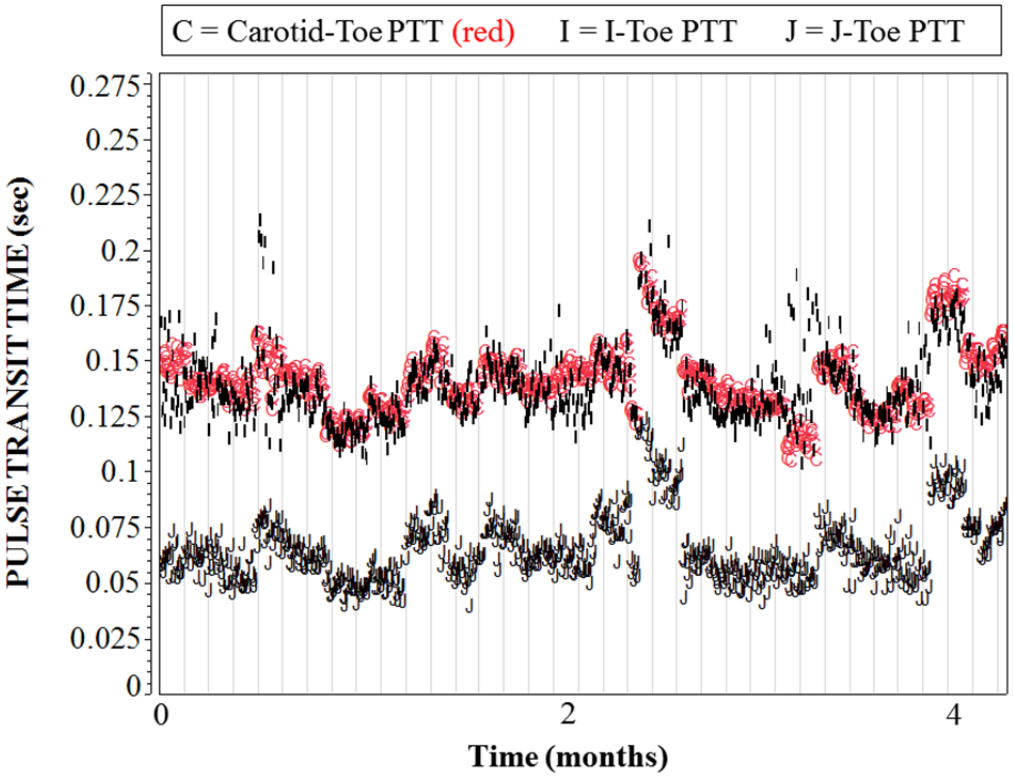

Figure 4.12: Individual arterial pulse transit timings (PTT-toe) for the carotid (C), BCG I-wave (I) and J-wave (J), referenced from the toe (T2). The vertical lines segment the data between 30-second recordings, over the four month study.

The pooled mean, pooled standard deviation, and [average within-day] standard deviation for pulse transit times were: 142 ms ± 15 ms [± 4.6 ms] (carotid-toe), 142 ms ± 17 ms [10.2 ms] (I-toe), and 66 ms ± 15 ms [6 ms] (J-toe). The I-wave PTTs within-day variability was two-fold that of the carotid and J-wave PTTs. Manual identification of the raw time traces confirmed that the signal processing was correct for point appearing to be outliers, so were left in the analysis. The PTT pooled standard deviations, however, were similar for all three timings since between-day arterial stiffness changes were larger compared to within-day variability.

4.2.3.3 Correlation of Arterial Stiffness Estimates (Raw Timings)

In this section, we examine the behavior of three vascular stiffness metrics by correlating each to the carotid-toe pulse transit time—the assumed gold standard (Figure 4.13).

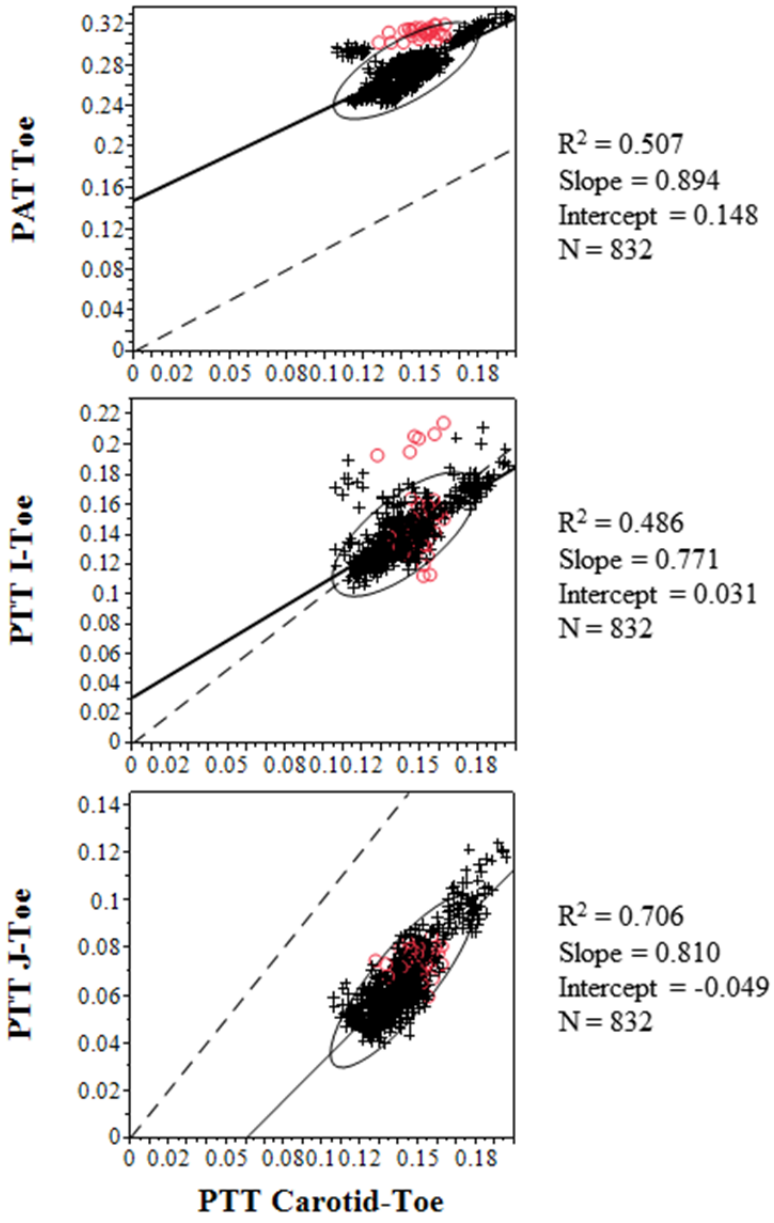

Figure 4.13: Regression plots for the R-toe PAT (top), I-toe PTT (center), and J-toe PTT (bottom), correlated to the carotid-toe PTT. Red circles depict the day the β-blocker was administered. The dashed line depicts the unity slope with zero intercept. Density ellipses depict 95% of the data points.

The first plot represents the pulse arrival time at the toe, referenced from the ECG R-wave (T0). The PAT-toe correlation was included in the analysis since it was deemed unsuitable to assess vascular stiffening, since the preejection period (PEP) was included in the timing—which confounds contractility changes with vascular stiffness changes [1]. The Pearson correlation coefficients were $r^2 = 0.507$ for PAT, 0.486 (I-toe PTT), and 0.706 (J-toe PTT).

The red circles in Figure 4.13 depict the measurements after the β-blocker administration. For PAT-toe, 100% of the points were significantly off the regression line, 21% for I-toe PPT points, and none for J-toe PTT. The β-blocker grouping was expected for the PAT regression, since preejection period increases which reduces contractility. The I-toe timings had the lowest correlation overall, even lower than PAT. Sub-populations of these timings were found to be significantly away from the regression line; however this was only for small proportions of the beats for the 30-second recordings.

4.2.3.4 Averaging Beats – Mean vs. Median

Since beat-by-beat BCG timings generally have higher variability than beat-by-beat carotid timings, averaging of the 30-second recordings was performed to improve BCG timing estimation. Some of this increased BCG timing variability is due to special causes such as motion artifacts (from body movements) and incorrect feature extraction (by the algorithm), which are infrequent in occurrence, but artificially increase the standard deviation—so the median may be a better estimate than the average. Therefore, to characterize averaging approaches, correlations were obtained for the median vs. mean of each 30-second recording and are presented in Table 4.1.

Table 4.1: Correlation of Median versus Mean Pulse Arrival Times

	Longitudinal Study Correlation Coefficient for PAT-Median vs. PAT-Mean [r^2]	**Age Study** Correlation Coefficient for PAT-Median vs. PAT-Mean [r^2]
$PAT_{carotid}$	0.999	0.995
$PAT_{I\text{-}wave}$	0.947	0.911
$PAT_{J\text{-}wave}$	0.996	0.990
PAT_{toe}	0.996	Not recorded

All 30-second recordings exhibited high correlation between the median vs. mean of their respective pulse arrival times (e.g. $r^2 > 0.99$) with the exception of the I-wave PAT, which was $r^2 = 0.94$. Again, these individual timings for the longitudinal study were reexamined by manual inspection and deemed as correct—so, the correlation analysis was also applied retrospectively to the age study. Again, all PATs in the age study were high and above $r^2 > 0.99$, except for the I-wave ($r^2 = 0.91$). Manual inspection of the age study data for the I-wave PAT outliers revealed a combination of (1) correct signal processing, and (2) missed I-waves due to low signal-to-noise for beat-by-beat data, and (3) motion artifacts in the signals. As a result of the analysis, the *median PATs* were deemed suitable for analysis, since the outliers were infrequent and large in variance. This averaging technique allows all data points to be valid without giving extra weight to outliers. Therefore, the correlations for the longitudinal study are reexamined with respect to the median value of the 30-second recordings, depicted in Figure 4.14.

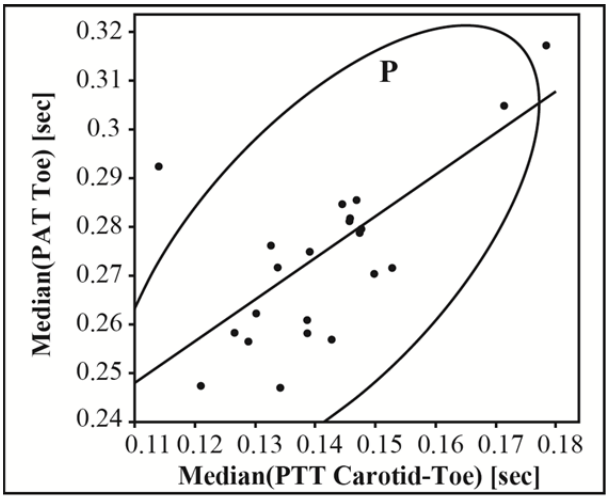

$R^2 = 0.429$
Slope = 0.854
Intercept = 0.153
N = 23

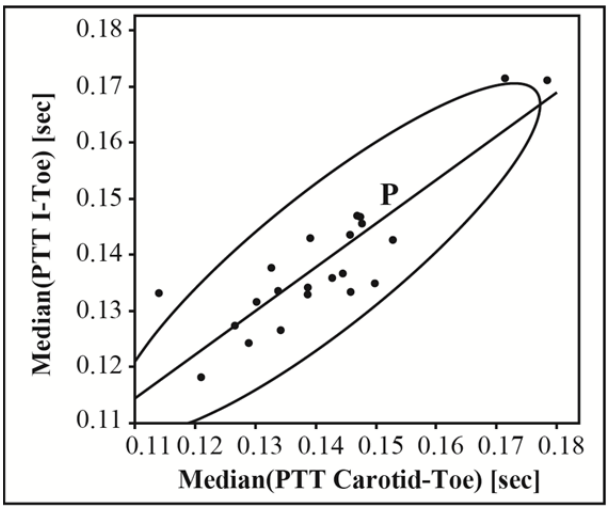

$R^2 = 0.773$
Slope = 0.780
Intercept = 0.028
N = 23

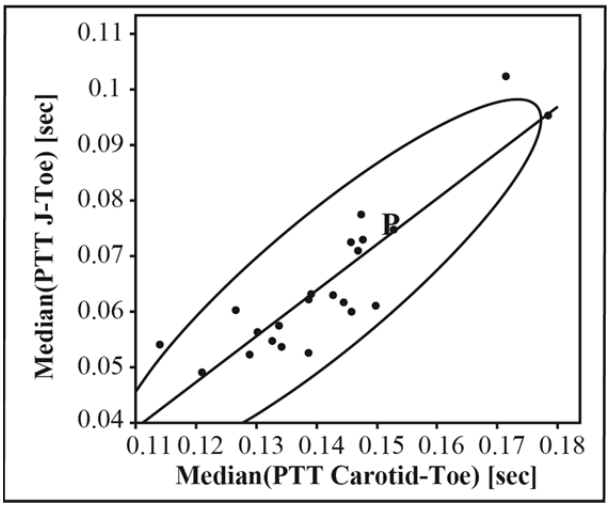

$R^2 = 0.792$
Slope = 0.827
Intercept = -0.052
N = 23

Figure 4.14: Regression plots for the median R-toe PAT (top), I-toe PTT (center), and J-toe PTT (bottom), correlated to the median carotid-toe PTT. The "P" data point depicts the day the β-blocker was administered. Density ellipses depict 95% of the data points.

The correlations changed significantly once median values were considered. The median correlations were $r^2 = 0.429$ (carotid-toe PAT), 0.773 (I-toe PTT), and 0.792 (J-toe PTT), when correlated to the median carotid-toe PTT. The "P" data point depicts the β-blocker (propranolol) administered where both "P" points fall onto the regression line for the BCG time points, while not the case for the PAT dataset.

4.3 Discussion

4.3.1 Validation of BCG Timings

The goal in this chapter was to examine the BCG in context of T1 timings to determine whether the BCG is an appropriate signal for arterial stiffness measurements. Two unique studies were conducted—*age* and *longitudinal*, which elucidated key patterns of the BCG supporting this aim. The following discussion summarizes key results supporting validation of the BCG as a T1 timing, evidenced by theoretical predictions and clinical performance.

4.3.1.1 Does the BCG Occur in the Arch, when Measured at the Feet?

The first aim in this thesis was to describe *where* cardiovascular forces are generated within the body. Womersley elastic theory in three-dimensions was used to model these forces, treating BCG forces as surface phenomenon interacting at the fluid-solid interface (FSI) of the vessel wall. In doing so, peak cardiovascular forces were localized to the aortic arch, which led to a hypothesis that the BCG IJ upstroke is related to PTT_{arch}. The model also predicted BCG forces in the left-right measurement axis, which have been measured by others in free-floating studies.

Measured BCG upstroke timings were also explained using a geometric model, by calculating the transit time along a semi-circular arch—the headward-footward force was related to the pulse pressure. This simplified analysis predicted forces and timings similar to the computer-based model. Thus, two independent physical models (FSI and geometric) demonstrated close agreement to the measurements, and consequently, early BCG forces and timings were localized to the arch—which support the PTT_{arch} hypothesis as an underlying timing parameter. The shape of the aortic arch is necessary to transduce aortic pulse pressure into headward-footward body forces. Consequently, these physical models formed a theoretical basis, to justify use of BCG in studies of arterial stiffening in human subject testing.

4.3.1.2 Discussion: Age Study

The age study was designed to investigate (1) absolute BCG timings gated from the ECG R-wave, and (2) BCG timings relative to the carotid pulse arrival time. Age was chosen as the study variable since aging encompasses greater likelihood of elastin degeneration and atherosclerosis, which alters arterial stiffness. The key findings were as follows:

First, the BCG RI interval timings were found to agree with theoretical PAT_{arch} predictions. The average QI interval occurred within 12% of the model, which suggests there is negligible time involved for the headward aortic arch to propagate down to the feet—which is further supported by non-significant correlations of RI interval to height and weight. Additionally, aortic arch stiffening behavior was identified when stratifying data into young/old age buckets (the RI and RJ intervals decreased with increasing age). This finding was unexpected and important since preejection period *increases* with age. Prior to this discovery, the BCG was only shown to change in accordance to PEP change. Therefore, it must be concluded that the BCG timings is related to both PEP and PTT; therefore *the early BCG timings are pulse arrival timings in the aortic arch*.

Secondly, QI and QJ intervals were compared relatively to carotid-PAT, since the carotid is the reference T1 timing for aortic stiffness measurements. With increased age, the RJ interval decreased by the same amount as the carotid-PAT (~11-14 ms between age groups). The IJ interval (independent of the R-wave) also decreased significantly with age, further supporting a stiffening pattern in the BCG timings. Assignable causes associated with PEP would have resulted in longer IJ intervals, but is not the case. The J-wave was considered for T1 timing since they were more robust in feature extraction (higher signal-to-noise) which is preferable. However, J-waves occur much later in the cardiac cycle; far beyond the aortic arch pulse arrival time (the J-wave timing may be the second-order timing response in the arch, while the I-wave is the first order but theory has not yet been developed to account for this). Subsequent physical models may include the propagation of CV forces through the body. When new models are developed, retrospective validations can be performed using the age study data from the prior chapter. Now, attention is directed to the expected outcomes in the PWV age study.

Consequently, the timings obtained from the age study (both absolute and relative) support a conclusion that the BCG I-wave represents the pulse arrival behavior in the arch—even when measured at the feet on a scale. Therefore, T1 timings could be extracted from BCG while standing on the scale, which could eliminate carotid applanation in PWV measurements. Furthermore, we conclude that the FSI physical model was reasonably accurate in predicting pulse transit times and the model was validated through human testing. BCG forces can now be treated as pressure-induced phenomena localized in the aortic arch.

4.3.2 Discussion: Longitudinal Study Correlations

Since the aortic stiffness assumptions were validated in the age study, a second study was initiated to baseline trending capability of the BCG to determine arterial stiffness changes. This study was preliminary in nature; however, the results strongly support using the BCG as a replacement to carotid applanation. They key results are as follows:

4.3.2.1 BCG-Based PTT Trending Capability

The results from the trending study revealed that PTT variability (BCG or carotid) was larger for *between-day* versus *within-recordings* by a factor of 2x to 3x. This empirical observation is important as it demonstrates that PTT (or PWV) changes can be trended using the scale. For this subject, the 30-second BCG-PTT recording resulted in an average measurement uncertainty of 7% (*e.g.*, 142 ms ± 10.2 ms) during the four-month study. For comparison, the FDA-approved SphygmoCor® CPV system (AtCor Medical) is the gold standard and reports PWV with ±10% relative uncertainty, otherwise their algorithm will not report a result—requiring a retest. PTT uncertainty is the same as PWV uncertainty, thus the BCG-PTT method has potential to meet current PWV accuracy requirements. This will be studied further in the next chapter.

4.3.2.2 Relative PTT Timing Changes

To characterize the BCG-toe timings, two additional pulse timings were measured as reference. The purpose of these reference timings were to quantify whether the BCG-toe timing behaved more like an arterial stiffness timing, or an ECG-based pulse arrival timing that changes with preejection timings. The (1) carotid-toe PTT was the arterial stiffness reference, while the (2) ECG R-toe signal was used as the PAT reference. The BCG I-toe and J-toe PTT's exhibited high correlation (r^2: 0.75 and 0.80, respectively) to the carotid-toe PTT, while R-toe PAT had low correlation (r^2: 0.48), see Figure 4.14. The low correlation of PAT to carotid-toe PTT was expected since PAT includes preejection timing changes of the heart. The BCG PTT's, on the other hand, had stronger correlation to carotid-PTT behavior, even in the presence of a β-blocker—which was an extreme outlier in the PAT regression plot. The β-blocker data point resulted in a large T1 change, while not changing arterial stiffness (T2-T1)—consistent in behavior with its method of action.

4.3.2.3 Supplemental Discussion: BCG Changes with β-blocker

As stated before, the β-blocker time point was revealing—which led to the following observations of the raw time trace, Figure 4.15. The heart rate decreased for the Day 1 time points, and BCG amplitude of the post- β-blocker administration decreased by a factor of 0.3x to 0.5x from pre-administration. For reference, this β-blocker (propranolol) is quickly and completely absorbed, with peak plasma levels achieved in 1-3 hours—and timing between these BCG recordings was 2.5 hours. Assuming contractility was reduced, the BCG amplitude would decrease as a result of lower pulse pressure. The BCG amplitude recovered to normal by the following day and was stable thereafter. A pharmaceutical study would be required to study drug effects more fully. However, from these findings it is suggested that a BCG-PTT system could be capable of monitoring antihypertensive drug therapies which alter myocardial strength (e.g. RI/RJ interval, BCG amplitude/power) from drugs such as β-blockers, and arterial stiffness from vasodilator drugs (e.g. PWV).

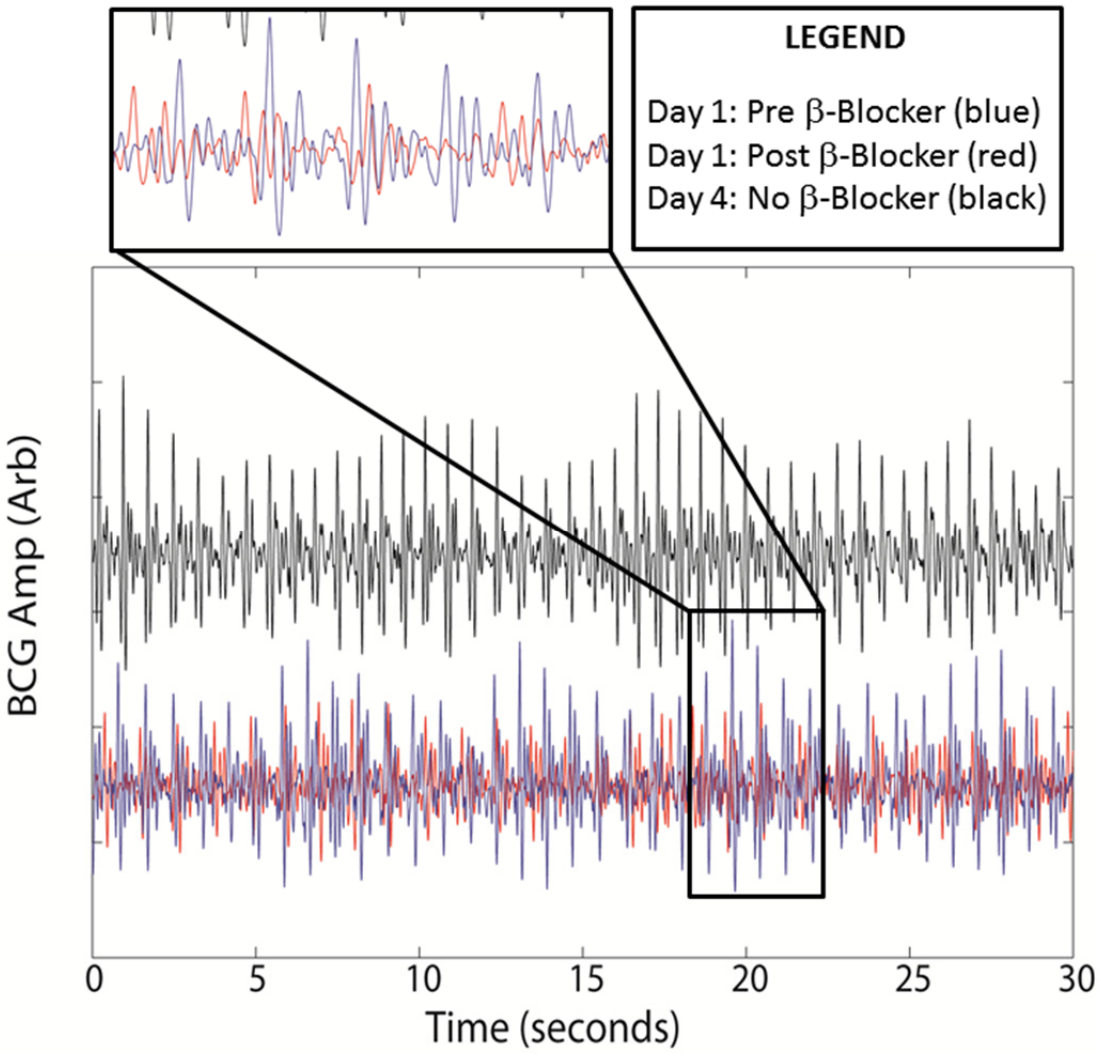

Figure 4.15: Observation on the effects of β-blocker on BCG amplitude. The red and blue traces were obtained on the same day—the blue trace obtained prior to the subject administered the β-blocker, the red trace 2.5 hours after the β-blocker. The BCG amplitude decreased by almost one-half, indicating reduced myocardial strength. The amplitude recovered (black trace) four days later.

4.4 Conclusions

In this chapter, an investigation was performed to characterize BCG timings relative to carotid artery timings, to challenge a hypothesis. The physical models developed earlier in this thesis were thus validated with clinical measurements from an age and longitudinal study, which in turn improves the basic understanding of the BCG signal genesis.

Practically, the standing BCG measurement was demonstrated to be a novel approach for measuring arterial stiffness, by validating BCG timings as T1 timings in the aortic arch. From a

convenience standpoint, standing on a BCG scale approach is simpler and more repeatable than carotid applanation (using tonometry)—thus removing the need for a trained operator. Finally, safety concerns related to fracturing carotid plaques are mitigated since applanation is not required.

With a validated BCG T1 method demonstrated, the next chapter is dedicated to clinical investigations of the standing pulse wave velocity (PWV) measurement—with the aim to improve detection of stiffened arteries responsible for increased CVD risk.

BIBLIOGRAPHY

[1] J. Allen, "Photoplethysmography and its application in clinical physiological measurement," *Physiological Measurement,* vol. 28, p. R1, 2007.

[2] O. T. Inan, M. Etemadi, R. M. Wiard, L. Giovangrandi, and G. T. Kovacs, "Robust ballistocardiogram acquisition for home monitoring," *IOP Journal of Physiological Measurement,* vol. 30, pp. 169-185, 2009.

[3] X. Wang, J. C. K. Jr, A. D. Struthers, and G. Z. Feuerstein, "Assessment of arterial stiffness, a translational medicine biomarker system for evaluation of vascular risk," *Cardiovascular Therapeutics,* vol. 26, pp. 214-223, 2008.

[4] W. W. Nichols and M. F. O'Rourke, *Mcdonald's blood flow in arteries, theoretical, experimental and clinical principles*, Fifth Edition ed. New York: Hodder Arnold, 2005.

[5] H. J. Montoye, P. W. Willis, G. E. Howard, and J. B. Keller, "Cardiac preejection period: Age and sex comparisons," *Journal of Gerontology,* vol. 26, pp. 208-216, 1971.

[6] J. Murgo, N. Westerhof, J. Giolma, and S. Altobelli, "Aortic input impedance in normal man: Relationship to pressure wave forms," *Circulation,* vol. 62, pp. 105-116, 1980.

[7] O. Inan, M. Etemadi, R. Wiard, G. T. A. Kovacs, and L. Giovangrandi, "Non-invasive measurement of valsalva-induced hemodynamic changes on a bathroom scale ballistocardiograph," *IEEE Engineering in medicine and biology society conference proceedings,* vol. 2008, pp. 674-677, 2008.

[8] M. Etemadi, O. T. Inan, L. Giovangrandi, and G. T. A. Kovacs, "Rapid assessment of cardiac contractility on a home bathroom scale," *Information Technology in Biomedicine, IEEE Transactions on,* vol. 15, pp. 864-869, 2011.

5 Standing Pulse Wave Velocity Measurements in a Normal Healthy Population

"…at the beginning a disease is easy to cure but difficult to diagnose; but as time passes, not having been treated or recognized at the outset, it becomes easy to diagnose but difficult to cure."

-Niccolo Machiavelli, II Principe, 1513

5.1 Background

As discussed in the introduction chapter, pulse wave velocity (PWV) is an arterial biomarker which, when utilized properly, can be used to improve estimation of cardiovascular disease (CVD) risk better than using blood pressure alone. Asymptomatic patients can reduce CVD risk by preventing early vascular aging (EVA) through earlier interventions as demonstrated in the *Aggressive Decrease of Atherosclerosis Modifiers* (ADAM) study. The potential impact of PWV can be fully appreciated when considering all major clinical studies investigating arterial stiffening over the past few decades. The theoretical receiver operator curve (ROC) in Figure 5.1 depicts this improvement in overall accuracy to assess CVD risk—the best performance is attained when an arterial biomarker (PWV) is used.

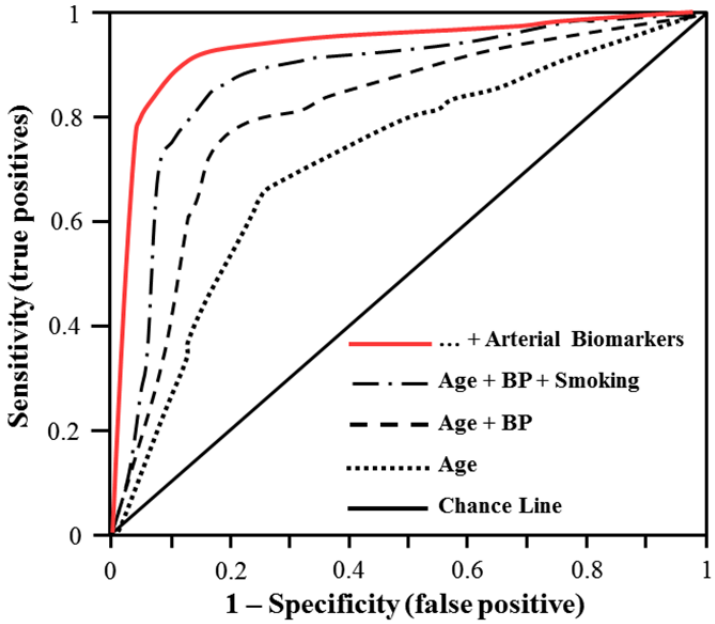

Figure 5.1: Receiver Operator Curve (ROC) depicting CVD risk factor identification. The best overall accuracy is achieved when: age, blood pressure, smoking history, and arterial stiffness are factored in together, redrawn after [1].

Currently, PWV measurements are not commonly performed. There are a few approved PWV devices on the market, however they are not widely accepted by the medical community for lack of knowledge regarding clinical utility, there is no reimbursement for testing, and there are no home PWV devices available for self-monitoring. These factors motivate the demonstration of a BCG-based PWV measurement system, which may enable broad adoption.

The study performed in this chapter is preliminary in nature; however, the results demonstrate performance similar to published data of large scale clinical trials performed over the past few decades, but using a far simpler, inexpensive approach.

5.2 Standing PWV Protocol Overview

The goal of this study is to record *standing pulse wave velocity* (sPWV) measurements with the BCG scale and correlate sPWV to age and blood pressure. PWV is normally measured in the lying down (supine) posture. Since the cardiovascular system adapts between supine and standing, it is imperative to characterize the BCG-PWV scale system in a standing population. To relate this information to hypertension, c*entral blood pressure* (aortic, cBP) was measured in this study, since cBP is more physiologically relevant than peripheral pressures in CVD risk assessment. Age, as discussed is the previous chapter, is the main study variable since the arteries stiffen from elastin degeneration and from atherosclerosis. There were no treatments or interventions in this observational study.

The BCG I-wave is considered suitable for sPWV timings, based on theory and experimental confirmation in the previous chapter. I-wave timings relative to the ECG R-wave were identical to the carotid pulse arrival—consequently, the pulse transit times and PWV should be similar to published literature—which is to be determined here.

5.3 Expected Hemodynamic Changes with Age

The population recruited for this observational study included healthy male and female subjects with ages covering seven decades of life. As such, changes in blood pressure and vascular stiffness are expected and described below.

5.3.1 Blood Pressure Changes with Age

Blood pressure (both peripheral and central) increases with age, as shown in Figure 5.2. The general pathology is an increase in both systolic (SBP) and diastolic pressures (DBP) up until the fifth decade of life, where the trend changes to become an *increase* in SBP and *decrease* in DBP. The increase/decrease pattern occurs in the fifth decade because of atherosclerotic hardening; faster wave reflections return to the heart augmenting systolic pressure, and consequently lowering DBP which decreases coronary perfusion. This condition, known as *Isolated Systolic Hypertension* (ISH), increases the pulse pressure (PP = SBP-DBP) significantly with age, along with PWV. To increase knowledge about

arterial blood pressure, both peripheral and central measurements are also performed in this study [2-5]. The aortic pressures are obtained noninvasively using a tonometer applied to the radial artery.

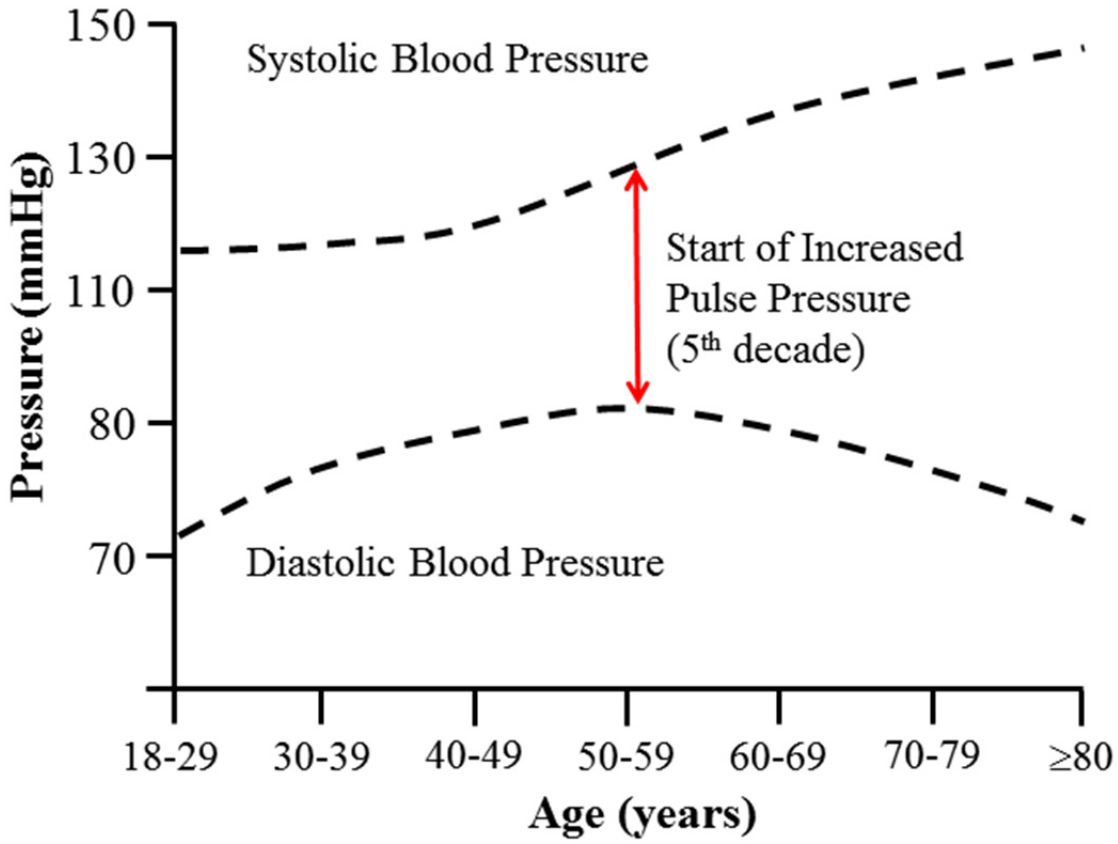

Figure 5.2: General relationship of peripheral blood pressure versus age, redrawn after [6].

5.3.2 Arterial Stiffness Changes with Age

Arterial stiffness changes with age, due to elastin degeneration and atherosclerosis. Figure 5.3 shows age-related PWV for the aortic-iliac and femoral-ankle segments in an urban population with low prevalence of atherosclerosis. The age-dependent PWV change is greater for the aortic-iliac branch (top) since the aorta was once highly compliant (higher elastin content)—whereas the leg arteries are more muscular (higher smooth muscle cell content) and less prone to change. These arterial segments were shown here, since the standing PWV measurement is comprised of both.

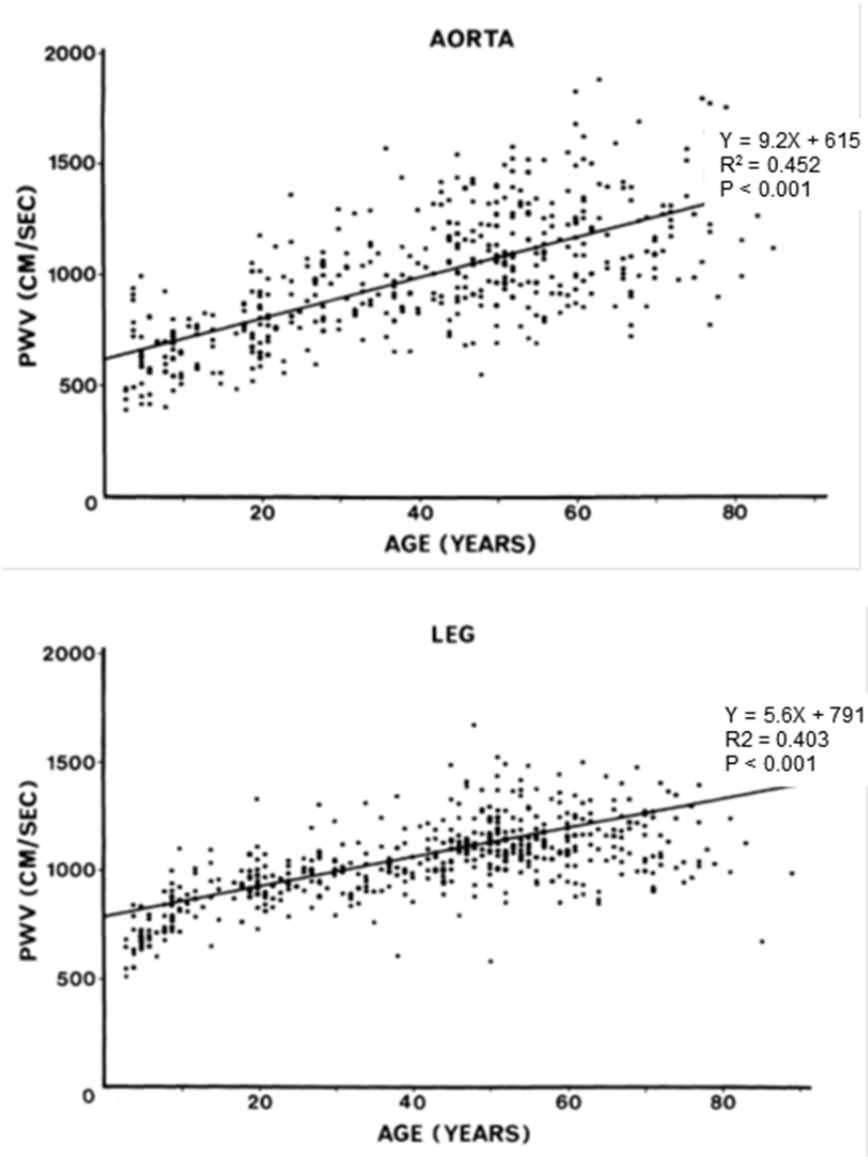

Figure 5.3: Pulse wave velocity relationships for aortic-iliac (top) and femoral-ankle (bottom) in 480 subjects with low prevalence of atherosclerosis in urban Beijing, used with permission [7].

5.4 Materials and Methods

5.4.1 Subject Preparation and Demographic Collection

Healthy subjects were recruited for this study to cover a target age range of 18-80 years old. Upon arrival to the study center, subjects were then asked to remain seated for at least ten minutes to achieve a stable cardiovascular resting baseline. During this time, subjects were asked to complete a questionnaire with basic demographic background, and information about medications and cardiovascular disease history.

Measurements were then taken of their weight, BMI, height, and limb measurements to determine pulse wave velocities along different arterial segments.

5.4.2 Peripheral Pressure Measurements

Brachial blood pressure (BP) measurements were then collected based on the American Heart Association recommended guidelines [8]. To reduce deviations, measurements were taken in a room with stable temperature. Subjects were seated in a chair with their feet flat on the ground, and arm positioned on a table with brachial artery at heart height. A sizing chart was used to determine the proper cuff size for the subject's arm circumference. Systolic and diastolic pressures were obtained using an HEM 7300 (OMRON Corporation, Kyoto, Japan) inflating oscillometric cuff, which has been validated to meet current standards developed by the Association for the Advancement of Medical Instrumentation (AAMI), British Hypertension Society (BHS) and the European Society of Hypertension International Protocol (ESH-IP), supported by clinical validations [9-12]. Three measurements were taken, allowing at least one minute of rest in-between and averaged together to determine the peripheral pressures. Measurements were also taken midway through the study to verify stable cardiovascular baselines.

5.4.3 Central Pressures Measurements

Ascending aortic blood pressure measurements were obtained using a SphygmoCor® CPV (AtCor Medical, Sydney, Australia) tonometer; where a pressure transducer is partially compressed against the radial artery, see Figure 5.4. The beat-by-beat radial artery trace was collected; with consistency verified by software quality controls for several portions of the waveform. A quality control (QC) score is computed when the recordings are completed. If the score is too low, a re-measure is required to ensure accuracy, with central pressure amplitude uncertainty of similar to a conventional cuff, since brachial cuff measurements are used for calibration. Central pressures were then estimated using a generalized transfer function embedded in the SphygmoCor® application software.

Figure 5.4: Example of applanation tonometry. The radial artery pressure waveform is recorded and transformed into the aortic pressure waveform, using a generalized transfer function and a brachial blood pressure measurement for amplitude calibration (not shown).

5.4.3.1 Utility of Central Pressure Measurements

Figure 5.5 depicts the utility of central pressure measurements. In the case below, two subjects had similar brachial systolic pressures around 140 mmHg. However, the estimated ascending aortic pressures were quite different (by over 20 mmHg), when using applanation tonometry at the radial artery. As mentioned above, the radial systolic and diastolic waveforms were calibrated to the brachial BP cuff measurements.

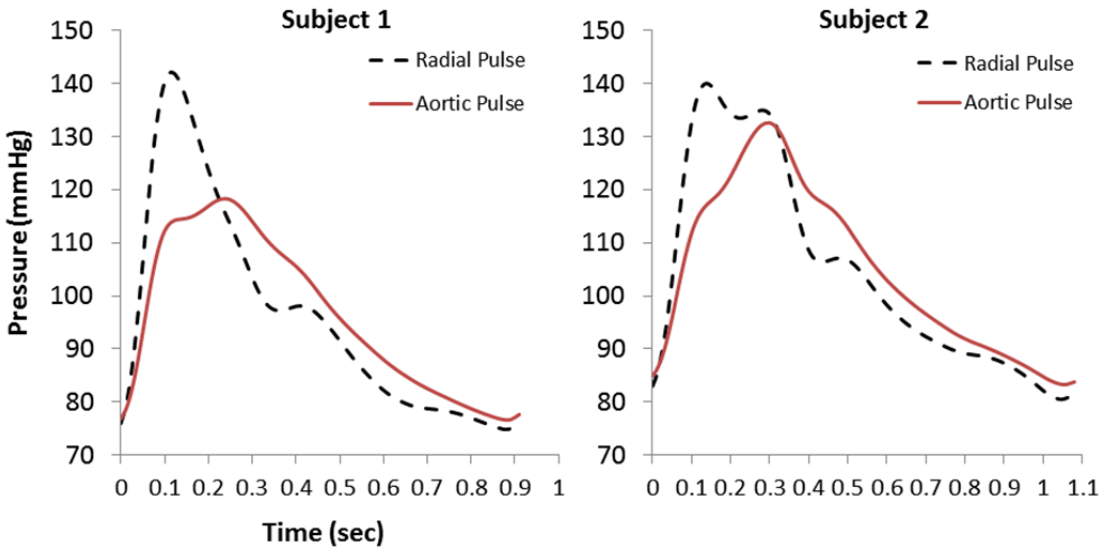

Figure 5.5: Example tonometry pressure waveforms obtained during the study. The two subjects (left and right) had similar brachial systolic pressures (~140 mmHg, dashed lines), but significantly different aortic pressures (solid lines).

5.4.4 Standing PWV Measurements

Following pressure recordings, subjects were instructed to stand for at least two minutes before taking PWV measurements, see Figure 5.6. The PWV measurement setup was comprised of a BCG scale to record I-wave timings for (T1), a photoplethysmograph (PPG) at the toe to record the pulse arrival (T2), and another PPG to record the pulse arrival at the finger (T3). The ECG was also recorded to use as a timing reference (T0) for signal processing. PWV was calculated using the distance from the suprasternal notch down to the feet (Figure 5.6), divided by the pulse transit time (T2-T1). It is important to note that the carotid artery timing was not recorded, to minimize variabilities caused by baroreflex stimulation, which are known to affect T1 timings [1].

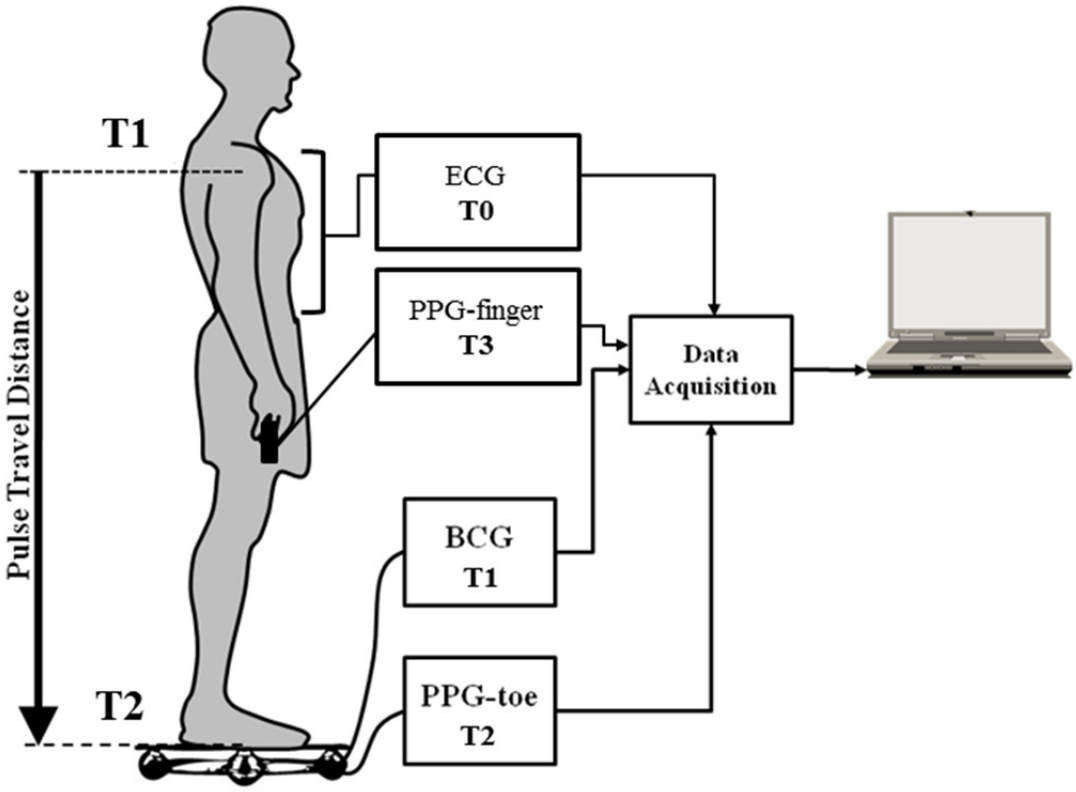

Figure 5.6: Standing PWV measurement setup

5.5 Results

5.5.1 Standing Pulse Wave Velocity versus Age

Figure 5.7 depicts the standing PWV measurement versus age for 50 subjects, using the BCG I-wave timing for T1. The linear best fit with 95% confidence bands (black solid and dotted lines) had a slope of 0.107 m/sec/year and intercept of 7.88 m/s. For comparative analysis, the regression lines from Avolio's studies (Figure 5.3, [7, 13]) are overlaid for the aortic-iliac PWV (red dashed line) and femoral-ankle PWV (green dotted line). Treating the Avolio studies as a historic baseline, the standing PWV intercept differed by +1.73 m/s for aorta-iliac PWV (significant) and -0.03 m/s for the femoral-ankle PWV (non-significant). The standing PWV slope has a 95% confidence interval of 0.094 to 1.20. The slopes in Avolio's study were 0.092 for the aortic-iliac PWV and 0.056 for femoral-ankle.

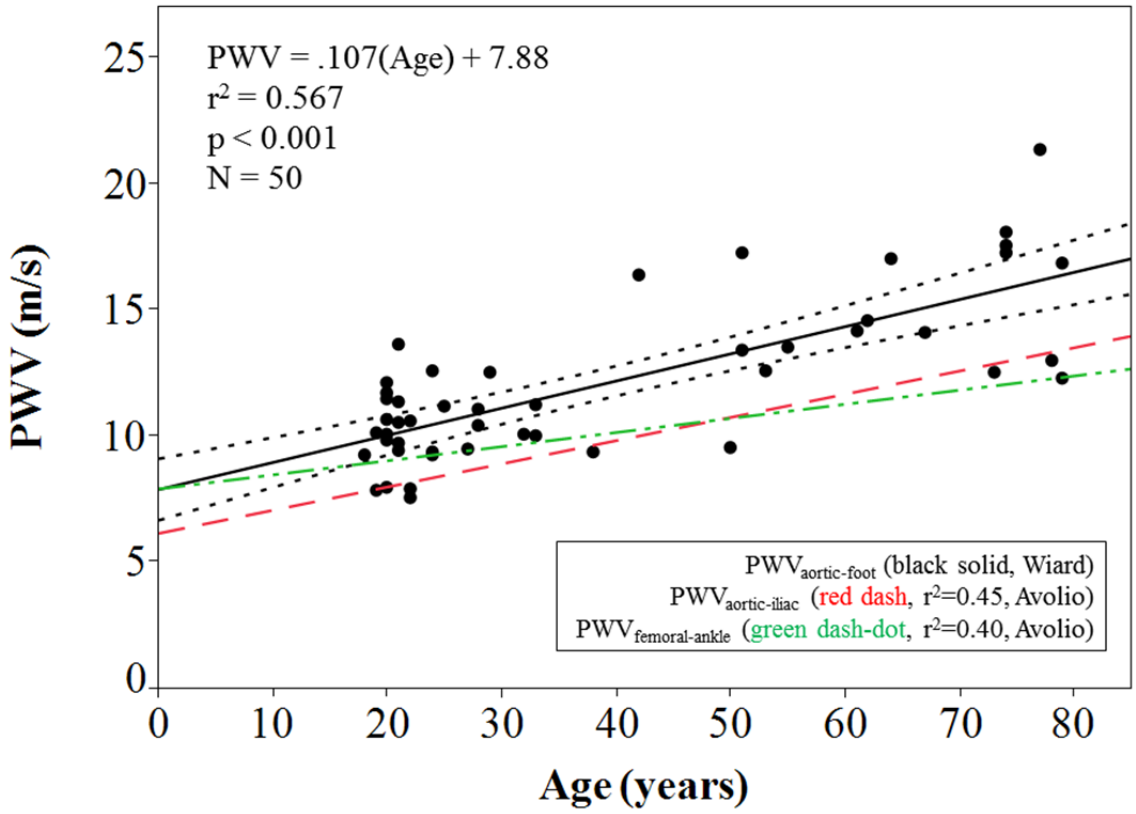

Figure 5.7: Standing pulse wave velocity versus age, compared to the Avolio studies for aortic-iliac (red dashed) and femoral-ankle (green dotted) PWV [1].

5.5.2 Standing Pulse Wave Velocity versus Central Pressures

Standing PWV regressions were also performed against other central pressure parameters such as central systolic, pulse pressure, augmentation pressure, and augmentation index. Standing PWV versus Central Systolic attained the best fit, Figure 5.8. The slope was 0.117 m/s/mmHg with intercept of -0.731 m/s. The 95% confidence bands for the regression line go through zero, such that a zero pressure would result in zero PWV.

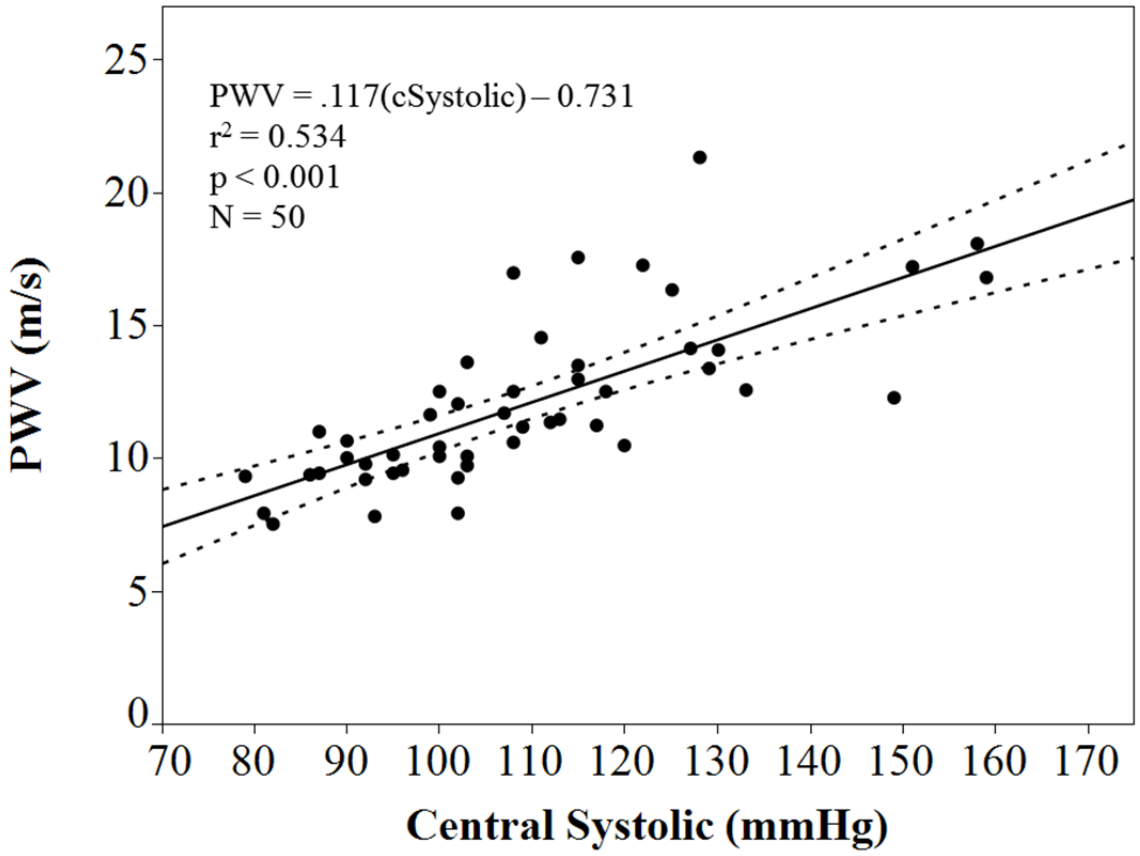

Figure 5.8: Standing pulse wave velocity versus ascending aortic pressure.

5.5.3 Bivariate Correlation Comparisons

The results section concludes with a summary in Table 5.1 of stiffness measures (e.g. PWV, PTT, PAT) along the aorta, aorta-toe, and arm—versus CVD risk factor parameters (age, central systolic pressure, and central pulse pressure). The purpose of this table is to provide a relative comparison of the novel standing BCG-PWV system developed in this thesis compared to those previously described in the literature. All correlations were calculated from this study. As can be seen, the standing PWV measurement had the highest significance for age and central pressures. For arm measurements, PTT_{arm} had a high correlation for age ($r^2 = 0.46$), but had low significance when correlated to central pressures. Comparatively, PWV_{toe} maintained the highest correlations in all three categories. The potential benefits of this correlation strength will be discussed in the closing chapter.

Table 5.1: Correlations (r^2) of Stiffness Measures versus Common CVD Risk Parameters

vs.	Age	Central Systolic Pressure	Central Pulse Pressure
PWV_{Toe}	**0.57**	**0.52**	**0.41**
PTT_{Toe}	0.55	0.49	0.33
$PWV_{Aorta, Est.}$	0.49	0.33	0.30
$PTT_{Aorta, Est.}$	0.56	0.46	0.32
PAT_{Toe}	0.49	0.37	0.28
PAT_{Arm}	0.39	0.19	0.15
$PAT\text{-}PWV_{Arm}$	0.36	0.09	0.12
PTT_{Arm}	0.46	0.30	0.20
$PTT\text{-}PWV_{Arm}$	0.37	0.17	0.13

5.6 Discussion

5.6.1 Validation versus Verification Protocol

It is important to understand key decisions behind this standing PWV study design before discussing the results and conclusions. At the highest level, this protocol was designed to characterize human physiology under the anticipated intended-use scenario of the device which is a requirement of validation. A validation protocol was considered—to directly compare against a known "gold standard," however, there are differences in physiological responses between predicate devices and this particular standing PWV system when used as intended due to posture and carotid applanation.

5.6.1.1 Physiological Differences due to Posture

In the previous chapter, the BCG I-wave was validated as a T1 timing to replace the carotid timing in standing subjects. However, that validation was not designed to certify PWV performance, since predicate PWV systems (e.g., SphygmoCor CPV) were validated in the supine position. Consequently, this PWV study was required to determine whether arterial stiffness physiology was similar between supine and standing positions. To illustrate such differences, Figure 5.9 shows example pulse transit times for the seated, standing, and supine positions for one subject. The standing (center) and supine (right) positions resulted in significantly different transit times but were stable over time—while transient behaviors were observed in the sitting position (left), which is characteristic of blood pooling in the lower leg (venous insufficiency) [14]. If sitting leads to insufficiency, then seated-PWV may be a disadvantageous posture to use, reducing accuracy, with methods proposed by [15, 16].

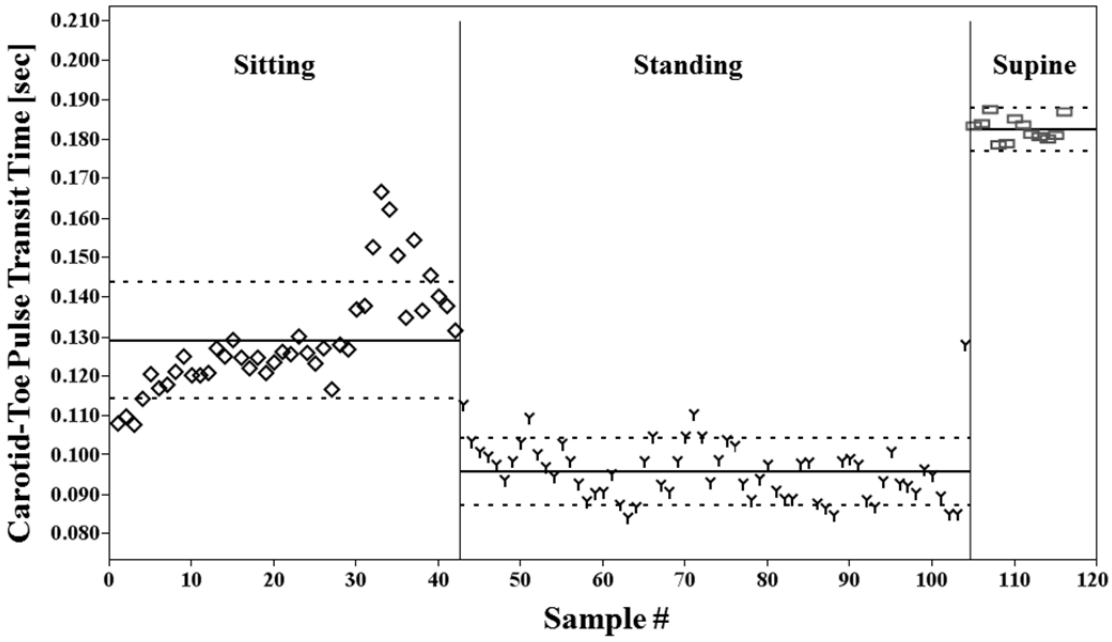

Figure 5.9: Example of postural (sitting, standing, supine) changes to pulse transit times for one subject, leading to different pulse wave velocity values. The standing and supine positions are different but stable, while sitting position leads to transient behavior suggestive of blood pooling in the lower leg (venous insufficiency) [14].

5.6.1.2 PWV Physiological Differences due to Carotid Stimulation

It was essential to perform this standing PWV protocol without simultaneous carotid measurements in order to characterize standing physiology, since the intended use of this device is without carotid applanation. Rubbing the carotid sinus activates nerve synapses in the nucleus tractus solitaries (NTS), which indirectly affects sympathetic and parasympathetic activity; decreasing heart rate and/or blood pressure [17]. However, the carotid and BCG timings have been correlated to each other in the previous chapter, with extensive characterization; both for age and longitudinal studies to confirm their synchronous behavior.

5.6.2 Discussion of Standing Arterial Stiffness (Aortic-Toe) Behavior

5.6.2.1 Comparisons of Standing PWV to Aortic PWV

The standing PWV method measurements demonstrate similar age-related increases as found in the literature, Figure 5.10 [7, 13]. The supine PWV values in Avolio's studies represent age-related changes for the aorta-iliac (red dashed line) and femoral-ankle (green dotted line) arteries. In contrast, the standing PWV measurement comprises both of these branches (from the suprasternal notch to toe) so there is a combined stiffening effect from a compliant aorta and the muscular arteries in the legs. Based on the data, the net behavior is best described as the slope as supine $PWV_{aortic\text{-}iliac}$, with the intercept of the

$PWV_{femoral\text{-}ankle}$. This behavior, however, is not simply the sum of the two branches in series or parallel. The standing PWV values are greater than the supine. Further observational studies are needed to determine whether there the standing versus supine response can be calibrated to each other to obtain universal PWV values. However, it is not clear if physiology differences would be consistent between this system and gold standards when taking into account gravitational loading on the arteries; fluid shifts between the chest, thorax, and down to the legs; and with/without carotid stimulation.

In light of these differences, age-related changes between standing PWV were comparable to $PWV_{aortic\text{-}iliac}$ for a Beijing population with high prevalence of hypertension (Figure 5.10) similar that to the United States [7]. The standing PWV slope obtained in this study could have been higher, but most (if not all) of the older subjects were taking at least one antihypertensive medication. Avolio's observational data for the urban Chinese population had low prevalence of atherosclerosis based on serum cholesterol values—however, it was unclear if those hypertensive subjects were taking blood pressure medications.

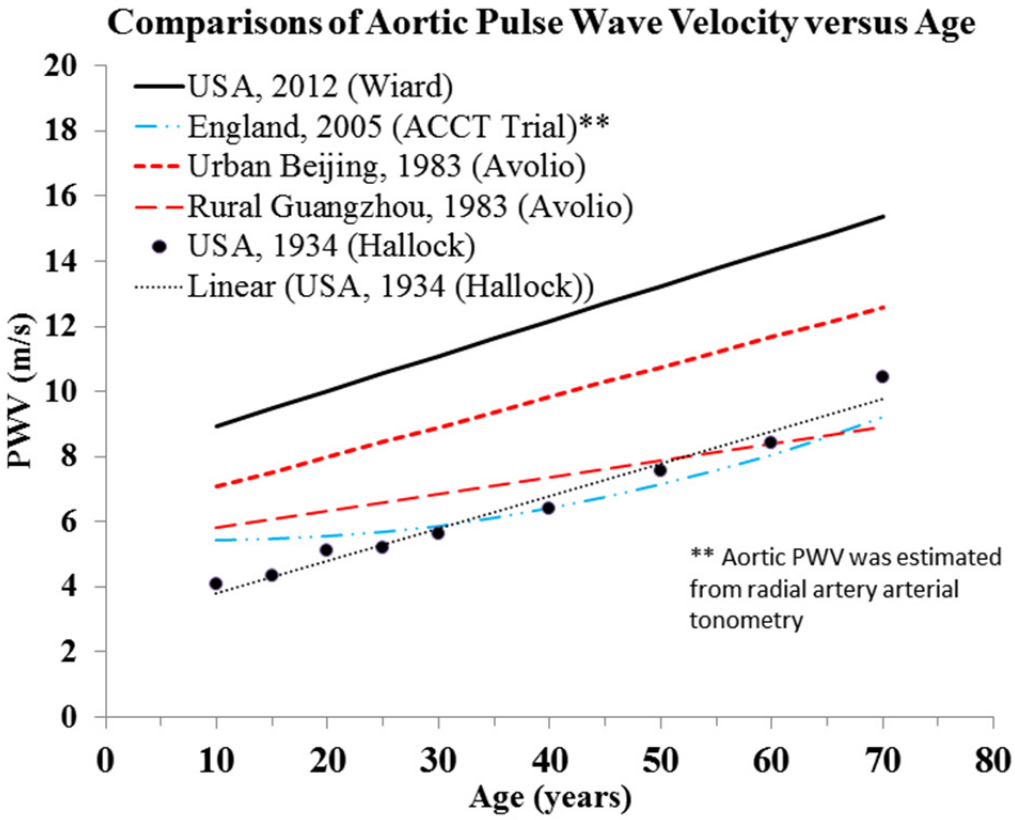

Figure 5.10: Comparison of standing PWV versus age compared to several major studies of aortic PWV. The arterial aging slopes are similar for developed countries and urbanized cities; noticeably steeper than rural Guangzhou—an area with lower prevalence of hypertension and atherosclerosis.

There are visually noticeable differences in PWV values between studies, with several potential causes for the differences [18]. First, the standing PWV in this thesis has the highest intercept which is most likely due to posture, since standing upright decreases pulse transit times compared to the supine position, as exemplified in Figure 5.9. Secondly, the intercepts may be different due to the prevalence of hypertension in particular regions. For example, Avolio chose to study urban versus rural areas in China because age-matched blood pressure levels were higher there than other countries, including the United States, likely due to high salt consumption. The rural Guangzhou region had much lower prevalence of hypertension, thus there is a smaller slope with age compared to Beijing. The Chinese study is highly informative, since the same measurement device and protocol were used at both sites. The Anglo-Cardiff Collaborative Trial (ACCT) regressing in non-linear because of the method used to estimate aortic PWV [18]. Radial applanation tonometry was used, with a generalized transfer function to reconstruct the aortic pressure pulse. After reconstruction, PWV was estimated based on the timing of the reflected pressure wave that augments central systolic pressure. Therefore, the PWV measurement used in the ACCT trial was indirect and nonlinear.

5.6.2.2 Alternative Measures of Arterial Stiffness

Also, it is important to discuss alternate methods to estimate arterial stiffness, such as using electrocardiography (ECG) and photoplethysmography (PPG) to measure pulse arrival time (PAT). This method has been investigated by others and a comprehensive review was done by Allen [19]. The main drawback is that the ECG contains preejection (PEP) timings which confound arterial stiffness measurements. Allen and Murray studied age-related PAT changes in 116 subjects and they concluded that ECG-toe PAT had the largest change with age, compared to the arm and ears. Their PAT-toe correlations were $r^2 = 0.48$ and $r^2 = 0.28$, for age and systolic BP, respectively [20]. The PAT correlation was similar in this study; as standing PAT_{toe} was measured as $r^2 = 0.49$ and $r^2 = 0.37$, respectively (Table 5.1). However, PAT correlations by Allen and Murray and those from this study were not as strong when compared to standing $PWV_{aortic\text{-}toe}$, $r^2 = 0.57$ and $r^2 = 0.52$, respectively. The $PWV_{aortic\text{-}toe}$ correlations are higher, like due to the subtraction of PEP. The strong mutual correlations of age and blood pressure to PWV illustrate the meaning of *interdependent* risk factor.

5.6.2.3 Conclusions on Standing PWV Measurements

Based on the comparative analysis (Figure 5.10), it was concluded that the standing PWV system quantifies aortic stiffness (based on slope)—which is the most clinically relevant PWV value to prognose CVD risk. The PWV scale is therefore a viable arterial biomarker device as alluded to in the introduction (Figure 5.1) and superior in correlation to arterial aging and systolic pressure measurements than similar PAT measures. Therefore, examples are given below to demonstrate the potential clinical utility of PWV to detect early vascular aging in young adults, using the PWV scale.

5.6.3 Predicting Cardiovascular Disease Risk

5.6.3.1 Improving Detection of Cardiovascular Risk in Younger Subjects

Approximately 10% of young adults in the United States, ages 18-39 years old, have hypertension [14]. However, diagnosing true hypertension in this demographic is problematic because of a phenomenon known as pulse pressure amplification. With amplification, aortic pressures can be very low (which is healthy) while measuring high brachial pressure, due to the differences in stiffness between the aorta and brachial artery [1]. Thus, pulse pressure amplification can falsely elevate brachial systolic pressure leading to misdiagnose of hypertension in the younger adult population—since younger aortas tend to be compliant.

Isolated Systolic Hypertension (ISH) is defined as systolic BP of at least 140 mmHg and diastolic BP 90 mmHg or less. These thresholds are reasonably accurate to diagnose hypertension in older adults—but are far less accurate when screening younger adults for hypertension, due to pressure amplification as discussed above. However, in a recent outcome study (HARVEST—Hypertension and Ambulatory Recording VEnetia STudy), Saladini reported on improved CVD risk detection in young adults when measuring central aortic pressure [21].

In HARVEST, 354 young subjects participated with 9.5 years of follow up to detect CVD events resulting from ISH and Systolic-Diastolic Hypertension (SDH). Subjects were placed in the hypertensive group if their brachial BP met the Stage-1 ISH 140/90 mmHg cutoff, and the control group were the remaining subjects below the cutoff [21]. Saladini then created hypertensive sub-groups based on their aortic pressure, measured noninvasively at the radial using applanation tonometry. He concluded that CVD risk was predictable in young adults when the central systolic pressure (cSBP) 125 mmHg or greater—the odds ratio (O.R.) was 6.0 when cSBP was above the cutoff, compared to an O.R. of 1.01 when below the cutoff. For the first time, central pressure measurements were confirmed to be more beneficial than brachial pressure for a young adult population.

The association of arterial stiffness to CVD risk in young adults was also investigated in HARVEST (indirectly) using applanation tonometry. Saladini confirmed that large and small artery compliance had decreased ($p < 0.05$) for the >125mmHg sub-group, but not the other group. In other words, young adults with higher CVD risk were more likely to have stiffer arteries.

In HARVEST, aortic blood pressure and stiffness were shown to be beneficial measures, offering hope to improve CVD risk detection in young adults. Therefore, PWV may be a beneficial measure to screen young adults for CVD risk. An example is presented in the following section, using the PWV scale described in this thesis, as a motivation for future investigations.

5.6.3.2 An Example Utilizing Standing PWV to Prognose CVD Risk in Young Adults

Assuming the PWV scale was properly validated to measure aortic stiffness in this thesis, an example is presented below describing a potential approach to prognose CVD risk in young adults. A sub-group (ages 30 and under) from the age study was examined to compare various stiffness measures (*e.g.*, PWV and pulse arrival time) to age, central systolic, and central pulse pressures, Figure 5.11.

Data points circle and triangle depict two 21-year old males from the study—their data points appear to be outliers with respect to PWV (circle) and central pressure (triangle) for the younger sub-group. Their BCG records were manually inspected and correct I-wave feature extraction was confirmed. Recall from Table 5.1 that the standing PWV measurement had the highest correlation to age, central systolic, and central pulse pressure—compared to several other pulse speed techniques. Therefore, it is more likely that PWV outliers based on age and pressures represent abnormal arterial stiffness. Thus, subject (triangle) has abnormally high central BP but normal PWV (Figure 5.11, top row). This may be interpreted as pre-hypertensive since the cSBP is below Saladini's 125 mmHg cutoff. Conversely, subject (circle) has abnormally high PWV (> 13.5 m/s) but normal central pressure (103 mmHg). Per Saladini's 125 mmHg cutoff, subject (circle) would not be considered at-risk for developing CVD. Based upon the PWV vs. Age regression per Figure 5.10, subject (circle) has an effective arterial age of a 48-year old and may benefit from vasodilator therapies to reduce the stiffening.

Pulse arrival times PAT_{toe} (Figure 5.12, middle row) and PAT_{finger} (Figure 5.12, bottom row) were also examined, since they are often cited in the literature as stiffness measures [19, 20, 22]. Unlike PWV, no unusual stiffness behavior observed for either subject using PAT—likely due preejection timings confounding the stiffness estimate. The example above highlights potential uses for PWV as a supplemental measure to central pressures for early detection of CVD-risk, however, it must be noted that further studies are required to confirm outcomes—which is motivation for future work. In particular, more subjects are needed for each age decade to improve the confidence intervals for the arterial age regression (Figure 5.10) and the subject should (ideally) be trended over the course of several years to determine odds ratios of developing certain forms of CVD.

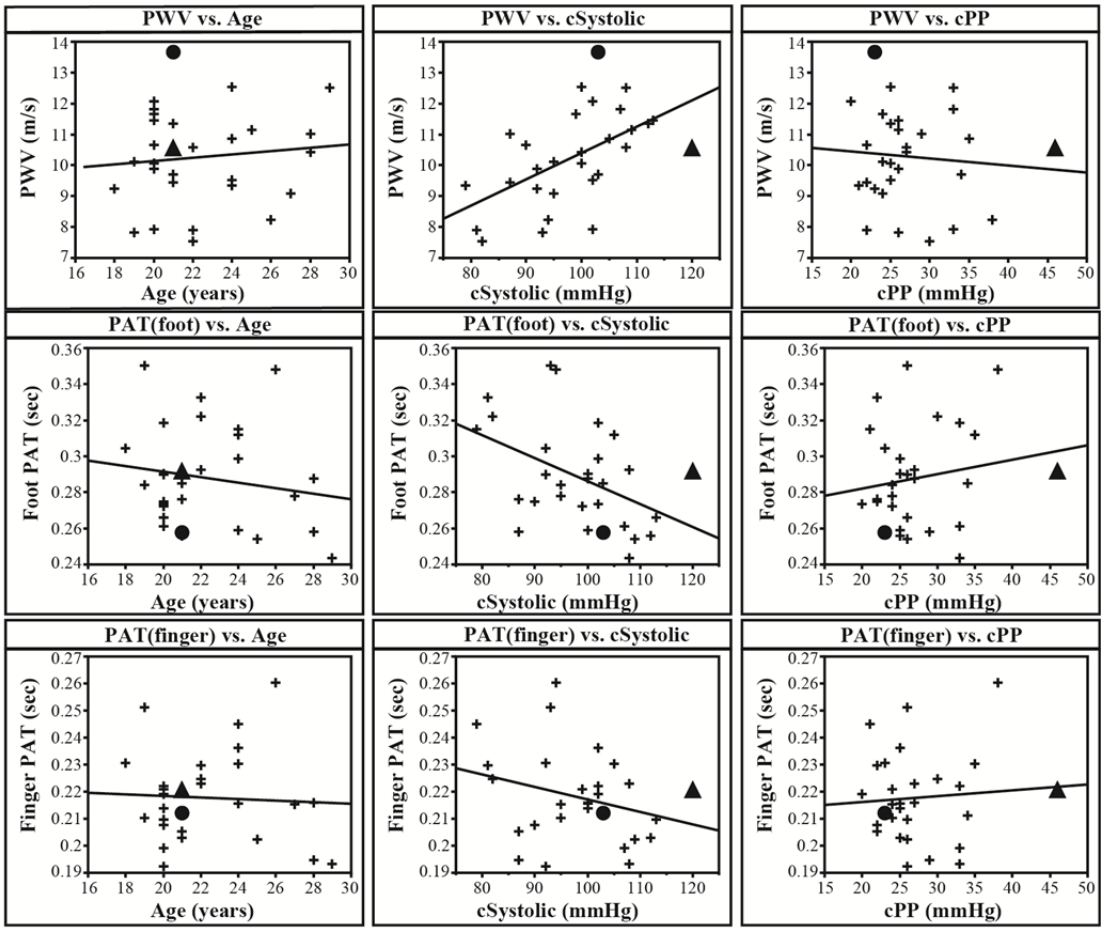

Figure 5.11: Comparison of standing PWV (top row), to PAT_{toe} (middle row) and PAT_{finger} (bottom row) for subjects 30-years and under (N = 29 subjects) for age, central systolic pressure, and central pulse pressure.

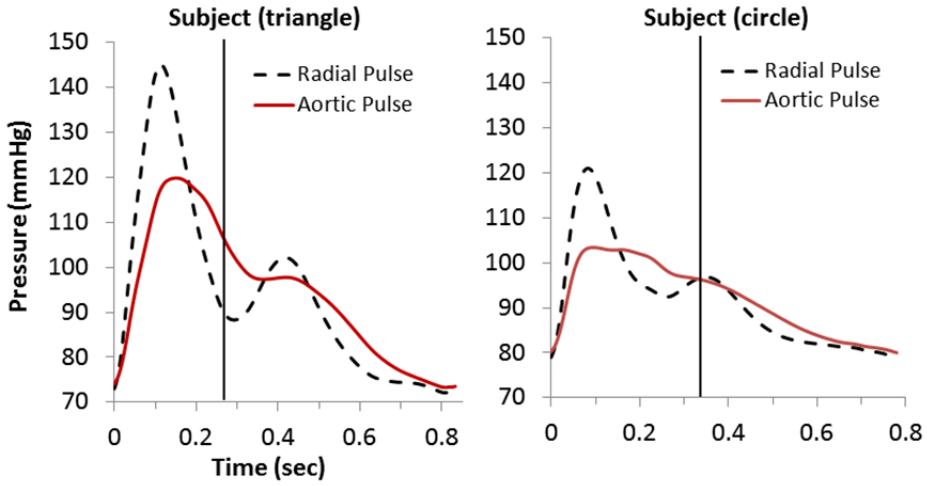

Figure 5.12: Peripheral and central blood pressures for two 21-year old males in the under-30 age demographic. Based on blood pressure alone, subject (triangle) has elevated systolic pressures, but normal PWV (see Figure 5.10). Subject (circle) has normal blood pressure, but his PWV is highest in the younger age demographic.

5.7 Conclusions

Age-related PWV changes have been measured in standing subjects. Physiological differences due to posture, and combined aortic-to-foot PWV have been characterized and compared to key studies in the literature. The age-related slope for the standing PWV measurement was found similar to carotid-femoral PWV, where the latter is the most clinically relevant PWV measurement to estimate cardiovascular disease risk. Furthermore, the standing PWV measurements had the best overall correlations to age and central pressures, when compared to ECG-based pulse arrival times for the arms and legs. The aforementioned correlations demonstrate the usefulness of ballistocardiography to de-confound preejection timing changes in order to estimate vascular stiffness. PWV is a recognized and accepted measurement in medicine, and the work in this thesis supports the use of BCG and PPG as another method to measure PWV. In conclusion, this work, combined with additional supporting clinical trials, should permit the realization of the first practical design for measuring arterial stiffness in the home setting within the next few years.

BIBLIOGRAPHY

[1] W. W. Nichols, M. F. O'Rourke, and D. A. McDonald, *Mcdonald's blood flow in arteries: Theoretic, experimental, and clinical principles*, 6th ed. London: Hodder Arnold, 2011.

[2] M. Karamanoglu, M. F. O'Rourke, A. P. Avolio, and R. P. Kelly, "An analysis of the relationship between central aortic and peripheral upper limb pressure waves in man," *European Heart Journal,* vol. 14, pp. 160-167, 1993.

[3] A. L. Pauca, M. F. O'Rourke, and N. D. Kon, "Prospective evaluation of a method for estimating ascending aortic pressure from the radial artery pressure waveform," *Hypertension,* vol. 38, pp. 932-937, 2001.

[4] A. P. Avolio, L. M. Van Bortel, P. Boutouyrie, J. R. Cockcroft, C. M. McEniery, A. D. Protogerou, M. J. Roman, M. E. Safar, P. Segers, and H. Smulyan, "Role of pulse pressure amplification in arterial hypertension: Experts' opinion and review of the data," *Hypertension,* vol. 54, pp. 375-383, 2009.

[5] M. R. Nelson, J. Stepanek, M. Cevette, M. Covalciuc, R. T. Hurst, and A. J. Tajik, "Noninvasive measurement of central vascular pressures with arterial tonometry: Clinical revival of the pulse pressure waveform?," *Mayo Clinic Proceedings,* vol. 85, pp. 460-472, 2010.

[6] A. V. Chobanian, G. L. Bakris, H. R. Black, W. C. Cushman, L. A. Green, J. L. Izzo, Jr., D. W. Jones, B. J. Materson, S. Oparil, J. T. Wright, Jr., and E. J. Roccella, "The seventh report of the joint national committee on prevention, detection, evaluation, and treatment of high blood pressure: The JNC 7 report," *JAMA: The Journal of the American Medical Association,* vol. 289, pp. 2560-72, 2003.

[7] A. Avolio, S. Chen, R. Wang, C. Zhang, M. Li, and M. O'Rourke, "Effects of aging on changing arterial compliance and left ventricular load in a northern chinese urban community," *Circulation,* vol. 68, pp. 50-58, 1983.

[8] T. G. Pickering, J. E. Hall, L. J. Appel, B. E. Falkner, J. Graves, M. N. Hill, D. W. Jones, T. Kurtz, S. G. Sheps, and E. J. Roccella, "Recommendations for blood pressure measurement in humans and experimental animals," *Hypertension,* vol. 45, pp. 142-161, 2004.

[9] M. Golara, A. Benedict, C. Jones, M. Randhawa, L. Poston, and A. H. Shennan, "Inflationary oscillometry provides accurate measurement of blood pressure in pre-eclampsia," *BJOG: An International Journal of Obstetrics & Gynaecology,* vol. 109, pp. 1143-1147, 2002.

[10] M. Golara, C. Jones, M. Randhawa, and A. H. Shennan, "Inflationary oscillometric blood pressure monitoring: Validation of the omron-mit," *Blood pressure monitoring,* vol. 7, pp. 325-8, 2002.

[11] C. E. Grim and C. M. Grim, "The omron elite 7300w home blood pressure monitor passes the european society of hypertension international validation protocol for women and men," *Blood pressure monitoring,* vol. 14, pp. 87-90, 2009.

[12] A. de Greeff, Z. Beg, Z. Gangji, E. Dorney, and A. H. Shennan, "Accuracy of inflationary versus deflationary oscillometry in pregnancy and preeclampsia: Omron-mit versus omron-m7," *Blood pressure monitoring,* vol. 14, pp. 37-40, 2009.

[13] A. P. Avolio, F. Q. Deng, W. Q. Li, Y. F. Luo, Z. D. Huang, L. F. Xing, and M. F. O'Rourke, "Effects of aging on arterial distensibility in populations with high and low prevalence of hypertension: Comparison between urban and rural communities in china," *Circulation,* vol. 71, pp. 202-10, 1985.

[14] N. Kaplan and R. Victor, *Kaplan's clinical hypertension*, Tenth ed. Philadelphia: Lippincott Williams & Wilkins, 2010.

[15] T. Koivistoinen, T. Koobi, A. Jula, N. Hutri-Kahonen, O. T. Raitakari, S. Majahalme, K. Kukkonen-Harjula, T. Lehtimaki, A. Reunanen, J. Viikari, V. Turjanmaa, T. Nieminen, and M. Kahonen, "Pulse wave velocity reference values in healthy adults aged 26-75 years," *Clinical physiology and functional imaging,* vol. 27, pp. 191-6, 2007.

[16] J. Alametsa, A. Varri, J. Viik, J. Hyttinen, and A. Palomaki, "Ballistocardiogaphic studies with acceleration and electromechanical film sensors," *Medical Engineering & Physics,* vol. 31, pp. 1154-65, 2009.

[17] R. Berne, Levy, M., *Cardiovascular physiology*, 8th ed. St. Louis: Mosby, 2001.

[18] C. M. McEniery, Yasmin, I. R. Hall, A. Qasem, I. B. Wilkinson, and J. R. Cockcroft, "Normal vascular aging: Differential effects on wave reflection and aortic pulse wave velocity: The anglo-

cardiff collaborative trial (ACCT)," *Journal of the American College of Cardiology,* vol. 46, pp. 1753-1760, 2005.

[19] J. Allen, "Photoplethysmography and its application in clinical physiological measurement," *Physiological Measurement,* vol. 28, p. R1, 2007.

[20] J. Allen and A. Murray, "Age-related changes in peripheral pulse timing characteristics at the ears, fingers and toes," *Journal of human hypertension,* vol. 16, pp. 711-7, 2002.

[21] F. Saladini, M. Santonastaso, L. Mos, E. Benetti, N. Zanatta, G. Maraglino, and P. Palatini, "Isolated systolic hypertension of young-to-middle-age individuals implies a relatively low risk of developing hypertension needing treatment when central blood pressure is low (the HARVEST study group)," *Journal of Hypertension,* vol. 29, pp. 1311-1319, 2011.

[22] J. Allen and A. Murray, "Variability of photoplethysmography peripheral pulse measurements at the ears, thumbs and toes," in *IEEE Science, Measurement, and Technology Conference Proceedings*, 2000, pp. 403-407.

6 Conclusions and Future Directions

"*Every now and then ballistocardiography is rediscovered, but even at this meeting its enthusiasts were unable to define a role where it helps in clinical cardiology…"*

-Dennis Krikler, Senior Lecturer in Medicine at the Royal Postgraduate Medical School address to the BCG research community in 1978, commenting on forty years of BCG research.

6.1 Conclusions

A novel technique was demonstrated to obtain proximal (near the heart) and distal pulse arrival timings using ballistocardiography and photoplethysmography, respectively, with both sensors placed in contact with the feet. By simply standing on a scale, arterial pulse wave velocity (PWV) can be estimated without the need to locate superficial arteries to measure localized pulsations. PWV measurements were attained with 30-second recordings using signal processing to extract timing features in the BCG and PPG. The BCG-PPG scale was validated as a useful tool to measure aortic-to-toe PWV while standing upright, through age and longitudinal trending studies. The PWV versus age regression slope was found to be similar to carotid-femoral PWV measured in several major clinical trials, but the scale is much easier to use.

A new physical theory called Central Aortic Forces (CAF) was developed during this work to explain how headward-footward BCG forces and timings can be attributed to pressure changes in the aortic arch. Clinical results demonstrated the validity of the model developed. Without such a theory, it would be challenging to physically explain the correlations between the BCG and carotid artery pulse timings. For example, the theory predicted the nominal timing for when headward BCG forces should begin and this was shown to be accurate for a patient population covering seven decades of age.

The theoretical pulse arrival timing in the arch was validated by comparing the theoretical timing to the RI interval in an age study—the timing results agreed within 12% error of each other. In relative comparisons, the average RI interval timings and carotid arrival timings were within 3 milliseconds of each other. When sub-grouped into young/old age groups, the BCG and carotid timings were shown to have the same age-related timing dependencies that exhibited patterns of stiffening. Faster wave velocities (earlier arrival times) due to stiffening were observable despite the large changes in preejection timings masking the effect. This work established, for the first time, the validation of the BCG as a surrogate timing for the carotid artery to determine vascular stiffness. As such, a major update to BCG physical theory was presented in this thesis.

With the validation completed, practical examples were presented to use the PWV scale system in conjunction with blood pressure measurements, to potentially improve early CVD detection in younger demographics—which are currently challenging. A four-month longitudinal study for one subject was performed to compare the stability of BCG-PWV measurements to carotid-PWV. The correlation between the two methods was high ($r^2 = 0.79$, $p < 0.01$) for twenty-four recordings captured over four months. Propranolol effects were studied showing that the BCG-PWV was insensitive to preejection period (PEP) changes when compared to electrocardiogram-to-toe pulse arrival timings (PAT). The between-day PWV variability were three times greater than the 30-second PWV recording variability—which suggests that measurement system is capable of detecting physiological changes in arterial stiffness. This trending capability would thus be useful to study the short and long-effects of vasodilating drugs to manage hypertension.

A study was also performed to characterize postural dependency of PWV measurements, since most clinical studies were performed previously in the supine position. The standing PWV measurements were shown to have similar age-related sensitivity (slope) to several major clinical studies investigating aortic PWV in the supine position. The standing PWV intercept was higher and was attributed to the physiological differences between postures.

Since the PWV scale demonstrated sensitivity similar to aortic stiffness, a young sub-group from the age study was examined for signs of early vascular aging. Based on their central blood pressures, examples were given to identify "abnormal" aortic stiffness to prognose early vascular aging. This example demonstrates the potential benefit of secondary measurements to supplement blood pressure measurements to forecast cardiovascular disease risk, which is motivation for future work.

6.2 Perspectives and Future Work

6.2.1 Improving the Biomechanical Models

The motivation to study arterial stiffness in relation to the BCG resulted from the theory developed during this work. The CAF theory was developed in parallel to the instrumentation and signal processing work of Omer Inan at Stanford University, to help develop sound intuition about cardiovascular (CV) forces as they relate to: stroke volume, pressure, shear stress, Young's modulus, arterial geometry, peripheral impedance, and other CV parameters. When the first model was completed, it was apparent that pressure and arterial geometry were the primary determinants of CV forces at the origin of the BCG. The BCG-PWV hypothesis was then formed and led to targeted clinical studies to test key aspects of the theory.

Improving the CAF theory is the next logical step to fully model the BCG. The primary factors in the model determined during in this thesis were pressure and arterial geometry. Geometry directly relates to the number of nodes in the fluid and solid mesh that need to be solved for by the Coupled Momentum Method algorithm—which is currently limited by available computer processing power. The next model

should incorporate both the aortic arch and iliac bifurcation, as the iliac branch introduces another geometric asymmetry which is likely related to the rather large K-wave amplitudes acting in the footward direction. Empirically, Nickerson demonstrated that the K-wave was absent in subjects with aortic coarctation, and "re-appeared" later when the coarctation was surgically removed, Figure 6.1 [1]. The CAF model in this work lacked the iliac branch likely necessary to model this downward force, see Figure 3.7.

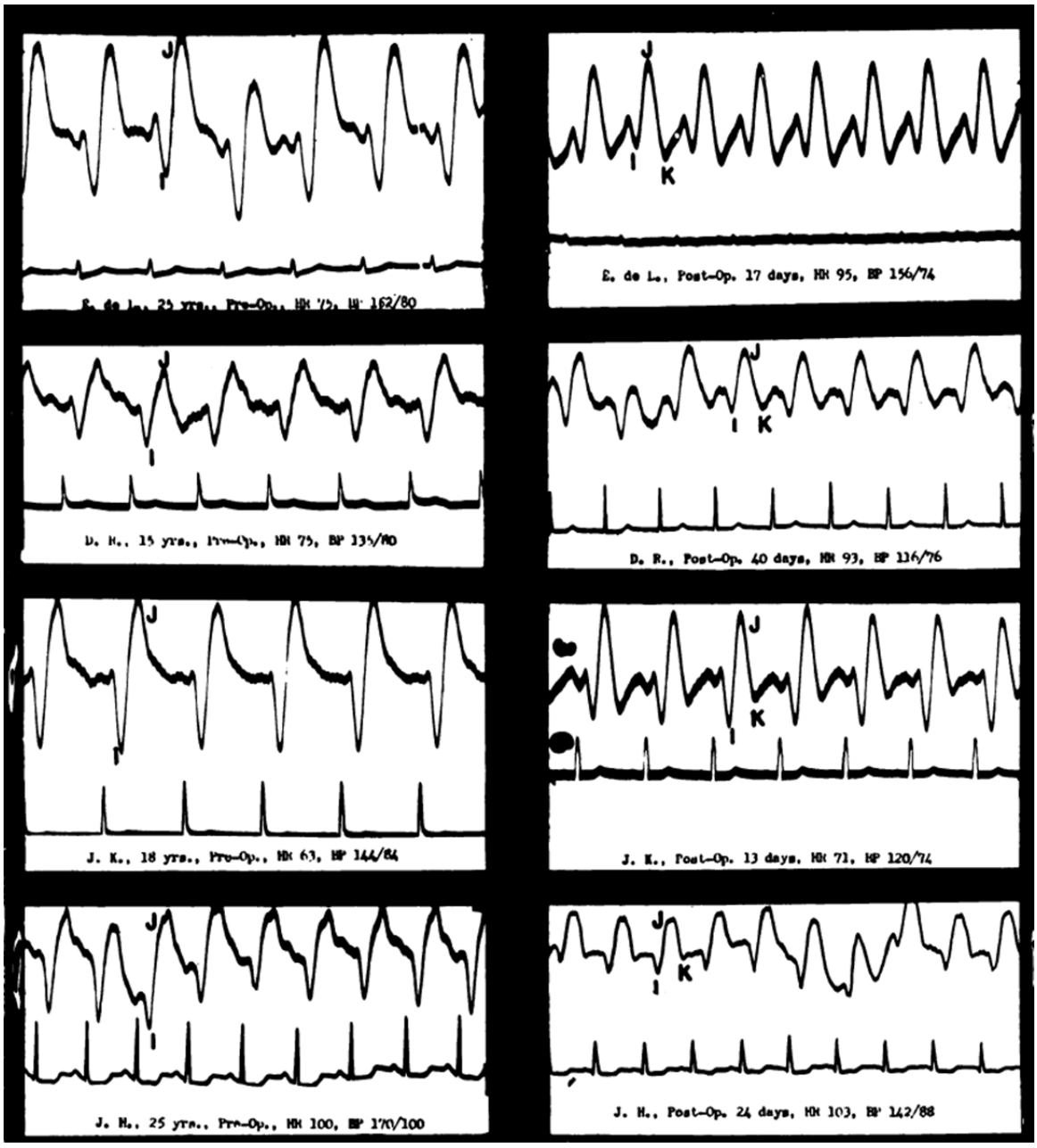

Figure 6.1: The absence (left) and appearance (right) of the BCG K-wave in four patients that underwent aortic coarctation removal. Used with permission [1].

6.2.2 Clinical Trials in Key Hypertensive Populations

A shorter-term step to characterize this PWV system further, is to include it in hypertension clinical studies. The potential capability for longitudinal trending was demonstrated in this work, which is important to understand physiological responses to certain antihypertensive medications such as angiotensin-renin blockers (ARBs) that cause vasodilation in the muscular arteries. Vasodilator drugs are highly effective but currently the most expensive forms of antihypertensives and they are normally only prescribed after trying less expensive medications such as diuretics and beta-blockers. The order these medications are tried is based on cost-benefit models using blood pressure (BP) as the only determinant of efficacy. However, as shown in Figure 5.1, knowledge of arterial stiffness is necessary to improve accuracy of CVD risk estimation. It is possible to have low BP and high PWV since they are independent. The PWV scale presented in this thesis could be easily used in conjunction with BP to manage hypertension.

Younger adults may also be a target population to study for Clinical studies with BP and PWV [2]. Due to pulse pressure amplification, this demographic is frequently misdiagnosed for hypertension. PWV may be a useful secondary index to compare with blood pressure, to improve true-positive identification while lowering false-positive diagnosis. Pulse pressure amplification also exists in older subjects, but at a lower incidence. Therefore, the younger segment offers a greater likelihood if detecting hypertension while minimizing the study size.

The on-going recruitment of healthy subjects should also be pursued to quantify the slope and intercept of standing PWV with age. The relationship between standing and supine PWV will require further quantification to determine normal standards and any transformations required to convert between the two. When sufficient data is obtained for both postures, a calibration factor could be calculated.

6.2.3 Improving the Prognosis of Cardiovascular Disease Risk

A long-term goal for using this PWV scale is to incorporate the PWV measurements into models to forecast CVD risk. However, such studies require years of follow-up to track which individuals actually develop hypertension and/or comorbidities—to establish odds ratios. A direct PWV measurement was lacking in the HARVEST study [2]. However, the indirect compliance measures were still correlated to those subjects who later developed hypertension. In HARVEST, patients took home continuous ambulatory BP monitors to wear and obtain better BP measures, which improved study accuracy. Likewise, the PWV scale can be taken home with subjects to trend PWV changes since a trained operator is not required. Recently, the National Institute of Health (NIH) initiated the multi-site SPRINT (Systolic Blood Pressure Intervention Trial) outcome study to determine whether systolic BP values should be re-adjusted for the Stage 1 and Stage 2 hypertension cutoffs. 9,000 participants will be enrolled in the study for the next four-to-six years [3]. Some of the SPRINT study sites will be measuring PWV. The data and validation described here could be used as a basis for amended studies using the PWV scale, especially for subjects where carotid applanation introduces unnecessary thromboembolism.

6.3 Concluding Remarks

This work, and follow-on studies could have significant impact on large populations to improve their overall health and quality of life. Prognosis and diagnosis are synonymous with leading and lagging indicators. Age, gender, blood pressure, cholesterol, and smoking history are currently the only indices used to routinely determine CV risks. There is active debate on the over-weighting of age in various 10-year CVD risk estimates; however, without additional measurements available to assess the CV system, the forecasting accuracy cannot improve. Pulse wave velocity may become the next CV measure available for this calculation and the hope is that a simple system, such as the one described here, would be readily available to make such determinations in the next few years.

BIBLIOGRAPHY

[1] J. L. Nickerson, G. H. Humphreys, R. A. Deterling, T. C. Fleming, and J. A. L. Mathers, "Diagnosis of coarctation of the aorta with the aid of the low frequency, critically damped ballistocardiograph," *Circulation,* vol. 1, pp. 1032-1036, 1950.

[2] F. Saladini, M. Santonastaso, L. Mos, E. Benetti, N. Zanatta, G. Maraglino, and P. Palatini, "Isolated systolic hypertension of young-to-middle-age individuals implies a relatively low risk of developing hypertension needing treatment when central blood pressure is low (the HARVEST study group)," *Journal of Hypertension,* vol. 29, pp. 1311-1319, 2011.

[3] D. M. Reboussin, J. T. Wright, A. Cheung, S. Oparil, D. Goff, and B. Cushman, "Systolic blood pressure intervention trial (SPRINT)," ed. Wake Forest University School of Medicine: National Heart, Lung, and Blood Institute (NHLBI), 2010.

Appendix: Pulse Transit Timing Calibration Process

Purpose

The purpose of this experiment was to quantify the first-order timing delays of the ECG, BCG, and PPG signals due to the amplifiers and filters from their analog conditioning circuits. Such delays need to be accounted for to obtain calibrated pulse transit (or arrival) times. The **group delay** (reported in milliseconds) is the phase delay versus frequency of output signal relative to the input signal, which becomes the calibration metric. If the circuit response is linear, a constant group delay will result and the output signal will be delayed with no phase distortion, which will be verified. These corrected times will be compared to the PAT_{arch} theory and the relative difference between optical and BCG measurements.

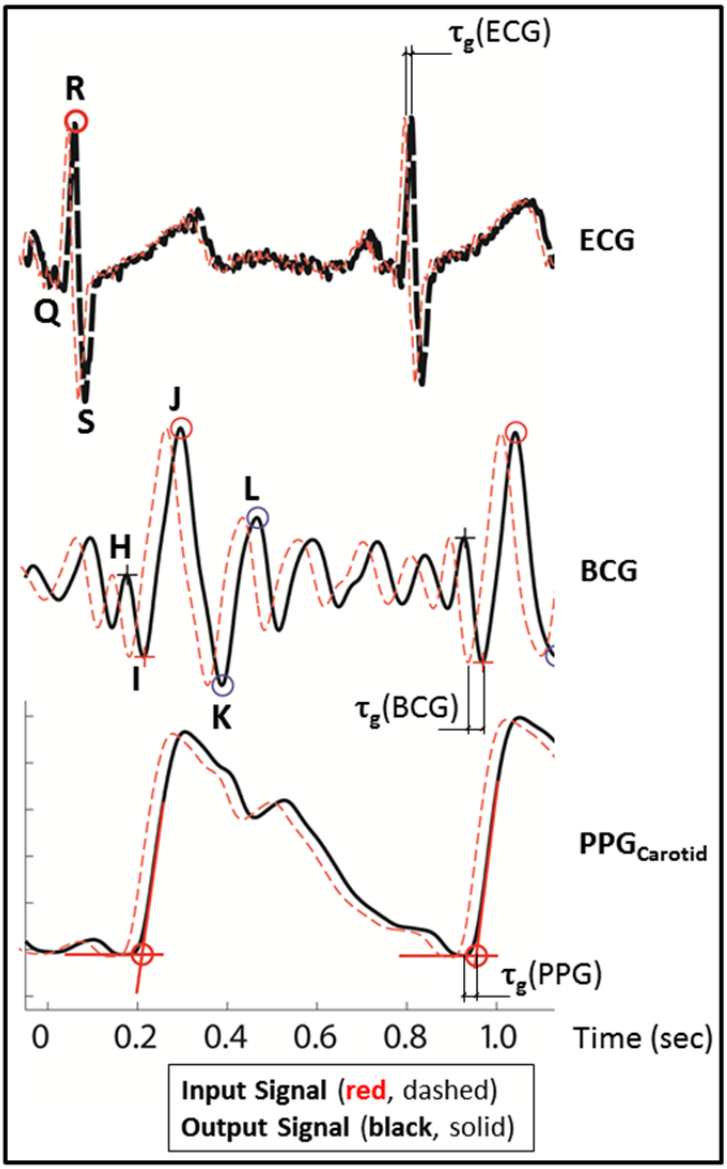

Figure A.1: Example of electronic group delays (τ_g), for the ECG, BCG, and PPG.

Methods

Group Delay Testing

The group delays for the ECG, BCG, and PPG circuits were determined by measuring their respective amplitude gain and phase responses using a dynamic signal analyzer (SRS-780, Stanford Research Systems, Palo Alto, CA). The signal analyzer was configured to drive a sinusoidal input voltage, $v_{in}(\omega)$, through a range of from 0.1 Hz — 1 kHz, with a minimum of 50 cycles at each frequency for averaging of the gain and phase response (Figure A.2).

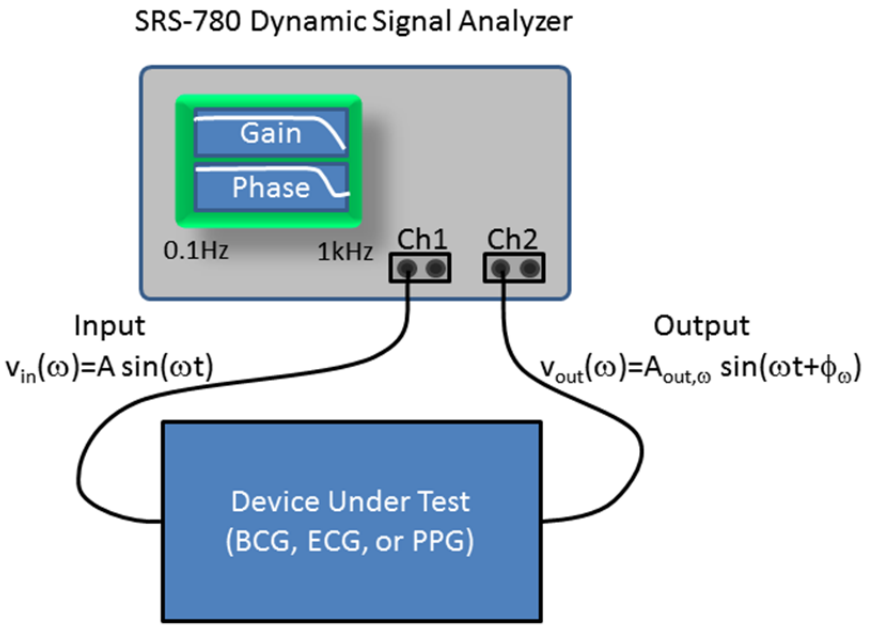

Figure A.2: Dynamic signal measurement setup for the ECG, BCG, and PPG circuits.

The gain and phase data for each circuit was measured, stored on a computer, and post-processed to obtain the group delay. The group delay τ_g is the frequency-dependent delay, which is the derivative of the phase delay $d\phi$ with respect to frequency (ω or f) and can be expressed as:

$$\tau_g(\omega) = -\frac{d\phi(\omega)}{d\omega} = -\frac{d\phi(f)}{df\times 360^\circ} \tag{A.1}$$

Results

Group Delay Testing

The gain and phase responses were obtained for the ECG, BCG, and PPG circuits using the SRS-780. The respective group delays were then calculated using Equation A.1 and are plotted in Figure A.5.

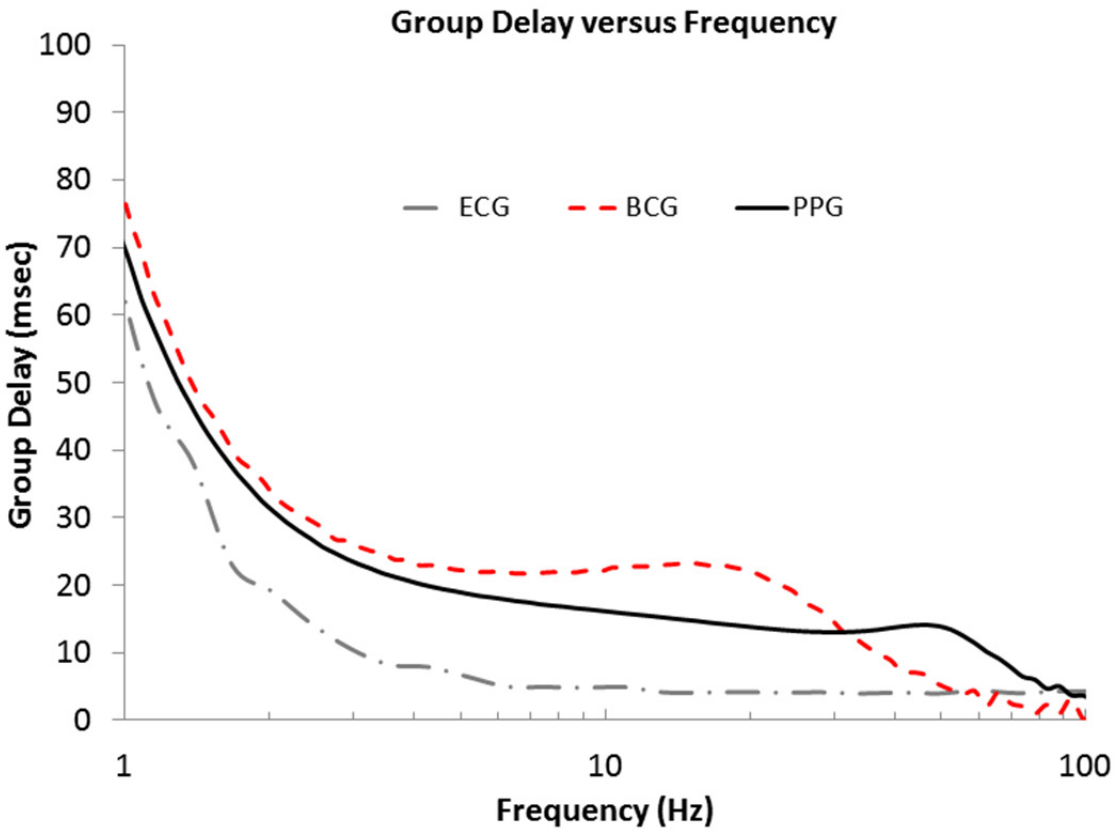

Figure A.5: Measured group delays for the ECG, BCG, and PPG circuits.

Discussion

Group Delay Testing

The group delays for each circuit decreased monotonically from 0.1 Hz and began to level out between 2-3 Hz. The ECG had the shortest group delay of 4 ms from 6 Hz onward, whereas the BCG and PPG delay were significantly longer, 22 ms and 19 ms, respectively. The short group delay of the ECG is attributed to the larger bandwidth with -3 dB cutoffs at (0.2 Hz to 125 Hz), compared to (0.2 Hz to 20 Hz) and (0.3 Hz to 20 Hz) for the BCG and PPG, respectively. At this point, the group delay for the ECG can be approximated as 4 ms, since the QRS complex is above 10 Hz, which is the timing feature used for ensemble averaging. Similarly, the BCG group delay can be approximated as 22 ms, since most of the BCG signal content is centered at 5 Hz as determined in the power spectral density analysis by Omer Inan (Stanford University) in his thesis [1]. A similar analysis of the PPG data collected for this thesis supports a 5 Hz band as a approximate frequency to estimate the PPG group delay, which is 19 ms. It must be noted that these offset values only approximate the delay of the signals. To properly correct these signals for dispersion, an all-pass filter should be implemented digitally based on the measured group delays, to vary the propagation delay with frequency, which is motivation for future work. At the present time, the delays for the ECG, BCG, and PPG timings are estimated, as a means to compare against the theoretical timings.

Conclusions

The group delays for the ECG, BCG, and PPG circuits were measured and quantified as a set of calibration offset values to be used in correcting pulse transit, and pulse arrival timings (Table A.1).

Table A.1: Summary of timing offsets based on group delays

Signal / Interval	f_r(Hz)	τ_g(msec) at f_r	Offsets (msec)
ECG	> 10	4	-
BCG	5	22	-
PPG	5	19	-
R-I Interval	-	-	-18
R-Carotid Interval	-	-	-15
I-Carotid Interval	-	-	-3

BIBLIOGRAPHY

[1] O. T. Inan, "Novel technologies for cardiovascular monitoring using ballistocardiography and electrocardiography," Ph.D Dissertation, Electrical Engineering, Stanford University, 2009.